Karin Plimon, BSc, MSc

Performance Analysis of the Impaired User Downlink in a High Throughput Satellite System Employing an Efficient Multi-User Detection Scheme

DOCTORAL THESIS

to achieve the university degree of

Doktorin der technischen Wissenschaften

submitted to

Graz University of Technology

Supervisor

Assoc.Prof. Dipl.-Ing. Dr.techn. Wilfried Gappmair

Institute of Communication Networks and Satellite Communications

Graz University of Technology

Advisor

Dipl.-Ing. Dr.techn. Johannes Ebert

JOANNEUM RESEARCH

Graz, February 2019

AFFIDAVIT

I declare that I have authored this thesis independently, that I have not used other than the declared sources/resources, and that I have explicitly indicated all material which has been quoted either literally or by content from the sources used. The text document uploaded to TUGRAZonline is identical to the present doctoral thesis.

Date	Signature

Acknowledgements

At this point, I would like to express my gratitude to Hannes and Wilfried, who were always on hand with advice and constructive discussion for me. Thank you for your patience!

Of course, I would also like to thank my office colleagues, especially Nemanja, Harald and Balazs for their support and good cooperation and the rest of the team for the exceptionally friendly working atmosphere. I really appreciate it!

I am also grateful for the support and motivation of my friends and family during this phase of my life. No need to list them all - They certainly know!

- Thank you!

Abstract

The satellite communication industry endeavors to increase the system capacity in order to meet the growing user demand for higher data throughputs. Trying to face this challenging goal of more system capacity, satellite operators currently launch a new generation of satellites, called high throughput satellites (HTS). While the capacity increase is the major benefit of these multi-beam systems, the aggressive frequency reuse and with that, a drastic growth in co-channel interference is the most critical drawback. Due to this fact, methods to cope with these interference levels are absolutely essential.

In this work the multi-user detection (MUD), an interference mitigation technique applicable at the receiving user terminal on ground in the forward link, is in the focus of interest. The aim of this work is to complete theoretical studies on the feasibility of MUD in the forward link by a profound performance analysis under system conditions close to reality. In the course of this action, the MUD performance in terms of capacity is initially investigated considering DVB-S2 and DVB-S2X modulation and coding (MODCOD) schemes. System impairments, such as channel estimation, phase noise, and nonlinearities are additionally considered to the 2-colouring scenario taking into account realistic system conditions. The performance of a traditional 4-colouring multi-beam system is regarded as benchmark for this study. Based on the obtained performance, scheduling algorithms were tested to optimize the performance also for adaptive coding and modulation (ACM) with respect to the propagation channel.

The study is completed by a detailed analysis of interference levels using a realistic antenna pattern and a short excurse on the stability of the satellite in a geosynchronous orbit and the effect on the interference levels on ground.

Kurzfassung

Die Satellitenbranche verfolgt momentan das Ziel den steigenden Anforderungen der Kunden nach größeren Datendurchsätzen gerecht zu werden. High Throughput Satellites (HTS) bilden die neue Generation am Satellitenmarkt, die einerseits den großen Vorteil der deutlich gesteigerten Kapazität erfüllen, andererseits aber durch den wiederholten Einsatz gleicher Frequenzen die Interferenzen im System dramatisch ansteigen lassen, was einen deutlichen Nachteil darstellt. Aus diesem Grund werden derzeit Methoden analysiert, mit denen man den Einfluss dieser Interferenzen im System mildern kann, um von der Kapazitätssteigerung zu profitieren.

Diese Arbeit beschäftigt sich mit Multi-User Detection (MUD) als Verfahren, bei dem trotz vorhandener Interferenz im System, mehrere Signale am Empfänger detektiert werden können. Das Ziel der Arbeit ist es, bereits durchgeführte theoretische Studien zur Anwendbarkeit von MUD im Vorwärtskanal durch eine umfassende Arbeit zu ergänzen, welche die Systemleistung in einer Umgebung erfassen kann, die nahe an der Realität liegt. Zu diesem Zweck wird zu Beginn die durch MUD erreichbare Kapazität für DVB-S2 und DVB-S2X Umgebungen untersucht. Im nächsten Schritt werden die Störeinflüsse am Kanal wie Schätzparameter, Nichtlinearitäten und Phasenrauschen für die Messung herangezogen, um möglichst reale Bedingungen zu schaffen. Um die Ergebnisse zu quantifizieren, wird die Leistung in einem traditionellen 4-Farbensystem herangezogen. Aufgrund der Ergebnisse werden darauf hin auch Management- bzw. Planungsalgorithmen getestet, um die Leistung auch bei adaptivem Einsatz von Modulationen und Kodierungen unter Einbezug von troposphärischen Einflüssen zu optimieren.

Diese Studie wird durch eine detaillierte Analyse von Interferenzwerten und -verhältnissen unter der Annahme einer realen Strahlungscharakteristik eines HTS-Systems, sowie einem kurzen Exkurs zur Bahnstabilität eines geosynchronen Satelliten und dessen Effekte auf die Strahlungscharakteristik und damit die Auswirkungen auf die Interferenzbeziehungen am Boden abgerundet.

Contents

List of Figures

List of Tables

Acronyms

ACM	adaptive coding and modulation
API	application programmer interface
APSK	amplitude-phase shift keying
ASIC	application-specific integrated circuit
AVX2	advanced vector extension
AWGN	additive white Gaussian noise
BF	bundled frame
BP	belief propagation
CCDF	complementary cumulative distribution function
CRC	cyclic redundancy check
CSI	channel state information
DA	data-aided
DVB-S2	digital video broadcasting standard for satellite, 2nd generation
DVB-S2X	extension to DVB-S2
FEC	forward error correction
FER	frame error rate
FF	forward error correction frame
FPGA	field programmable gate array
FR	frequency reuse
GEO	geostationary earth orbit
HPA	high power amplifier

HPBW	half power beam width
HTS	high throughput satellite
IAN	interference as noise
IBO	input power back-off
IMT	interference mitigation technique
IMUX	input multiplexer
ITU	international telecommunication union
LDPC	low-density parity check
LLR	log-likelihood ratio
MAC	multiple access channel
MF	matched filter
MIMO	multiple input multiple output
MISO	multiple input single output
MODCOD	modulation and coding
MS	min-sum algorithm
MUD	multi-user detection
NDA	non-data-aided
OBO	output power back-off
OMUX	output multiplexer
OSI Model	open systems interconnection model
QEF	quasi error-free
QPSK	quadrature phase shift keying
PSK	phase shift keying
RRCos	root-raised cosine filter
RX	receiver
SC	single carrier
SFFI	superframe format indicator

SIC	successive interference cancellation
SimFile	simulation configuration file
SNIR	signal-to-noise plus interference ratio
SNR	signal-to-noise ratio
SOSF	start of superframe
STS	single tree search
TD	total degradation
TLE	two-line element
TRL	technology readiness level
TWTA	travelling wave tube amplifier
TX	transmitter
UT	user terminal
VSAT	very small aperture terminal
WH	Walsh-Hadamard

CHAPTER 1

Introduction

Along with the technologic progress, the amount of data sent over the globe is steadily increasing. This effect can also be observed in the satellite communication industry. Satellite communications in the early days provided predominantly telephone and TV broadcast services. Since the 1990s internet traffic is an application on the rise in the satellite communication business in terms of capacity demand, and this trend is stable for the future. Satellite operators carefully analyze the traffic and try to predict future trends in terms of traffic demand considering the improving technological aspects, demography and behaviour for the next 10 - 15 years ahead, because the planning and manufacturing of a satellite requires several years and the system usually has a nominal operational lifetime of approximately 10 years in orbit. The first communication satellites provided services to large areas or even whole continents by a single spot beam. The ever-increasing demand for capacity requested a new technology to meet these requirements.

The concept of high throughput satellites (HTS) revolutionized in some ways the concept of the traditional satellite systems. HTS operate multi-spot beams to service a certain coverage area instead of a single-spot beam per continent. The use of multiple spot beams allows the reuse of frequencies in the individual spot beams, a technique that provides more bandwidth and thus more capacity to the system. The combination of the technologic progress, allowing higher data throughput, and the increasing amount of users, as demonstrated in the example in Figure 1.1 showing the growth in the number of operated very small aperture terminals (VSATs) over the years 1985 to 2011, alter the request for bandwidth on a steady basis. Satellite operators constantly try to meet the increasing requirements by new technologies and approaches in the satellite industry. Applications that are the driving factors for the ever-increasing bandwidth demand according to Hughes [1], a provider of broadband satellite services, are:

- **Internet access:** the application with the fastest growing demand
- **Remote areas:** complement the terrestrial 3G infrastructure as backhaul or instantaneously enhance the bandwidth for enterprise networks
- **Mobile services:** provide services for land, maritime and airborne vehicles

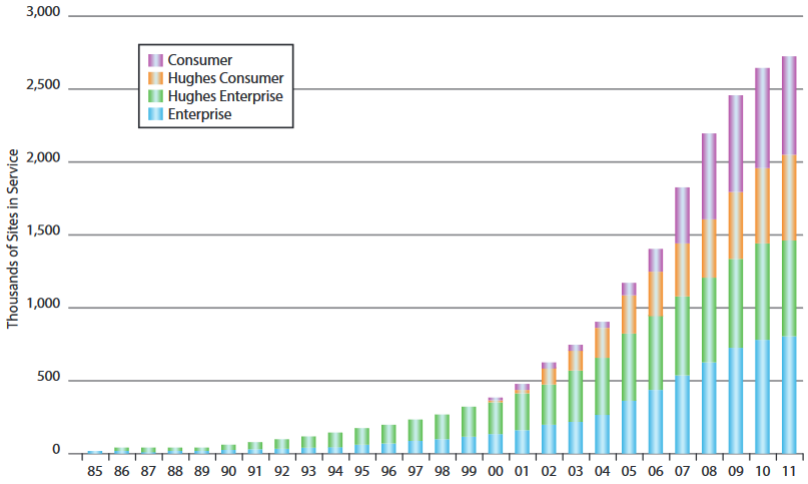

Figure 1.1: Demand for satellite services reported by Hughes [1]

Flexibility is another aspect driving advances in the satellite industry resulting from the situation described before. This demand for flexibility is desired by the satellite operators and is based on the fact that traffic demand is not uniformly distributed in the coverage area. Traffic is thus a function of location and time, since demographic hot spots, irregular events as well as daytime and season determine traffic demands. For this reason, flexibility is a hot topic in order to allocate the available resources optimally to meet the variable demand. Methods that provide this kind of flexibility, for instance beam hopping, strongly depend on the satellite hardware architecture, a topic that exceeds the scope of this work. Finally, the driving factor for the satellite industry is also the relation between service and demand that must not be neglected. With better and affordable service, the number of customers on ground is expected to increase. In addition to that, as long as the performance of the devices on ground improves on a steady basis, the quest for more efficient methods of data transfer over satellites persists.

Having outlined the reason for the introduction of HTS systems, this work turns now the spotlight on the achievable system performance. The fact that multiple users are serviced on the same frequency band at the same time instance increases the co-channel interference, the component contributing most to the intra-system interferences. Higher interference levels are a severe drawback to the system performance that need to be investigated in order to benefit from the increased bandwidth. Interference mitigation techniques (IMTs) are therefore required to counteract the present interference and, thus, allow exploiting the full potential of the increased bandwidth.

In general, there are mitigation techniques that are applicable at the receiver, such as multi-user detection (MUD) or at the transmitter, like precoding [18] [19] [20]. In the course of this work the analysis concentrates on MUD, the former method, applicable for receiver terminals on ground aiming to reduce the introduced co-channel

interference in the system.

The idea of MUD in satellite communications is not new and was initially considered for the return link where different detection algorithms were investaged by [21], [22], [23]. For the application in the return link however, a full frequency reuse is usually assumed [24], [25]. Many algorithms applicable for MUD such as for instance by Colavolpe [22], Studer [26], [27] and the BCJR algorithm [28] exist, to name a few. The approach of MUD as well as its applicability for HTS in the forward link has been studied extensively later by [29], [30], [9], [31] and [32] including also first system performance analysis results. These results revealed potential performance gains especially at the edge of the spot beam. Nevertheless, computational complexity was reported as an obstacle to analyze a wide range of scenarios with high reliability in terms of frame error rate (FER).

This PhD thesis complements the research on MUD analysis by a high performing software-based system demonstrator allowing performance analysis of different scenarios in terms of MODCOD combinations for a joint MUD detection up to a FER of 10^{-6}. The performance analysis is enhanced in a further step by system impairments simulating a satellite system close to real conditions. In parallel, the work pursues the objective to not only optimize the processing speed, but also considers the restricted requirements for a potential future hardware implementation and evaluates potential performance degradations caused by inaccuracy as well as feasibility limits.

1.1 Motivation and Objectives

The demanding user requirements lead to the design of high throughput satellites with multiple spot beams and the idea to apply an aggressive frequency reuse to increase the system capacity. The capacity gain is however traded for raised co-channel interference levels. The co-channel interference calls for mitigation techniques in order to actually profit from the capacity gain. The call for mitigation techniques in the forward link of a satellite system motivated this work that focuses on multi-user detection as possible mitigation technique applicable at the user terminal on ground.

This thesis aims to develop a performance efficient implementation of MUD in view of a potential prototype in the future considering hardware requirements, to evaluate the performance indicators for multi-user detection in a satellite receiver and to determine the achievable peak performance by MUD.

In addition to that, a realistic scenario considering system impairments including channel estimation is considered in order to evaluate the average system throughput of MUD using appropriate scheduling with adaptive coding and modulation.

1.2 Outline of the Thesis

This thesis is structured as follows. In chapter 2 the scope of this thesis is defined. Chapter 3 introduces the scenarios utilized for the system performance evaluation. The system model is covered by chapter 4 and the concept of multi-user detection

is explained in chapter 5. The software framework is detailed in chapter 6 with the according implementation steps explained in chapter 7. Chapter 8 shortly introduces the system impairments considered for a realistic environment. The obtained performance results for MUD including the peak and average system performance compared with a realistic spot beam antenna pattern are provided in chapter 9. The work is finally wrapped-up in chapter 10.

1.3 Research Contribution

This work targets the analysis of a ground-based interference mitigation strategy for HTS systems considering frequency reuse. For this activity, MUD is implemented in the receiver of a HTS software system demonstrator operating DVB-S2 and DVB-S2X in the forward link. This work aims to raise the processing speed and technical readiness level (TRL) of a MUD application in a satellite receiver to a TRL 3 by analysis of MUD in a realistic system demonstrator allowing the assessment of critical functions, performance characteristics and proof-of-concept. The concept of TRL is explained in more detail in section 6.1.

The selected procedure for this work determines FR-4, based on single carrier (SC) performances, as benchmark to analyze MUD performance on an ideal additive white Gaussian noise (AWGN) channel. In order to achieve results close to reality, synchronization, parameter estimation and system impairments such as nonlinearities and phase noise are considered in the system as well. The performance in terms of capacity, throughput and availability of the overall system is analyzed and compared in order to provide initial information on the feasibility, expected throughput and potential problems for the development of a future prototype and field tests. Results of this analysis help to identify dependencies between parameters that determine the system performance, i.e. interference levels, modulation and signal-to-noise ratio (SNR). Along with that, also requirements for the scheduling algorithm and overall system performances under certain conditions can be identified. In parallel to this aspect, the system implementation is hardware oriented in order to gather information about the feasibility and accuracy of this method for hardware requirements (bit-accurate). At the end of the work, topics are identified where, based on the obtained results, future activities could be required to add to the picture of MUD.

CHAPTER 2

Scope

The HTS systems in this work are considered to be geostationary satellites providing service to a certain area on the planet. A geostationary satellite is characterized by the fact that the position of the satellite seems stable from perspective of the Earth. The satellite is located in an orbit approximately 36 000 km from the surface of the Earth and orbits Earth with a constant speed relative to the speed of the Earth.

Depending on the size of the coverage area and the purpose of the mission, the number of spot beams operated by a HTS system can vary between a few tens of beams up to more than 200 spot beams. Amongst the multi-spot beam design, also the applied frequency reuse is a characteristic of a HTS system. These satellites aim to increase the system capacity by applying a frequency reuse that is more aggressive than a traditional 4-colouring scheme (FR-4).

Figure 2.1 illustrates the effect of the frequency reuse scenarios of 4 colours, 2 colours (FR-2) and 1 colour (FR-1), also denoted as full frequency reuse, in a multi-beam setup.

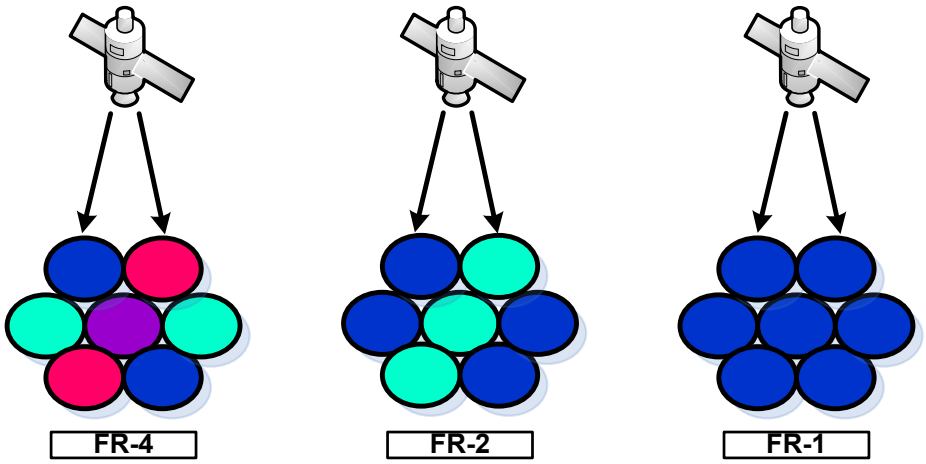

Figure 2.1: Colouring schemes applicable in a multi-beam satellite system: frequency reuse 4 (FR-4), 2 (FR-2) and 1 (FR-1)

2.1 Interference in Satellite Systems

In general the interferences in a satellite system can be roughly categorized into intra-system interferences, describing interference caused by different signals transmitted by the same system and inter-system interference, which denotes interference from signals that were transmitted by other systems [33]. For the purpose of this work, the focus is on the former. The individual sources contributing to intra-system interference are discussed in the following.

2.1.1 Co-Channel Interference (CCI)

Signals transmitted on the same frequency at the same time instance interfere with each other. In multi-beam systems, this interference is caused by frequency reuse in individual spot beams. This interference can only be reduced by adequate physical distance between the spot beams [33] leading to the effect that the contributing side lobes of other beams are reduced. The CCI represents the strongest contribution to the inter-system interference in a HTS system.

2.1.2 Adjacent Channel Interference (ACI)

Channels at adjacent frequencies can cause interference in the observed carrier. These effects can be mitigated by accurate filtering and channel allocation with appropriate intervals [34]. In multi-beam systems this interference can occur in multi-carrier-per-transponder systems.

2.1.3 Intermodulation Interference (IMI)

As explained by Lutz in [35], the nonlinear behaviour of the satellite amplifier causes intermodulation and thus introduces additional interference to the system. This effect can be mitigated either by linearization of the amplifier or by adequate selection of the output power back-off (OBO). The OBO represents a parameter that allows the setting of the operating point of the amplifier. More specifically, selecting the operating point is always a trade-off between linearity and SNR. Operating the amplifier in a linear region therefore results in lower SNR values.

For this application an OBO is selected in the linear region of the high power amplifier (HPA) to avoid the presence of IMI.

In the further analysis, we limit the scenarios to single-carrier-per-transponder setups. This leaves ACI aside and puts CCI at the heart of the following analysis.

2.2 Antenna Beam Pattern

The assumed antenna pattern consists of individual spot beams and stretches over the whole coverage area. Its gain however, is not constant like the pattern of a single spot beam satellite that drops towards the beam border, but is rather inhomogeneous since it consists of several spot beams aligned next to each other. For the design of a multi-spot beam antenna pattern the cross-over level is therefore an essential parameter that defines essentially the distance of the beam centers to each other. Due to this setting, the interference level on ground experienced by the user terminal is highly dependent on its position within the coverage area. The user terminal is assigned to a dedicated spot beam identified by the strongest receive power.

Following this definition all other beams transmitting at the same frequency are declared as co-channel interfering beams for this user terminal. Since the gain of the dedicated spot beam is strongest in the beam center, the receiver will experience the strongest CCI levels at the beam border, that is defined by the cross-over level, of its dedicated beam.

For the analysis in the following, the terminals are assumed to be located stationary within the coverage area at a specific GPS position. The user is assigned to a specific spot beam for service based on this position and the spot beam pattern of the satellite. To describe different setups, the terms main beam and strongest interferer are now introduced:

- The **main or dedicated beam (B_0)** for a user is defined as the assigned beam that is typically received as the strongest signal at the user terminal position.

- The **strongest interfering beam (B_1)** is defined as the beam that the user terminal receives as second strongest signal at the same colour, or in other words, at the same frequency as the main beam for this terminal.

2.2.1 Contour Loss

Due to the shape of an antenna pattern and its directivity, the gain at the center of the spot beam is normalized to 0 dB. The level of observed contour loss towards the beam border depends on the individual spot beam shape. The curvature of the surface of Earth together with the satellite angle usually distort spot beam shapes that are located close to the edge of the coverage area which causes stronger contour losses for these spot beams.

2.2.2 Cross-over Level

The cross-over level is a design parameter that defines the spacing between the adjacent spot beam centers. Traditionally, a 3 dB cross-over level is applied, indicating that neighbouring beams (independent of their individual colour) overlap each other at the half power beam width (HPBW), i.e. -3 dB gain level. The coverage area of a single spot beam is thus in this case defined by its HPBW. Depending on the design also other cross-over levels could be applied which affects the interference levels within the system.

2.2.3 The Contribution of Adjacent Spot Beams to the Co-channel Interference

The co-channel interference levels for neighbouring spot beams at the same colour depend on the location of the user terminal within the main beam. If the user terminal is located directly at the border of the spot beam, the carrier-to-interference C/I_1 level (referred here to the strongest interferer I_1) is 0 dB. For user positions closer to the beam center the C/I_1 ratio increases. The maximum achievable C/I_1 ratio is thus obtained at the beam center (i.e. position of the maximum received power) of the dedicated beam. In a multi-beam pattern with multiple adjacent spot beams operated at the same colour, the total CCI level at a certain user position is not only caused by the closest beam at the same colour (B_1) but also by other beams at a farther distance that are operated at the same colour as well. Without doubt, the main lobe of a beam would cause the highest interference levels, but also the side lobes of beams at a farther distance can still contribute to the overall co-channel interference level observed at a certain user terminal position in the main beam (B_0). The significance of the contribution certainly depends on the shape of the spot beam antenna pattern and its distance to the actual user terminal position of interest.

2.3 Bandwidth and Signal-to-Noise Ratio (SNR)

Throughout this work, different colouring schemes are inspected. However, a comparison is only meaningful if it is done on the same basis. For this reason, the topic of C/N in different frequency reuse schemes is addressed in this section to generate a common understanding of the situation. Throughout this work C/N will be used instead of SNR, denoting the relation between the power of the carrier of interest C to the present noise N. In FR-4 the available bandwidth in a single beam is 250 MHz, in FR-2 and FR-1 it is 500 MHz, though. This comparison is illustrated in Figure 2.2, Figure 2.3 and Figure 2.4.

The bandwidth per user in FR-1 achieves however 1 GHz since two carriers (both polarizations) are utilized for the data transmission to a single terminal.

Assuming a constant carrier power of 0 dB for both cases, there is a difference in terms of noise due to the doubled bandwidth in the FR-2 and FR-1 case. Taking this situation into account the C/N in a 2 and 1 colouring scheme is reduced by 3 dB,

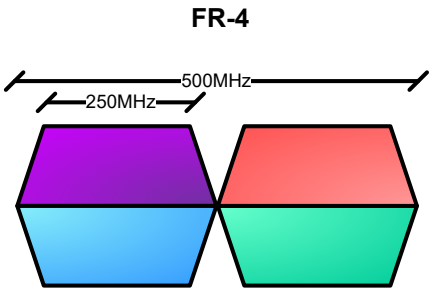

Figure 2.2: Bandwidth per beam in a FR-4 colouring scheme

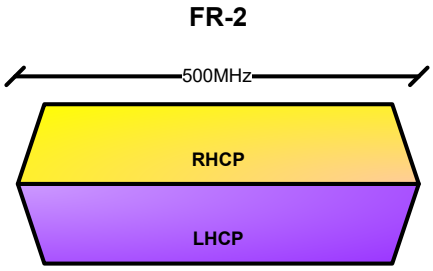

Figure 2.3: Bandwidth per beam in a FR-2 colouring scheme

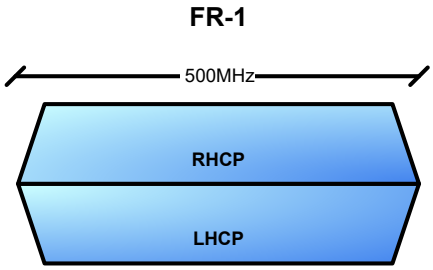

Figure 2.4: Bandwidth per beam in a FR-1 colouring (full frequency reuse) scheme

respectively 6 dB. Since FR-4 is considered as benchmark, it will be used as reference for the result analysis. For this reason, the results will be compared in terms of C/N at FR-4 beam center considering that C/N is 3 dB lower when talking about schemes that are operated with 500 MHz per beam. Figure 2.5 illustrates this situation for FR-4 and FR-2.

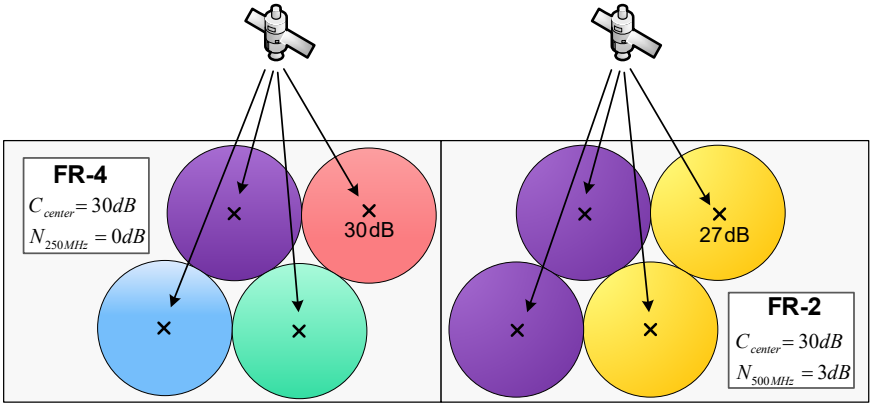

Figure 2.5: Colouring specific noise in a spot beam

As Figure 2.5 indicates, the performance obtained with FR-4 at 30 dB C/N and FR-2 at 27 dB C/N are compared at equivalent C/N = 30 dB at FR-4 beam center.

2.4 Signal-to-Noise plus Interference Ratio (SNIR)

The main reason to implement a 4-colouring scheme at early multi-beam satellite designs was to keep the CCI in the system low. Especially in aggressive frequency reuse systems, the system performance becomes inevitably interference-limited. The C/N, as discussed before, is thus less relevant as performance indicator. The interference needs to be taken into account and with that the signal-to-noise plus interference ratio (SNIR) (2.1) becomes the significant performance indicator:

$$SNIR = \frac{C}{N + I}. \tag{2.1}$$

The parameter C denotes the main carrier, I is the interference component that represents the co-channel interference sources in the system and N represents the AWGN from the channel. For the purpose of this work the parameter I represents the number of interfering carriers at the same frequency from the perspective of the user terminal of interest.

2.5 Satellite Links

A satellite system is usually composed of the following types of links, as illustrated also in Figure 2.6.

- Uplink (from ground to space)
- Downlink (from space to ground)
- Forward Link (from the gateway via the satellite to the user terminal)
- Return Link (from the user terminal via the satellite to the gateway)

This analysis focuses solely on the forward link and to be more specific, on the CCI mitigation performance in the user downlink. This means that the satellite is considered as the transmit part and the user terminal on ground is considered as the receive part.

The channel, the free space between the transmitter and the receiver is influenced by AWGN, interferences and impairments that are contributing to the performance degradation. As shown in Figure 2.6 the Digital Video Broadcasting Standard for satellite in the second generation (DVB-S2) [5] and its extension (DVB-S2X) [2] are considered for the user downlink. Since this work focuses on the user downlink performance, an optimum feeder link is assumed for the examined scenarios in this work.

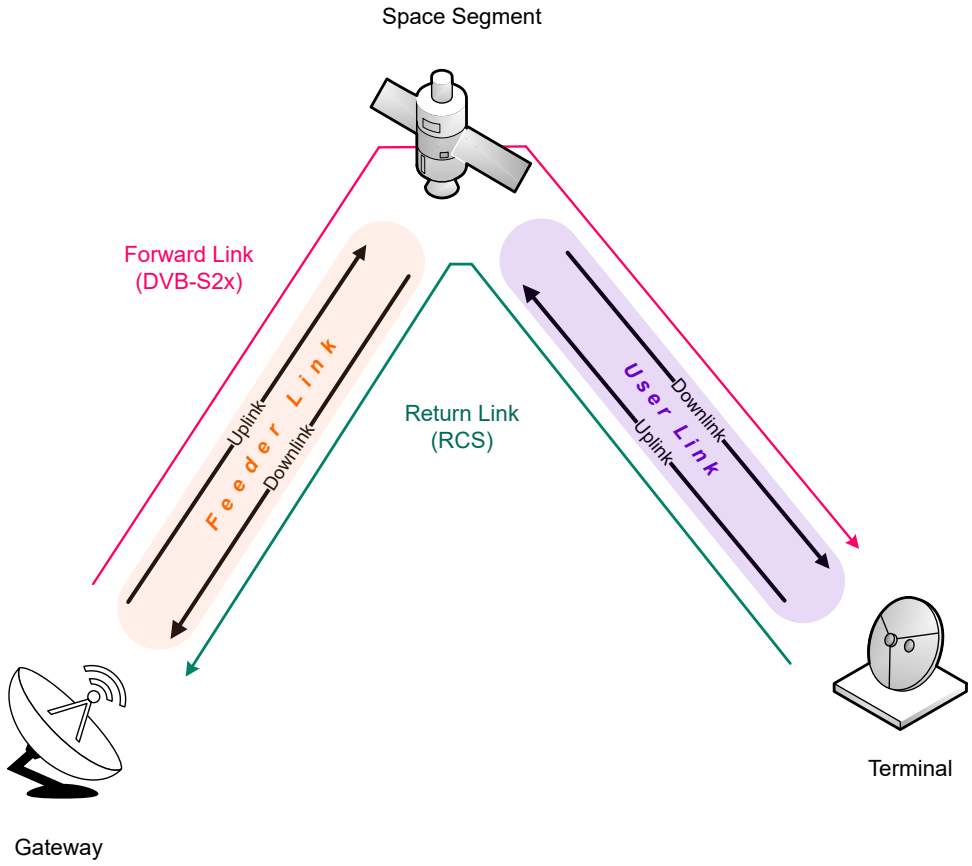

Figure 2.6: Links in a satellite system

2.5.1 DVB-S2X Framing

Considering the DVB-S2 and DVB-S2X standard, the scenarios focus on the DVB-S2(X) MODCODs, an acronym for modulation and coding (MODCOD), QPSK, 8PSK, 16APSK and 32APSK. The superframe format is introduced for data transmission by the DVB-S2X standard. This superframe format is specified for the data basis of short and normal forward error correction frame (FECframe) lengths, shown in Figure 2.7 and Figure 2.8, respectively.

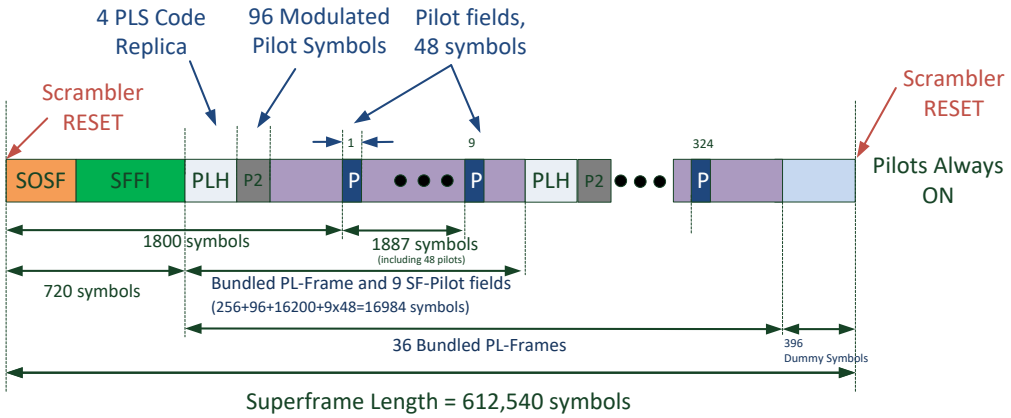

Figure 2.7: DVB-S2X superframe format with short FECframes [2]

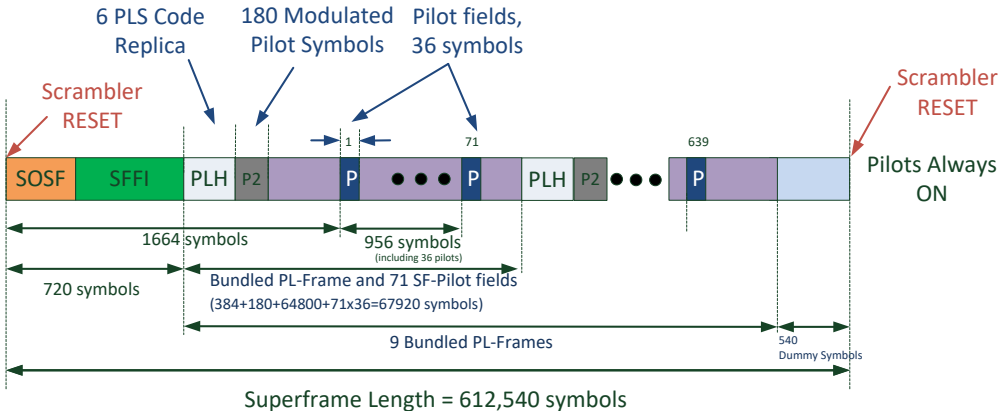

Figure 2.8: DVB-S2X superframe format with normal FECframes [2]

These short, respectively normal frames are grouped to bundled frames, shown in Figure 2.9 and Figure 2.10 that offer a constant frame length. The short bundled frame consists of 16 200 payload symbols, where the normal bundled frame has a length of 64 800 symbols. This constant frame length is an essential feature for MUD. In order to apply MUD at the receiver and perform successful CCI mitigation, it is required that the transmitted symbols of adjacent carriers fully overlap in time.

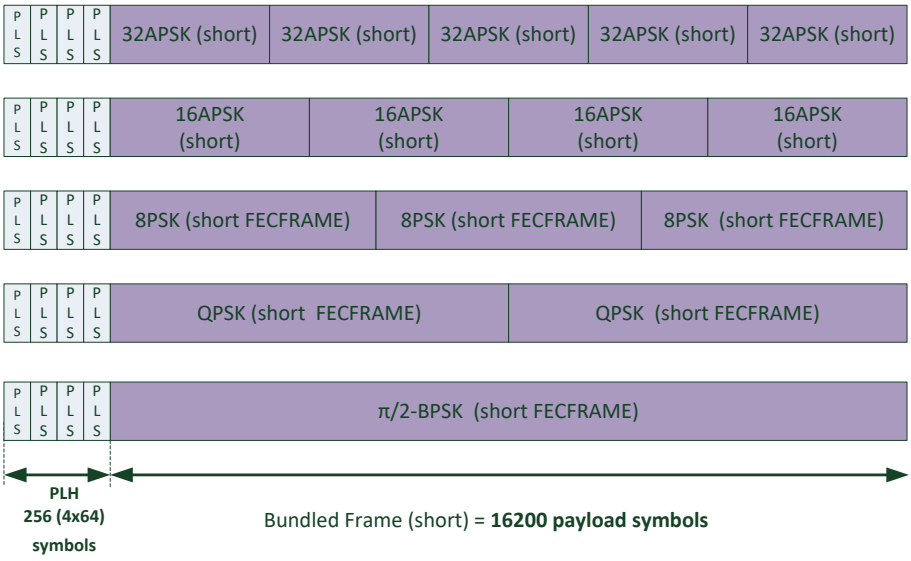

Figure 2.9: DVB-S2X bundled frame with short frames [2]

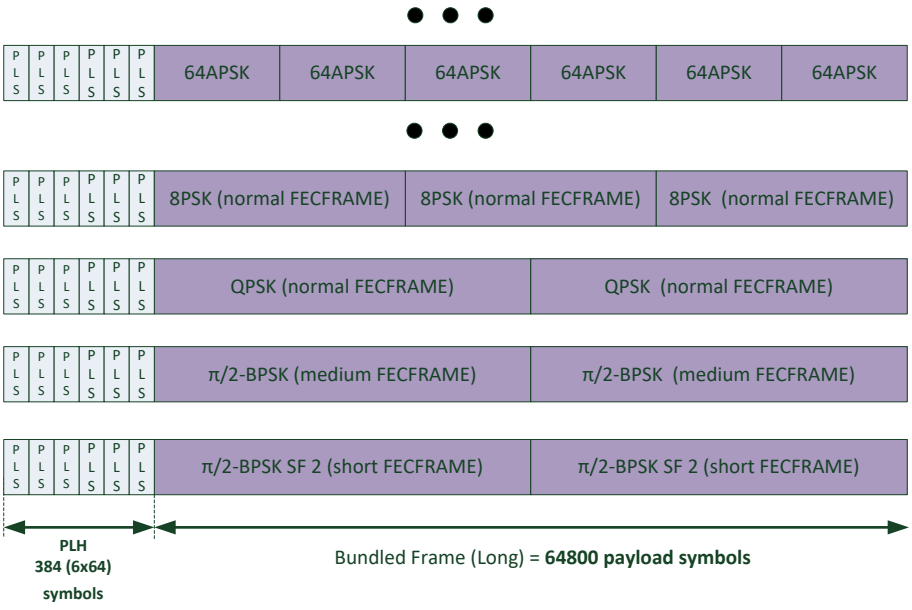

Figure 2.10: DVB-S2X bundled frame with normal frames [2]

The figures demonstrate that independent of the selected modulation for the individual carrier, a constant frame length is kept. This concept allows the transmission of individual MODCODs in different spot beams and enables detection using MUD for a single user terminal.

While the number of bundled frames per superframe is specified by the standard with 36 for short, and 9 for normal frame, the number of FECframes per bundle however, depends on the modulation order, as summarized in Table 2.1.

Modulation	**Order**	**FECframes per bundle**
QPSK	2	2
8PSK	3	3
16APSK	4	4
32APSK	5	5

Table 2.1: Modulation specific number of FECframes per bundled frame

In-between the bundled frames are physical layer headers and pilot fields. Together with the SOSF (start of superframe) and SFFI (superframe format indicator) field, that mark the header of each superframe, they are essential for the synchronization and parameter estimation at the receiver terminal.
Because this work investigates the MUD performance at the receiver, the focus is put on the bundled and FECframe structure.

CHAPTER 3

Scenario Definition

In order to assess the performance of MUD as interference mitigation technique for CCI applied at the user terminal, a definition of the assumed interference scenarios is required. For this purpose, this section is dedicated to specify the selected interference scenarios for FR-1, FR-2 and FR-4, and analyzes the resulting SNIR levels as performance measure.

3.1 Interference Scenarios

Statistically averaged CCI scenarios obtained from a realistic 200 spot beam system, as provided in Table 3.1, are considered for FR-4, FR-2 and FR-1. These interference scenarios represent the basis for the MUD performance analysis. As shown in Table 3.1, only the five strongest interferers are considered to contribute with their side lobes to the co-channel interference in the system for an individual user terminal. The contribution of the remaining beams at the same colour in the pattern is quite low due to their distance, and is therefore neglected for this study.

The reason why FR-4, in contrast to FR-2, has only a single CCI scenario is the fact that the CCI level is assumed to be constant within a single beam based on the large distance between beams that are operated at the same frequency. In other words, the interference at FR-4 is independent of the position of the user terminal. At FR-2, the individual CCI scenarios basically represent different user positions within a single beam. For example the scenario characterized by $C/I_1 = 0\,dB$ represents a user position directly on the beam border, next to a beam of the same colour. The interference scenario characterized by $C/I_1 = 10\,dB$ on the other hand, describes the interference situation for a user located at a position close to the center of a spot beam, where the signal strength of the own beam is significantly stronger than the signal of the strongest interfering beam at the same colour.

The interference scenarios are defined via the colour and their scenario ID, which becomes useful if the scenarios are compared to each other later in this work. If only single scenarios are adressed however, they are referred to by their characteristic C/I contribution of the strongest interferer, denoted as C/I_1 [dB], for simplicity.

FR-4					
	C/I_1 [dB]	C/I_2 [dB]	C/I_3 [dB]	C/I_4 [dB]	C/I_5 [dB]
	22	22	22	22	22
FR-2					
Scenario ID	C/I_1 [dB]	C/I_2 [dB]	C/I_3 [dB]	C/I_4 [dB]	C/I_5 [dB]
1	0	25	25	27	30
2	2	26	26	27	30
3	4	27	26	27	30
4	6	27	26	27	30
5	8	26	26	27	30
6	10	22	26	27	30
FR-1					
Scenario ID	C/I_1 [dB]	C/I_2 [dB]	C/I_3 [dB]	C/I_4 [dB]	C/I_5 [dB]
1	0	4	10	25	25
2	2	3	10	18	25
3	4	5	11	18	26
4	6	7	12	17	25
5	8	10	12	18	20

Table 3.1: FR-4, FR-2 and FR-1 carrier to interferer (C/I) levels [dB]

3.2 SNIR Analysis

The SNIR in general represents the performance measure for the successful detection and decoding. This parameter involves the C/N level and the interference but includes also the effects of present system impairments and tropospheric attenuation. The SNIR is therefore a good indicator that describes the whole system. For this reason, a special focus was set on the SNIR level for the analysis of the MUD performance. With MUD a user terminal is challenged to decode the information transmitted by two carriers in parallel. The information is transmitted by the main carrier (B_0), representing the dedicated beam of a user terminal, and the strongest interferer (B_1), operated at the same frequency. This implies that not only the SNIR of the dedicated beam but also the SNIR of the strongest interferer determines the performance at the user terminal. In order to avoid confusion, the following terms are introduced describing the SNIR from the perspective of the individual beams B_0 and B_1.

The SNIR from the perspective of B_0 and B_1 are computed as in (3.1) and (3.2) respectively.

The SNIR from the perspective of the main carrier (B_0) is given by

$$CNI_1^5R = \frac{C}{N + \sum_{i=1}^{5} I_i}, \tag{3.1}$$

whereas the SNIR from the perspective of the strongest interferer (B_1) develops as

$$I_1NCI_2^5R = \frac{I_1}{N + C + \sum_{i=2}^{5} I_i}. \tag{3.2}$$

When creating a MODCOD pair using two vastly different MODCODs, the individual carriers might be successfully decoded at quite different SNIR levels. This can lead to the effect that one of both carriers is successfully detected clearly before the FER of the second carrier begins to drop. In this case however, the SNIR level begins to raise for the perspective of the remaining carrier to be decoded, since one of the carriers is already known to the detector. Considering this scenario, the SNIR for the remaining carrier can be computed as follows.

Since both scenarios can occur, the formulas are given for the viewpoint of C, as well as I_1. The other, successfully decoded carrier is already known to the receiver and thus does not contribute to the SNIR.

The SNIR from the perspective of the main carrier (C) of beam B_0, if the strongest interferer is decoded first, can be written as

$$CNI_2^5R = \frac{C}{N + \sum_{i=2}^{5} I_i}. \tag{3.3}$$

The SNIR from the perspective of the strongest interferer (I_1) transmitted by beam B_1, if the main carrier is decoded first, is expressed as

$$I_1NI_2^5R = \frac{I_1}{N + \sum_{i=2}^{5} I_i}. \tag{3.4}$$

Note that, which carrier is successfully decoded first, depends on the assigned MODCOD pair for the present interference scenario and C/N by the scheduler and with that on the SNIR.

Based on the interference levels given in Table 3.1 the theoretical performance in terms of SNIR for C and I_1 are examined. Figures 3.1 to 3.4 as well as Figures 3.5 to 3.8 provide the comparison for FR-1 and FR-2, respectively, while keeping FR-4 as a reference for comparison reasons only. There, the performance for the main carrier, denoted with C, describes the SNIR. The performance of the strongest interferer, denoted with I_1, assumes that the main carrier is already perfectly decoded. This analysis was executed for the individual interference scenarios denoted by the significant strongest interferer $C/I*$, where $*$ represents the interference level C/I_1 [dB] of each scenario.

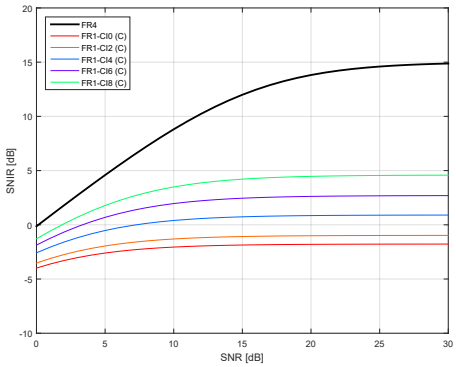

Figure 3.1: FR-1 CNI_1^5R performance

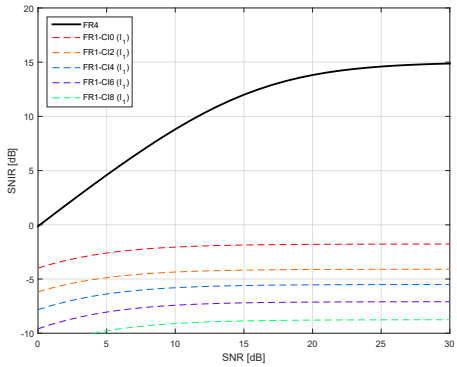

Figure 3.2: FR-1 $I_1NCI_2^5R$ performance

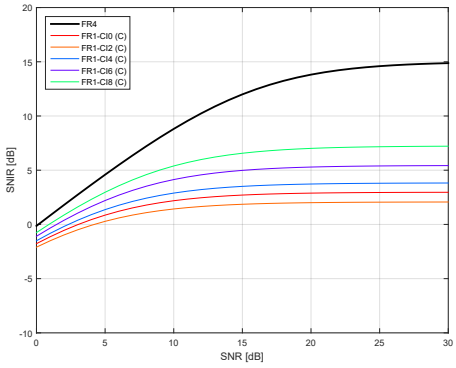

Figure 3.3: FR-1 CNI_2^5R performance

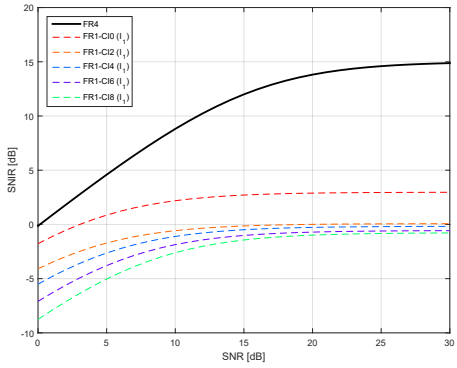

Figure 3.4: FR-1 $I_1NI_2^5R$ performance

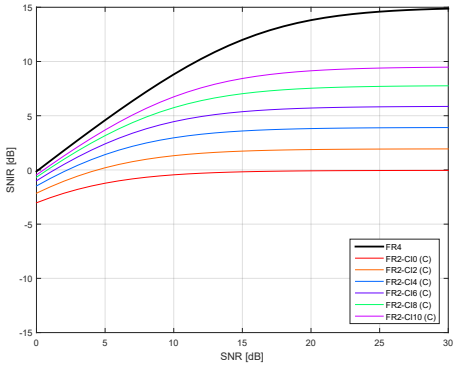

Figure 3.5: FR-2 CNI_1^5R performance

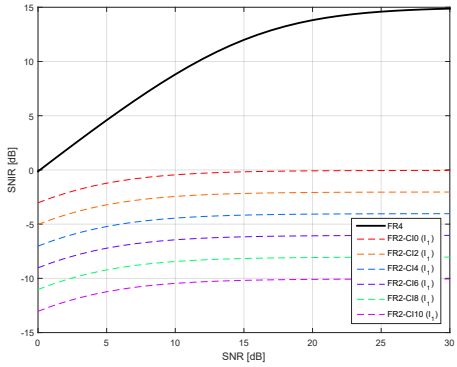

Figure 3.6: FR-2 $I_1NCI_2^5R$ performance

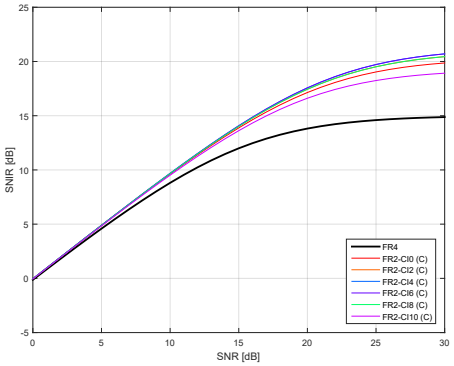

Figure 3.7: FR-2 CNI_2^5R performance

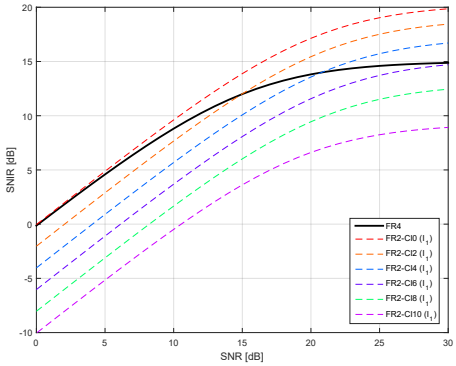

Figure 3.8: FR-2 $I_1NI_2^5R$ performance

On inspection of the FR-1 and FR-2 SNIR analysis the following conclusions of the situation can be drawn. The FR-4 performance is noise limited but becomes clearly interference limited at high C/N values, above 20 dB. Comparing the performance of FR-1 with FR-2, the initial situation is not dissimilar but as expected, the FR-2 performance achieves higher SNIR levels. The major difference becomes obvious, once one of the carriers is successfully removed. Due to the higher C/I levels of the remaining interferers I_2 to I_5 in the FR-2 scenarios, the interference limitation for the detection of the remaining carrier is dramatically improved compared to the situation in FR-1.

Based on this finding it can be concluded that for the application of MUD in a full frequency reuse (FR-1) scenario clearly more than the detection of the dedicated carrier and the strongest interferer is required. Despite the expected performance gain for FR-1 reported by [32], the detection of more than two carriers would unfortunately add significantly more complexity to the detector in the user terminal, a major drawback that was also adressed by [36] and [37], and potentially leads to instabilities in the joint detection process. Based on these facts, it was decided to exclude FR-1 from further analysis of the interference mitigation performance using MUD in the user terminal.

3.3 Frequency Reuse Scenarios

The parameter setting for the analyzed scenarios are provided in this section. The FR-4 scenario configuration, used as benchmark performance, is described in Table 3.2. The FR-2 scenario to be investigated using the application of MUD is given in Table 3.3. Both scenarios assume static user positions on ground and investigate the full range of C/N levels w.r.t. FR-4 at beam center from 0 dB to 30 dB. In general, a single carrier per transponder setup is assumed in any scenarios. In the FR-2 case, the $C/I_1 = 0\ dB$ scenario denotes a user position directly at the cross-over level of the dedicated spot beam to its adjacent beam which equals the assumed -3 dB. The contour loss at $C/I_1 = 2\ dB$ is taken into account with -1 dB.

FR-4 Scenario Reference	
C/I scenario	FR-4 scenario in Table 3.1
Feed setup	single feed per beam
Carrier setup	single carrier per transponder
Beam bandwidth	250 MHz
Number of beams	200
Number of TWTAs	100
Interference mitigation	deactivated
Format	DVB-S2, DVB-S2X

Table 3.2: FR-4 scenario parameter configuration

FR-2 Scenario	
C/I scenario	FR-2 scenarios in Table 3.1
TWTA configuration	single feed per beam
Carrier setup	single carrier per transponder
Beam bandwidth	500 MHz
Number of beams	200
Number of TWTAs	200
Interference mitigation	multi-user detection
Format	DVB-S2, DVB-S2X

Table 3.3: FR-2 scenario parameter configuration

3.4 Realistic Antenna Pattern Interferences

The MUD performance analysis is commonly done on statistically averaged interference levels as in [36], [31], [38] and [9]. This approach is justified since studies of innovative approaches require certain assumption in order to keep the number of variables to a manageable amount. Before a system can be installed and tested, system models are required that approximate reality as close as possible in order to understand the acutal complexity, challenges and limits of a system. In order to achieve that, understanding the influence and effect of individual factors in isolation and in interaction is essential. Hence, the results so far were based on statistically averaged but representative interference scenarios obtained from a realistic spot beam pattern of 200 beams.

The target of this section is now to approximate reality a bit closer and investigate in more detail the discrepancy between the assumed SNIR, respectively C/I_1 levels and those SNIR levels that are present in an actual representative spot beam. The assumed C/I scenarios for this analysis, as introduced in Table 3.1, are statistically

averaged interference scenarios. Thus, this chapter examines actual interference levels within individual spot beams closer to assess if the applied interference scenarios actually represent realistic interference conditions for the user terminal.

Based on this analysis the performance comparison between FR-4 and FR-2 is performed again for the present co-channel interferences at the specific location. In addition to that the assumption regarding the cross-over levels between adjacent beams, which was assumed to be constant at 3 dB is revised. This is a consideration that is likely be violated by a realistic beam pattern due to the elliptical stretching of the spot beams, especially visible at the border of the coverage area, caused by the curvature of the Earth.

In more detail, a realistic multi-spot beam HTS antenna pattern with 200 spot beams for a coverage area of Europe, provided by ESA, is utilized to determine realistic interference levels. The antenna pattern provides the co-polar gain for each spot beam over the whole coverage area of Europe. The spot beam centers in terms of maximum receive power were identified and an ID was assigned to the individual spot beams. To simulate the colouring schemes of interest, colours were assigned to the spot beam IDs for the representation of the 4- and 2-colouring schemes.

In the following a sample 4- and 2-colouring scheme, shown in Figure 3.9 and Figure 3.10 respectively, is applied to this realistic antenna pattern to analyze the interference and SNIR levels within representative spot beams. The coloured contour lines represent the power levels [dBW]. The individual spot beam center in terms of power levels is illustrated by a marker that is coloured according to the applied colouring scheme.

The beam centers at FR-4 are categorized in green, cyan, blue and magenta, whereas the beam centers in the 2-colouring scheme are identified by blue and cyan markers. The FR-2 antenna pattern in Figure 3.10 nicely demonstrates the need for interference mitigation techniques due to the presence of adjacent spot beams operating at the same colour.

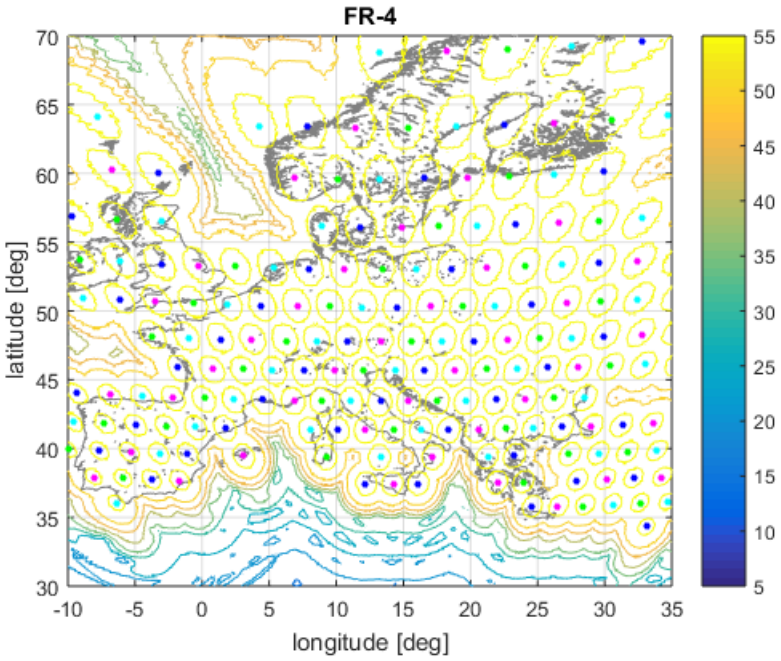

Figure 3.9: FR-4 applied to a realistic spot beam antenna pattern with coloured power levels [dBW] for the coverage area of Europe using [3]

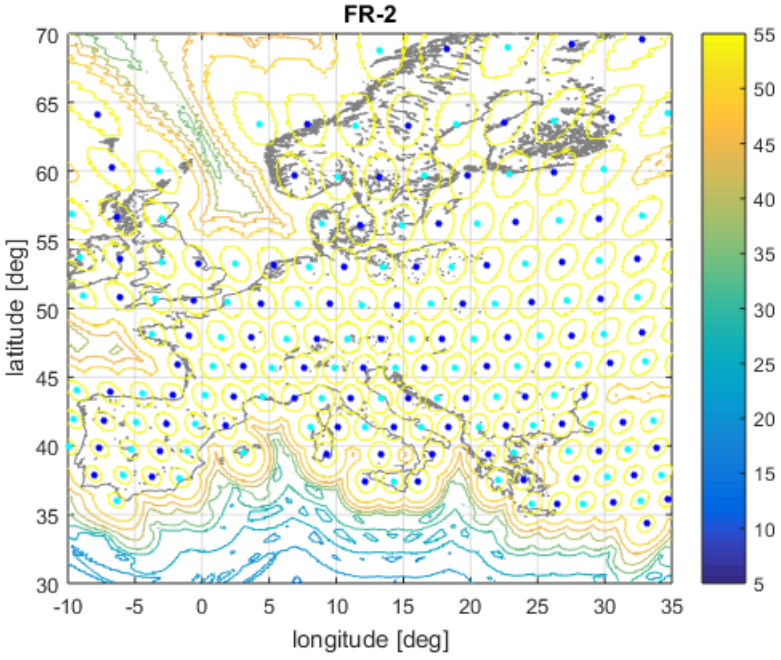

Figure 3.10: FR-2 applied to a realistic spot beam antenna pattern including coloured power levels [dBW] for the coverage area of Europe using [3]

3.5 Realistic Interference Levels

The multi-spot beam antenna pattern for the coverage area of Europe, as assumed in this chapter, is not uniform. The individual spot beam shapes are adapted to demographic and with that to traffic demands. Paired with the curvature of the Earth this leads to the effect that especially beams that are located on the edge of the coverage area are more distorted to an elliptical shape than beams in the center of the coverage area which can be approximated by a rather circular shape.

Taking this situation into account, the analysis of this chapter is based on two sample beams, one representing the situation at the coverage center and the other demonstrating the situation in a more elliptical spot beam, located at the border of the coverage area.

The interference levels C/I [dB] at FR-2 are provided from the view point of the main carrier C/I_1^5 in (3.5) and the strongest interferer I_1/I_2^5 in (3.6):

$$C/I_1^5 = \frac{C}{\sum_{i=1}^{5} I_i} \tag{3.5}$$

$$I_1/I_2^5 = \frac{I_1}{C + \sum_{i=2}^{5} I_i} \tag{3.6}$$

3.5.1 Center of Coverage Area

The beams at the center of the coverage area show that the interference levels are approximately symmetric. In order to provide the complete picture the half power beam width level at -3 dB, selected as cross-over level, is illustrated by the red circle, while the beam center in terms of receive power is indicated by the small circle in magenta.

Interference levels in terms of C/I_1^5 in a realistic spot beam at the center of the antenna pattern are shown in Figure 3.11 for the FR-4 case and in Figure 3.12 for the FR-2 case. The I_1/I_2^5 scenario, representing the perspective of the strongest interferer for FR-2 is illustrated in Figure 3.13.

The FR-4 results confirm a rather constant interference and significantly higher C/I_1^5 ratio within the spot beam due to the wider distances of co-channel beams, while the FR-2 case shows, as expected, various interference scenarios C/I_1^5 that are characterized by the strongest interferer I_1. The I_1/I_2^5 levels represent the contrasting picture from the perspective of the strongest interferer. Similar interference levels can be observed while the interferer experiences even slightly higher ratios.

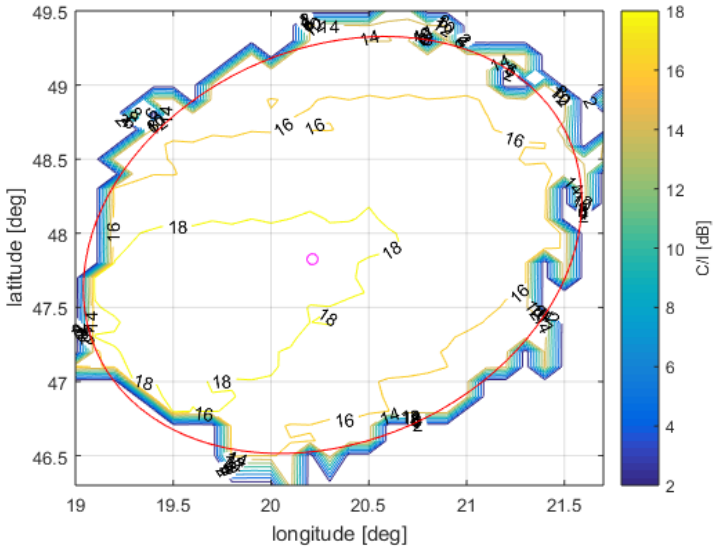

Figure 3.11: C/I_1^5 levels of a representative spot beam in the center of the coverage area with FR-4

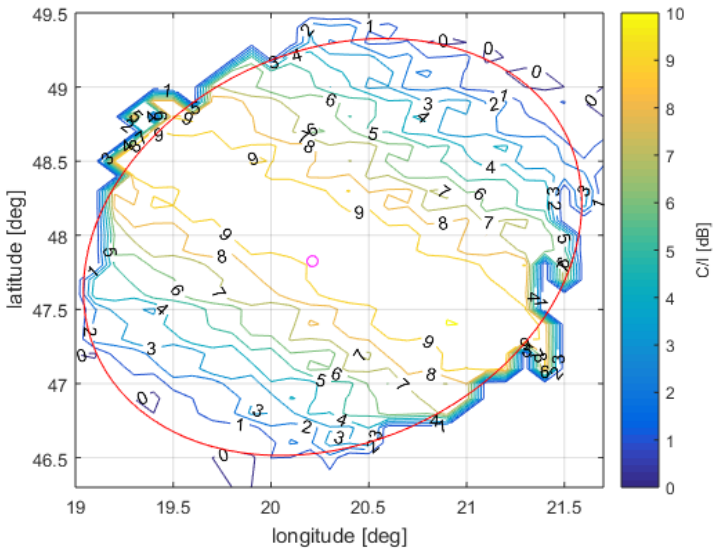

Figure 3.12: C/I_1^5 levels of a representative spot beam in the center of the coverage area with FR-2

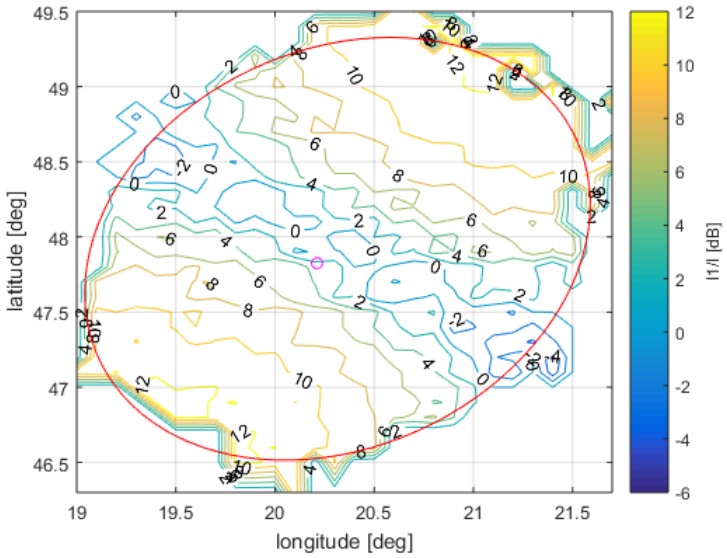

Figure 3.13: I_1/I_2^5 levels of a representative spot beam in the center of the coverage area with FR-2

3.5.2 Border of Coverage Area

In this section the interference in a spot beam located at the border of the coverage area of a realistic antenna pattern is investigated. The C/I_1^5 scenario at FR-4 is shown in Figure 3.14, while Figure 3.15 represents the situation considering a 2-colouring scheme.

To complete the picture, Figure 3.16 provides the I_1/I_2^5 levels for the FR-2 case from the perspective of the strongest interferer. In contrast to the beam located at the center of the coverage area, as shown before, this beam is heavily distorted. This effect causes the presence of even negative C/I_1^5 ratios. However, these regions are located far beyond the assumed cross-over level of 3 dB and are therefore not relevant.

It is notable that the obtained C/I levels for the beam at the border are higher than those obtained for the beam located in the center of the coverage area.

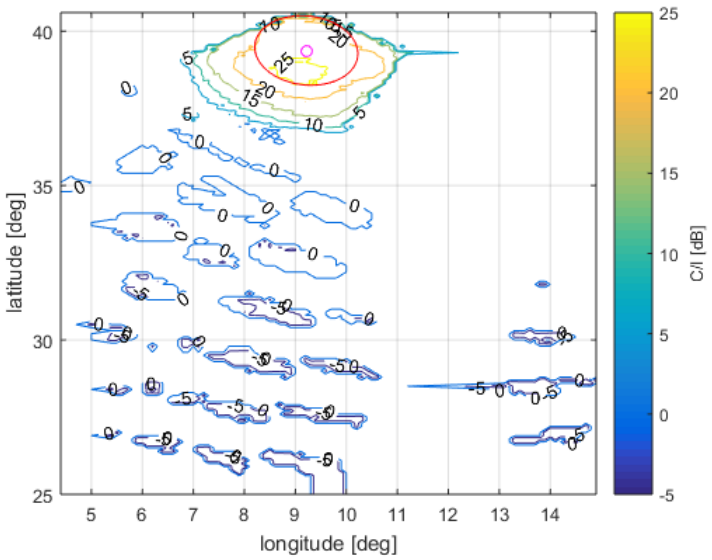

Figure 3.14: C/I_1^5 levels of a representative spot beam at the border of the coverage area with FR-4

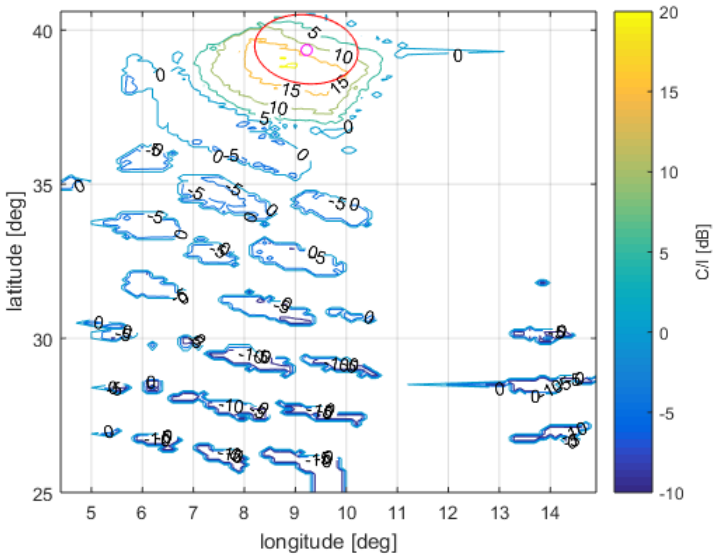

Figure 3.15: C/I_1^5 levels of a representative spot beam at the border of the coverage area with FR-2

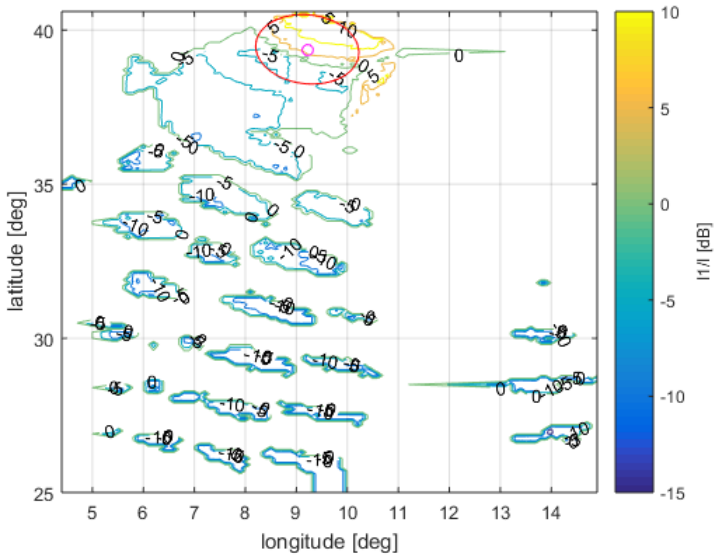

Figure 3.16: I_1/I_2^5 levels of a representative spot beam at the border of the coverage area with FR-2

3.6 SNIR Level Analysis

The analysis of the achievable performance at different C/I distributions is an extensive process since the spectral efficiency levels of all MODCOD pairs would need to be investigated for every C/I distribution scenario considering all interferers in the system. For this reason, the generalization by focusing only on the C/I_1 of the strongest and with that representative interferer was a reasonable step for the analysis in the previous chapter. Fortunately, the SNIR levels can as well be utilized to predict the expected performance achievable by MUD.

Regarding MUD, in general it can be stated that the SNIR must be sufficiently high in order that both carriers reach the SC QEF performance. Nevertheless, there are MODCOD pairs where this requirement can be violated because due to the contribution of the interferer that modifies the QEF performance. The examples shown in the following demonstrate the SNIR levels from different perspectives at C/N = 20 dB.

The comparison with realistic interference levels is done again based on the SNIR that is relevant for the MUD detector at the receiver. The SNIR examples in the following are provided from the perspective of the main carrier (3.1) and the perspective of the strongest interferer (3.4), once the main carrier is removed.

Again, two single spot beams, different from the chapter before, were selected as example to represent the situation in the center and the border of the antenna pattern to analyze the present SNIR levels. Since the MUD performance at FR-2 is compared to the traditional FR-4 performance as reference the SNIR at FR-4 is provided as well.

The results for the central beam including the FR-4 SNIR performance and the FR-2 performance in the center and border are shown in Figure 3.17, Figure 3.18 and Figure 3.19 respectively. Whereas, the corresponding results determined from a spot beam at the border of the coverage area are shown in Figure 3.20, Figure 3.21 and Figure 3.22.

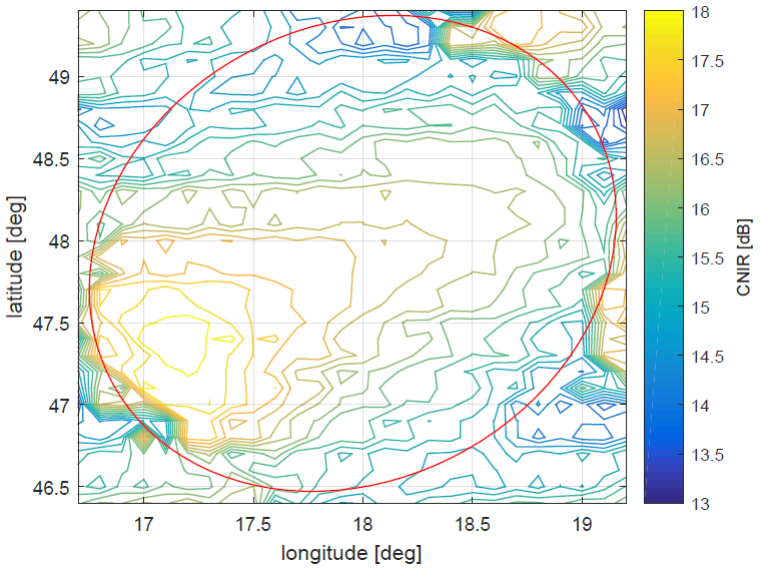

Figure 3.17: FR-4 SNIR at C/N = 20 dB, center beam

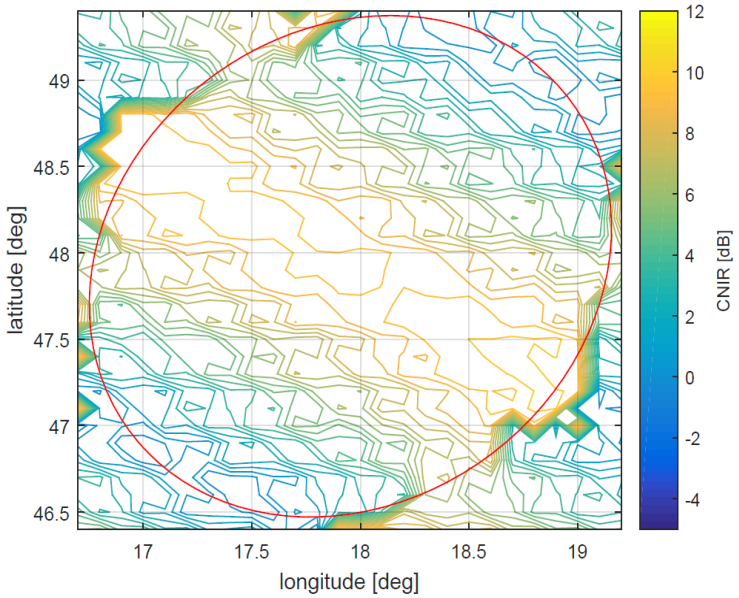

Figure 3.18: FR-2 CNI_1^5R at C/N = 20 dB, center beam

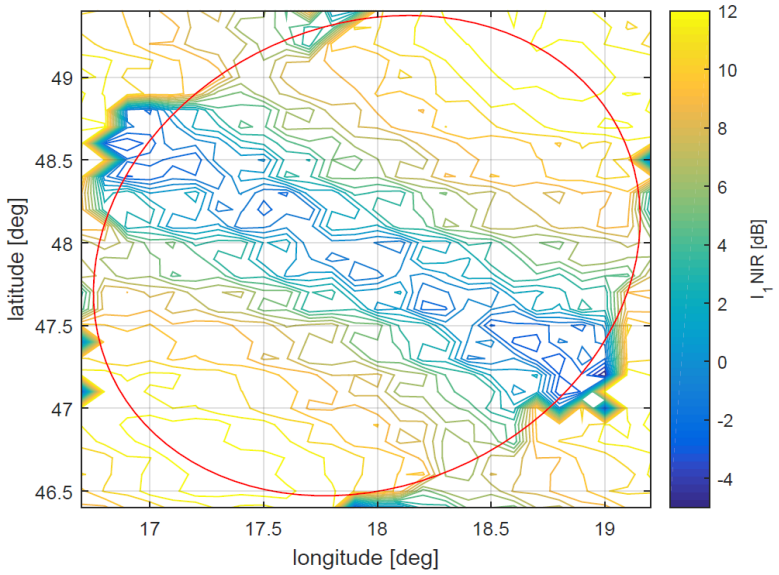

Figure 3.19: FR-2 $I_1 N I_2^5 R$ at C/N = 20 dB, center beam

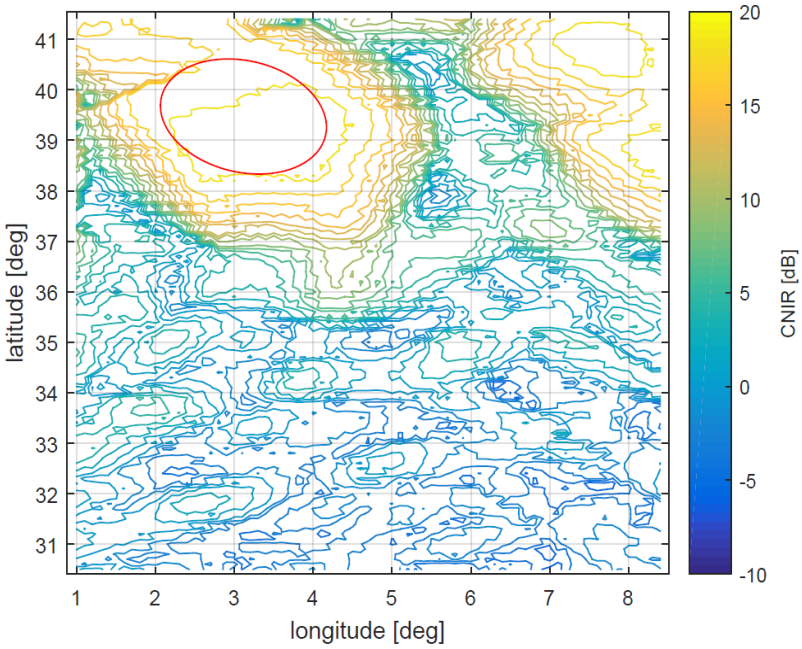

Figure 3.20: FR-4 SNIR at C/N = 20 dB, border beam

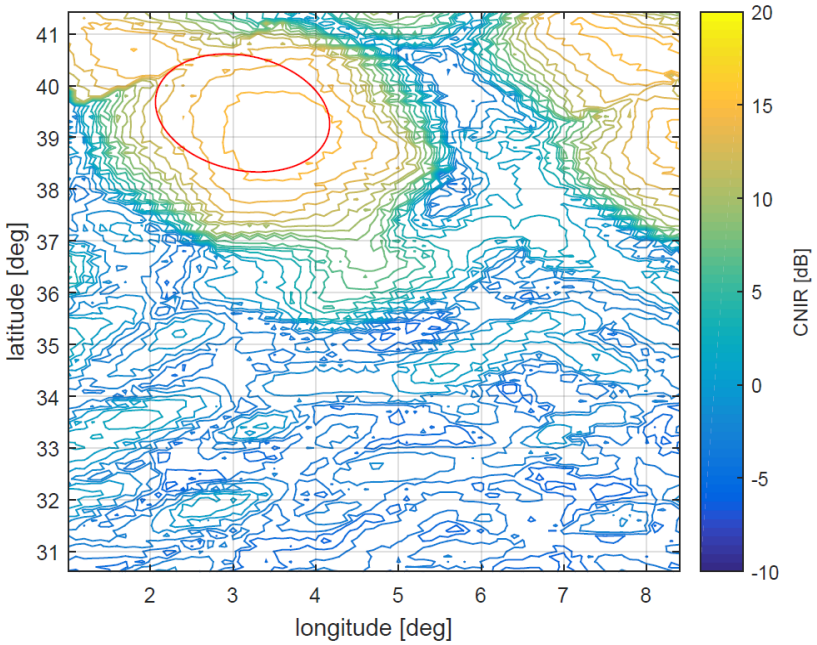

Figure 3.21: FR-2 CNI_1^5R at C/N = 20 dB, border beam

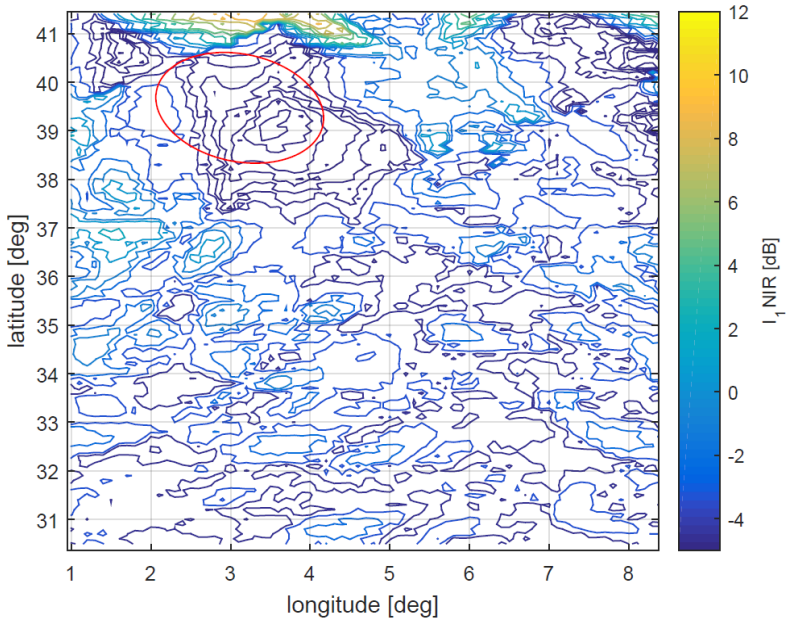

Figure 3.22: FR-2 $I_1NI_2^5R$ at C/N = 20 dB, border beam

By inspection of the two representative spot beams, substantial differences in the SNIR and INIR levels can be determined between the averaged scenarios, in Figures 3.5 and 3.8, and the realistic conditions. It can be observed that those regions, where the CNI_1^5R is quite high and the $I_1NI_2^5R$ very low, in the order of 0 dB, are not covered by the averaged discrete scenarios in Table 3.1. Positions with vice

versa CNI_1^5R and $I_1NI_2^5R$ levels and balanced settings are in contrast well covered by the averaged scenarios. The $I_1NI_2^5R$ for low SNIR around zero is also rather overestimated by the given scenarios, indicating that perhaps more interfering beams need to be considered. A similar behaviour was observed at other C/N levels and spot beams.

Achievable CNI_1^5R and $I_1NI_2^5R$ levels and the present C/N are the parameters that affect the MODCOD selection by the scheduler in a HTS system that is operated with MUD. The beauty of a geostationary (GEO) system, compared to a low Earth orbit, is the mostly static interference pattern. Based on this fact, that the main variation in the system is in the C/N that is influenced by the system impairments and the propagation channel. Assuming a realistic HTS system where adaptive coding and modulation (ACM) is applied, the scheduler requires a performance table for all possible C/N and SNIR scenarios to select the appropriate MODCOD pair for both beams.

For the performances in terms of capacity and throughput, the realistic interference conditions have to be analyzed in detail and MUD performances have to be identified for those scenarios considering also system impairments used as input for the scheduler.

It was determined that the averaged and realistic co-channel interference in the beams indeed varies by the order of some dB, which was expected. The MUD performance can be derived from the SNIR levels of both the main carriers. This comparison revealed that the statistically averaged interference scenarios do cover the observed cases but sometimes underestimate the obtained SNIR levels from the realistic pattern.

These findings however, support the theory that the MUD performance analysis has to be conducted based on each individual HTS antenna pattern in order to provide mapping tables for the scheduler to achieve the best possible throughput by optimum MODCOD pair assignment under the present conditions.

3.7 Payload Hardware Requirements

This section represents a short excurse on the payload hardware requirements. In order to analyze the payload hardware setup for the individual colouring scheme [30], the relation between the colouring scheme and the number of required TWTAs is illustrated in Figure 3.23. An overall transponder bandwidth of 500 MHz per TWTA is assumed. To illustrate how an aggressive frequency reuse affects the hardware setting on board of a satellite, FR-1 is listed here for completeness, but will not be covered by any performance analysis in the following.

In case of FR-4, 1 TWTA can serve 2 beams with a beam bandwidth of 250 MHz. FR-2 requires 1 TWTA per beam with a beam bandwidth of 500 MHz and FR-1 requires 2 TWTAs in order to serve a single beam with a beam bandwidth of 1 GHz.

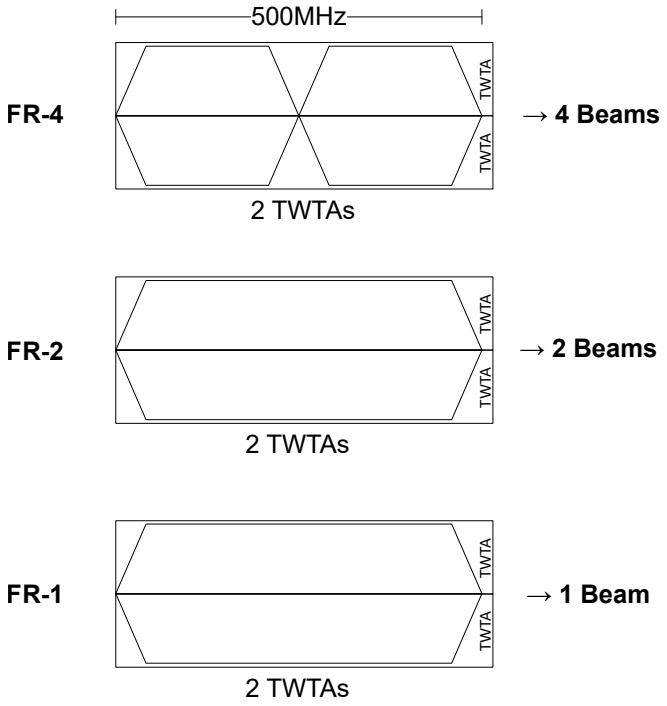

Figure 3.23: Colouring specific number of required TWTAs per number of beams

Considering a fixed amount of spot beams to completely cover the area of Europe, FR-1 would require 200 TWTAs, FR-2 100 TWTAs and FR-4 50 TWTAs on board of a satellite. An aggressive frequency reuse thus not only introduces additional interferences into the system but also has a significant effect on the payload mass [24]. However, the payload mass requirement becomes less critical since technologies to reduce the payload mass are available. Digital beam forming using phased antenna arrays [39], for instance, would be one option that could solve this issue.

3.8 Interference Pattern Stability on Ground

GEO satellites are considered as fixed satellite services since their orbit follows the cycle of a sidereal day. Due to this fact, the satellite seems to stay at the same point in the sky from the perspective on the surface of Earth. As explained by the ITU Recommendation ITU-R S.484 [16] this fixed position can be achieved when the following conditions are fulfilled by the satellite orbit:

- Semi-major axis: 42 165 km
- Eccentricity: e = 0
- Inclination = 0 deg

This ideal state however, cannot be preserved by the artificial satellite in space since perturbation forces are present and act on the satellite. The fact that the Earth is not a perfect sphere, the existing Earth's gravitational field, the solar radiation pressure and the present gravity of Sun and Moon are forces acting constantly on the satellite and thus influence its orbit. As regulated in the ITU Recommendation [16] the satellite must maintain its assigned position within ± 0.1 *deg* to avoid collisions. This calls for station keeping maneuvers in order to correct the position when the present drift gets close to this limit. In some cases, for instance, experimental missions, this limit is even restricted to ± 0.05 *deg*. Station keeping maneuvers are executed with onboard thrusters to ensure proper position in longitude and latitude within the assigned rectangular position box, called "deadband" in space [40]. Towards the end of the lifetime, this maneuver becomes more difficult due to hardware degradation and expiring fuel.

Having studied the interference conditions in a realistic antenna pattern at the beginning of this section, the main question arises, if these drifts in the orbital position affect the interference scenarios for the user terminals on ground since up to now the interference pattern was assumed to be static. Potential shifts of the pattern on ground could lead to the fact that users will face varying interference levels and perhaps get assigned to beams of a different colour during the course of a day which would demand additional intelligence in the scheduler.

The following considerations assume that the antenna beam pattern is fixed on the satellite and the satellite drift is not compensated in order to keep the pattern stable on ground, hence representing the worst case scenario. Assuming a fixed antenna pattern, the pattern and interference relations do not change within the pattern as such but with respect to a fixed position on the surface on Earth. As reported in the ITU Recommendation [16] and summarized in Table 3.4, the drift process is a quite slow but steady process and its rate depends on the actual satellite position in orbit.

For this reason a station keeping maneuver might be required at intervals of several months up to a year, indicating a rather slow change of the situation for the receiver on ground followed by a sudden change as a result of a maneuver.

To optimize the performance of the scheduler, regular updates of the interference map and re-evaluation of the user-to-beam assignment are required to assure correct information of the current colour and interference level. A regular update of the user terminal interference map on ground might be required for the scheduler.

According to the maximum drift range of ± 0.1 *deg* in longitude, shown in Figure 3.24, an antenna pattern movement on the surface of Earth can be observed, assuming no compensation measures by the satellite operator. Considering these assumptions, a worst-case scenario is estimated in the following, which implies that the actual movement has to be determined for the individual mission design.

Cause	Effect	Drift rate [deg/time]
Distortions of Earth's gravitational field due to the non-spherical shape	Semi-major axis deviation of the synchronous radius by a distance of $\Delta a\,[km]$	$-0.013\Delta a$ degrees per day
Solar radiation pressure and a small contribution from the gravitation of the Moon	A present eccentricity e causes a diurnal liberation motion in longitude	$\pm 2e + \frac{180}{\pi}$ degrees per day
Tidal force due to the gravity of Sun and Moon	The presence of an inclination i $[deg]$ induces a half-diurnal liberation motion; These inclination rate changes vary between 0.75 and 0.95 deg per year	$\pm\left(\frac{i^2}{4}\right)\cdot\left(\frac{180}{\pi}\right)$ degrees

Table 3.4: Description of cause and rate of potential drifts [16]

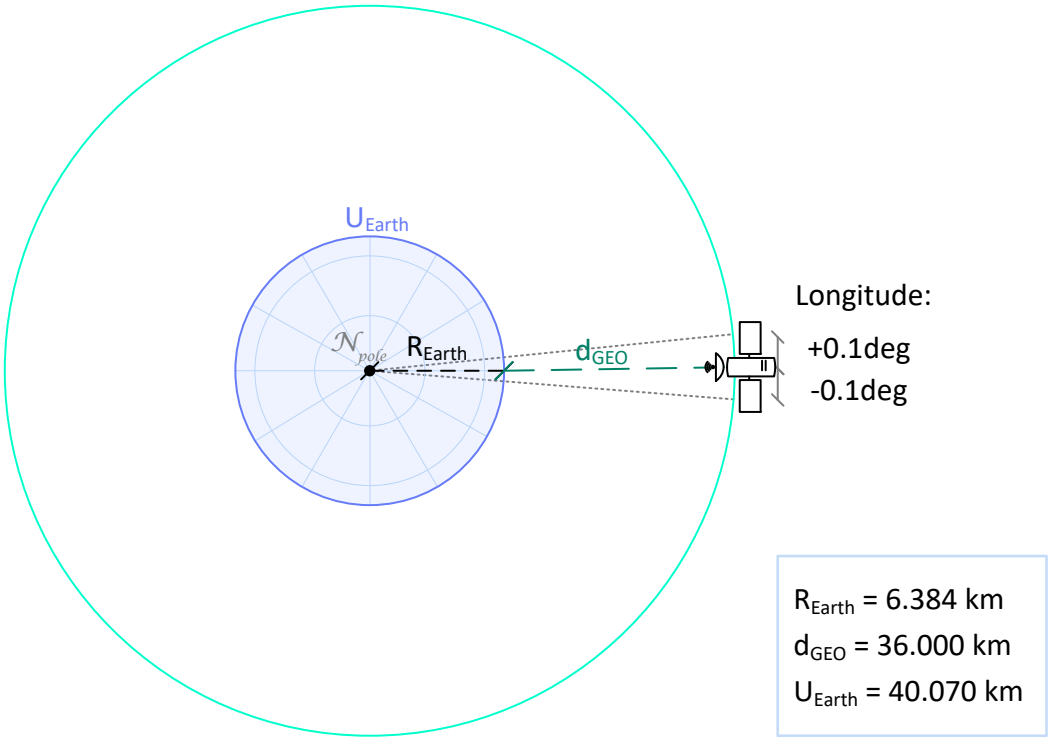

Figure 3.24: Effect of the maximum allowed satellite movement in longitude (Earth from top view, north pole)

$$\begin{aligned} 1\ deg \quad latitude &= \frac{U_{Earth}}{180} = 222.61\ km \\ 0.1\ deg \quad latitude &= 22.26\ km \end{aligned} \tag{3.7}$$

$$\begin{aligned} 1\ deg \quad longitude &= \frac{U_{Earth}}{360} = 111.31\ km \\ 0.1\ deg \quad longitude &= 11.13\ km \end{aligned} \tag{3.8}$$

Taking the orbital movement of KA-SAT, a multi-spot beam satellite operated by Eutelsat that services a coverage area of Europe, as a sample the two line elements (TLE) that describe the satellite position and predict the position in the near future of an approx. 24 h track describe the following motion, shown in Figure 3.25. The long-term motion is shown in Figure 3.26 covering the satellite motion of approximately one week for comparison.

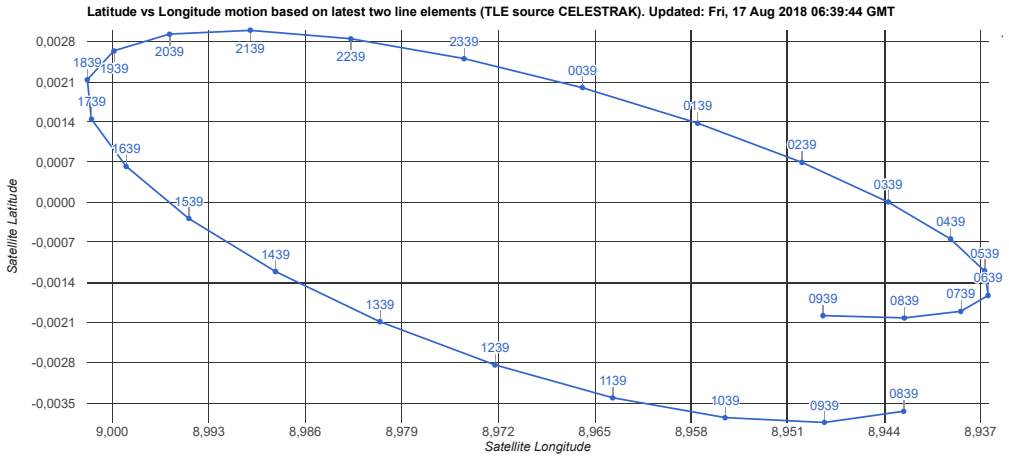

Figure 3.25: Sample orbital movement in latitude and longitude over approx. 24 h of KA-SAT operated by Eutelsat [4]

The worst-case 24h and 1h antenna pattern movement in (3.9) and (3.10) can be derived from the longitudinal motion of KA-SAT in Figure 3.25.

$$24\ h \ \rightarrow \sim 0.063\ deg \ \ longitude \ = \ 7.0123\ km \tag{3.9}$$

$$1\ h \quad \rightarrow \sim 0.014\ deg \ \ longitude \ = \ 1.5583\ km/h \ = \ 0.4\ m/s \tag{3.10}$$

The motion in latitude is comparable to the motion in longitude negligible, but is listed for sake of completeness in (3.11) and (3.12).

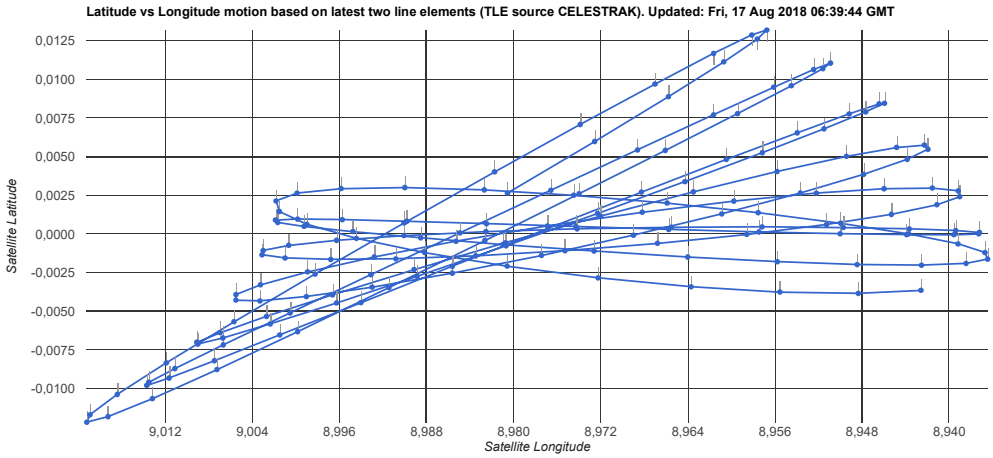

Figure 3.26: Long-term orbital movement of KA-SAT in latitude and longitude [4]

$$24\ h\ \rightarrow \sim 0.0063\ deg\ \ latitude\ =\ 1.4\ km \tag{3.11}$$

$$1\ h\ \ \rightarrow \sim 0.00026\ deg\ \ latitude\ =\ 57.9\ m/h\ =\ 0.016\ m/s \tag{3.12}$$

While HTS systems are most probably equipped with the required technology to stabilize the beam pattern and compensate the satellite's motion, a residual error is nevertheless expected. The example of KA-SAT assumes the worst case scenario with the maximum, uncompensated satellite drift regulated by the ITU.

Despite the worst case scenario is unlikely to happen, since satellite operators are well aware of the interference problematic in HTS systems, the residual error might be still be affecting the antenna pattern drift in a way that could affect and with that degrade the mitigation performance. For this reason, a channel state information (CSI) [41] feedback by the user terminal providing the updated interference situation at its location would be required by the scheduler to ensure accurate interference mitigation.
Detailed research on the actual pattern drift and compensation accuracy of a HTS mission would be of interest for the implementation of an efficient interference mitigation method.

The need for a return channel due to satellite motion was examined in this section and updated interference levels deemed as valid information for an optimized scheduling performance. Despite the relevance of a return channel in the system, a stable situation with ideal return channel is considered in the following by the system demonstrator in order to keep the scenario complexity to a moderate level.

CHAPTER 4

System Model

For the application of MUD in the user downlink, the AWGN channel is considered. The channel capacity together with the signal-to-noise plus interference ratio (SNIR) are important performance measures in this context. This chapter gives an overview on the system model for MUD and summarizes the theoretically achievable rate regions for the different scenarios. In addition to that, it discusses the computation of log-likelihood ratios, since MUD operates on soft bits, and shortly introduces the bit-to-symbol mapping.

4.1 AWGN Channel

In a single carrier setup consisting of one transmitter and one receiver with an AWGN channel, the symbol r received by the user terminal is defined as

$$r_n = c_n + w, \tag{4.1}$$

where c_n is the n-th transmitted symbol by the carrier and w represents the noise from the AWGN channel. In an interfered system, the N interfering carriers i_k are added linearly, resulting in the received symbol

$$r_n = c_n + \sum_{k=1}^{N} i_{k,n} + w. \tag{4.2}$$

The general definition of the AWGN variable y [42] with mean x and variance σ^2 is defined as

$$P(y) = \frac{1}{\sqrt{2\pi\sigma^2}} \exp\left(-\frac{(y-x)^2}{2\sigma^2}\right). \tag{4.3}$$

This indicates that the AWGN adds a scalar noise from a normal distribution with zero mean and variance $\sigma^2 = \frac{N_0}{2}$, where N_0 denotes the noise spectral density, resulting in the random variable y at the output.

4.2 AWGN Channel Capacity

As elaborated in [42] the capacity C of the AWGN channel is a crucial performance indicator. According to Shannon's noisy channel theorem, C denotes the maximum achievable rate on a channel with an arbitrarily small bit error probability. This theorem hence implies that reliable communication is only possible with rates lower than C.

The capacity C is a function of the bandwidth B and the signal-to-noise ratio (SNR) expressed as

$$C = B \cdot \log\left(1 + SNR\right), \tag{4.4}$$

where the noise N is defined as $N = N_0 B$.

4.3 Modulation Schemes

The transmitted symbols by the main carrier or the interferers represent a modulated bit stream. The DVB-S2(X) modulations considered in this work are QPSK, 8PSK, 16APSK and 32APSK. Their constellation diagrams are shown in Figures 4.1, 4.2, 4.3 and 4.4, respectively.

These modulations, as listed in the DVB-S2 and DVB-S2X ETSI standard in [5] and [2], use Gray coding.

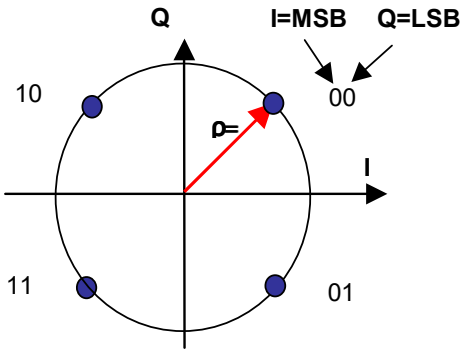

Figure 4.1: QPSK constellation diagram [5]

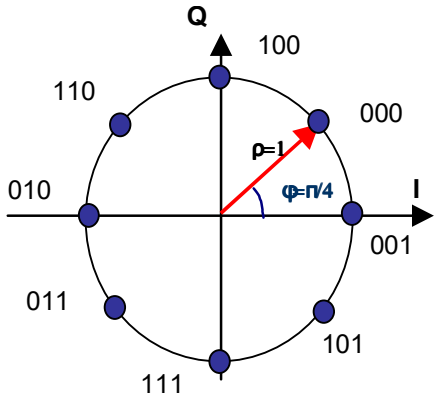

Figure 4.2: 8PSK constellation diagram [5]

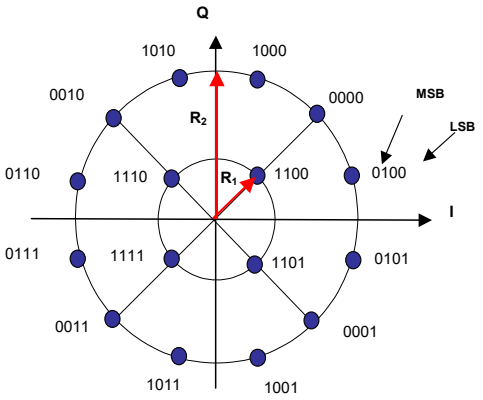

Figure 4.3: 16APSK constellation diagram [5]

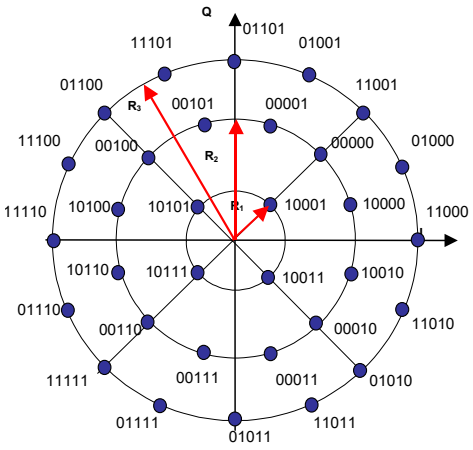

Figure 4.4: 32APSK constellation diagram [5]

4.4 Combined Constellation Diagram

The user terminal on ground receives a linear combination of the dedicated carrier and all interferers plus the AWGN added on the channel. A sample of the combined constellation diagram with QPSK in the main carrier and 8PSK in the strongest interfering carrier is shown in Figures 4.5 to 4.8 including the combined constellation after amplitude and phase correction. The figure illustrates a scenario where the signal strength of the main carrier is stronger than the signal strength of the interfering carrier. The rotation is corrected by the synchronization and parameter estimation implemented in the receiver. The effect of further interferers in the system on the combined constellation diagram shown in this example would depend on the present C/N value. If the system is noise limited at low C/N values, the effect of additional weak interferers is minor compared to a high C/N scenario.

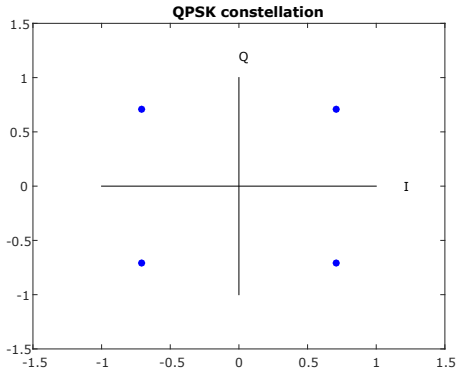

Figure 4.5: QPSK constellation diagram [5] of the main carrier

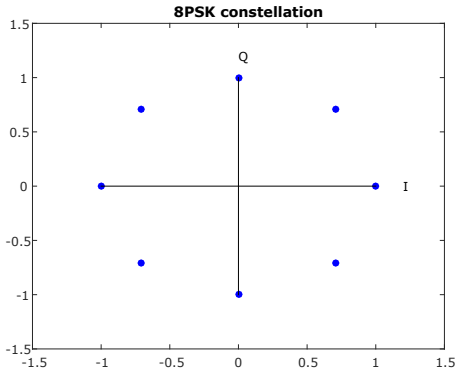

Figure 4.6: 8PSK constellation diagram [5] of the strongest interferer

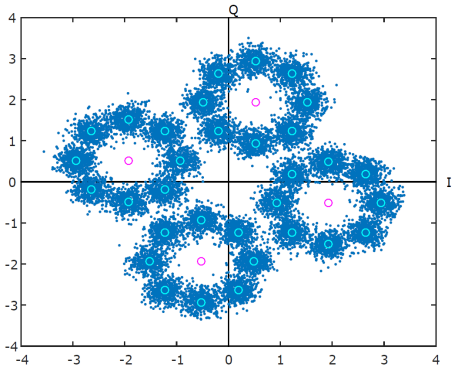

Figure 4.7: Combined constellation diagram arriving at the user terminal

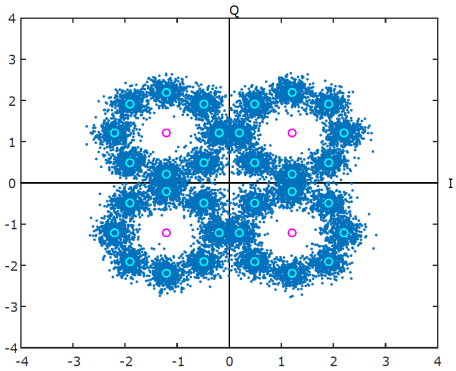

Figure 4.8: Combined constellation diagram after amplitude and phase correction in the receiver

4.5 Hard and Soft Decisions

A single information bit is able to represent two different states of information, which are denoted as 0 and 1. When operating a detector and decoder however, the information bit can either be processed as so-called "hard decision", meaning that a single bit is represented either by 0 or 1, or alternatively, as real valued scalar, which is then denoted as "soft decision" [43], [44]. The hard bit decision method determines the most likely state depending for example on the Euclidean distance of a received symbol (decision regions) of a value and sets the bit either to 0 or 1.

The idea of the soft bit decision method is to preserve the available information. Soft bits are real numbers indicating a tendency, if the bit is rather in the state 0 or the state 1. With soft bits, information is treated more sensitively, allowing a received symbol close to the decision edge to be treated with more uncertainty than at received symbol that was received with a significant distance to the decision border. In an iterative system, where information is gained with each iteration cycle, soft bits can be modified and the information can be preserved and improved. Hard decisions, on the other hand, do not provide any information about the certainty of the decision. For this reason, soft decisions are selected for the information exchange between the detector and the decoder in this work.

4.6 Log-likelihood Ratio

The applied joint MUD approach exchanges soft bit information between the detector and decoder in form of log-likelihood ratios (LLRs). Following the definition in [44] the log-likelihood ratio of a binary random variable b with the elements $\{+1, -1\}$ is defined as in (4.5), where -1 represents the binary state 0 and +1 represents the binary state 1:

$$LLR\,(b) = \log \frac{P\,(b=+1)}{P\,(b=-1)}. \tag{4.5}$$

This log-likelihood ratio is also denoted as so-called "soft" information since it contains the probabilities and expresses thus also the reliability of a decision that is based on the sign of $LLR(b)$. The situation changes once the random variable b is conditioned on another random variable or vector r. In this case the conditioned log-likelihood ratio is written as

$$LLR\,(b|r) = \log \frac{P\,(b=+1|r)}{P\,(b=-1|r)}, \tag{4.6}$$

where, considering the application of MUD, the parameter r denotes the input at the detector.

Since the probability $P(b)$ cancels out as explained by [44], it can be stated that the joint log-likelihood $LLR(b,r)$ equals the conditioned log-likelihood $LLR(b|r)$.

4.7 Multiple Access Channel (MAC)

The concept of MUD generally describes a situation, where that information is sent via more than one transmitter to several receivers. As a first approach, this setup can be described by the multiple-input single-output (MISO) channel [45]. The general MISO setup is illustrated in Figure 4.9.

In this Figure the MISO broadcast channel has two transmitters that transmit the same information s to a single antenna that receives both transmitted signals as y_0 and y_1.

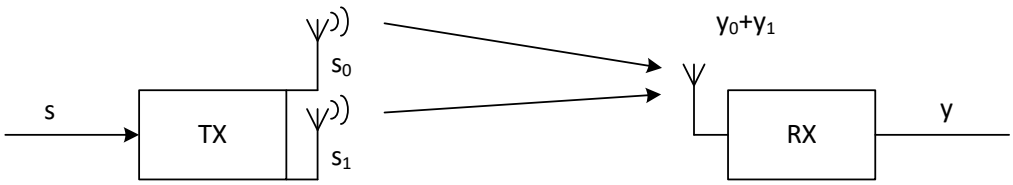

Figure 4.9: Multiple-Input Single-Output (MISO) broadcast channel

This concept however suggests that all transmitters send the same information to all receiver stations at the same time. Due to this fact the following two constraints need to be applied to the MISO broadcast system in order to approximate a satellite forward link more accurately:

- transmitted signals are statistically independent
- service is limited to a single user terminal per time slot

A system that obeys both listed criteria then basically describes the concept of a multiple access channel (MAC) channel [46]. The general setup of the broadcast channel is shown in Figure 4.10.

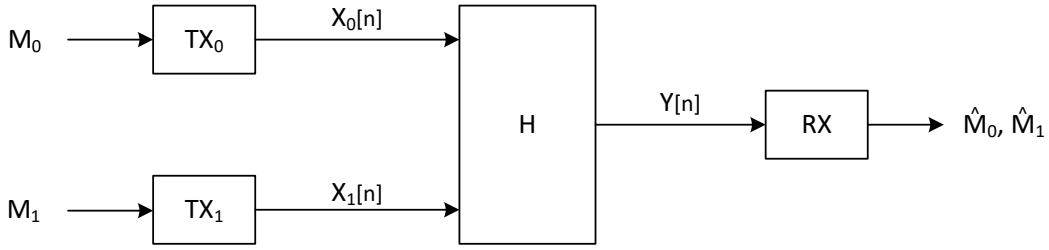

Figure 4.10: Multiple access channel (MAC)

In the example of the MAC channel two independent messages M_0 and M_1 are transmitted via a common channel H. A single unit receives both transmitted messages during its dedicated time slot as $\hat{M}_0$ and $\hat{M}_1$.

This model now represents the actual situation in a satellite forward link, where two transponders simultaneously send information to a common MUD enabled receiver on ground. For this reason this setting is denoted as MAC-MUD in the following.

Applying the general MUD concept to the satellite forward link results in the following situation. The information stream s intended for transmission to UT_0 is divided in two substreams s_0 and s_1 that are independently but simultaneously transmitted by two transponders, representing the main carrier and the strongest interferer from the perspective of UT_0. The two substreams arrive as linear combination $r = y_0 + y_1$ together with additional co-channel interference I and additive white Gaussian noise w at the terminal and are jointly detected as well as decoded by two distinct decoders that are integrated in the receiver. Once both substreams are successfully decoded, they are recombined to a common stream $s = s_0 + s_1$ at the receiver to obtain the full information of the actually transmitted stream s, as illustrated in Figure 4.11.

Since the acronym MAC is commonly used in different contexts, the contexts are discussed shortly in the following in order to clarify the situation. MAC can be the acronym for media access control. In the context of the Open System Interconnection (OSI) Model in Figure 4.12, MAC is a sublayer of the *L2 – Data Link Layer* and is concerned with the access control to the data in the physical layer as well as integrity checks of the sender etc. to list only a few tasks. This study in contrast however, concentrates on the data flow on the physical layer exclusively. The *Physical Layer* (Layer 1) focuses on the transmission of physical signals and thus aims to operate on data bits and grouping data bits to symbols for transmission.

Another meaning of the acronym MAC is, as already mentioned before, the "multiple access channel". In this context, MAC denotes a setup where two or more transmitters communicate over a common channel with a single receiver. The latter MAC concept of multiple access will be utilized for further MUD information theoretical analysis.

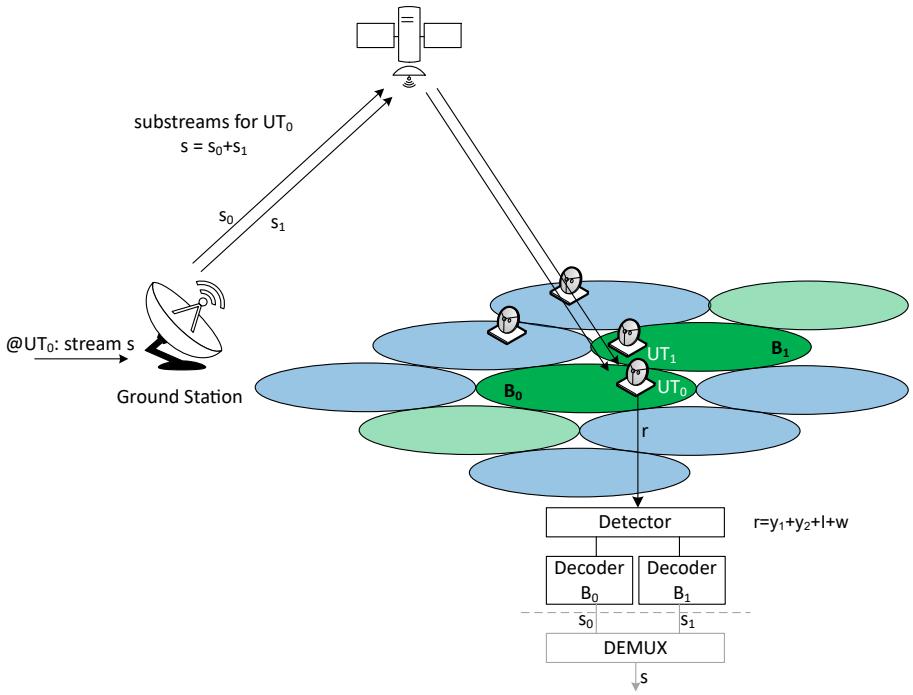

Figure 4.11: The MAC concept in the forward link of a multi-beam satellite system

OSI Model		
Layer	Name	Information
L7	Application	data
L6	Presentation	data
L5	Session	data
L4	Transport	segments
L3	Network	packets
L2	Data Link	frames
L1	Physical	bits

Figure 4.12: 7-Layer OSI model

4.8 Information Flow

The simplest way of data transmission, here denoted as information flow, is from a single transmitter (TX) to a single receiver (RX). Assuming a more complex setup with multiple TX and several advanced RX, different kinds of information flows can be installed.

Figure 4.13 and Figure 4.14 illustrate the information flows considered in this work which are listed below and described in more detail in the following.

- **Single beam per user**
  Data is transmitted to a single user via a single beam for 100% of the time.
- **Multiple beams per user**
  Data is transmitted to a single user via two beams for 50% of the time.

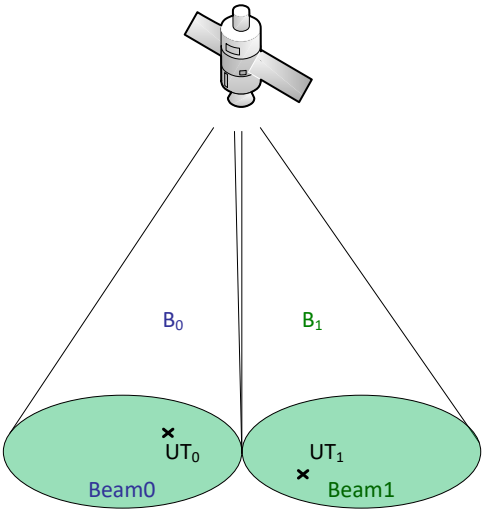

Figure 4.13: Single beam per user, single carrier transmission 100% of the assigned time slot

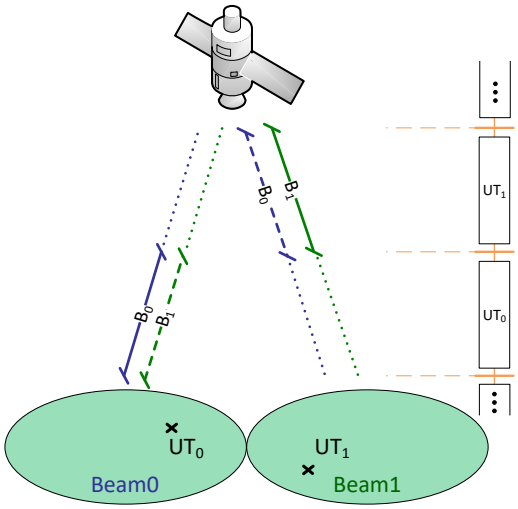

Figure 4.14: Multiple beams per user, transmission using two carriers (borrowing the strongest interferer) for 50% of the assigned time slot

4.8.1 Single Beam Per User Terminal

It is assumed that each user terminal on ground is assigned to the individual spot beam that is received with the strongest power on ground. This method implies that the user terminal is serviced only by the dedicated beam, denoted as main carrier. Usually, this mode is applied in traditional FR-4 schemes, where interference is at a moderate level and therefore does not require interference mitigation methods.

Nevertheless, accepting the losses due to higher interference levels, this information flow would of course also be feasible for more aggressive frequency reuse schemes.

4.8.2 Multiple Beams Per User Terminal

A multi-beam per user information flow describes the scenario where the user terminal is not only served by the dedicated beam but also by a second beam, ideally the strongest interferer, that is operated at the same colour.

This information flow is applicable for receivers on ground that are equipped with MUD, which allows them to actually profit from higher interference levels in the system. FR-2 systems, as investigated in the course of this work, would be suitable for this information flow.

4.9 Reception Modes at the Receiver

Assuming a MUD enabled user terminal on ground, different potential RX modes are feasible. This section lists and illustrates the set of RX modes categorized according to their required information flow.

4.9.1 Reception Modes for Single Beam Per User

This section introduces two reception modes applicable in a single carrier per user transmission scenario.

Interference as Noise (IAN)

Following the example of a FR-4 system that treats the present interferers as noise, this is theoretically also an option in a two-colouring scheme. The simple reception technique however, is a suboptimal reception method since the present co-channel interference levels in a FR-2 setup are vastly higher than in the reference FR-4 case. The implemented concept of IAN is illustrated by Figure 4.15, demonstrating the independent data transmission to two adjacent spot beams in FR-2, operated at the same frequency and polarization. In the concept of single carrier transmission, the scheduler assigns each terminal the optimal MODCOD for data transmission.

Single Carrier Multi-User Detection (SC-MUD)

A MUD capable terminal has the possibility to apply the joint detection process despite a single carrier data transmission mode. The idea of this concept is to utilize the strongest interfering signal for the detection process and abort the detection, once the dedicated carrier is successfully decoded. Since the strongest interferer does not provide any relevant information for the user terminal, potentially decoded information from the strongest interferer is simply discarded. This transmission and detection scenario is quite challenging for the scheduler since the data transmission in both adjacent beams is independent but the detection performance in both beams is not. In other words, careful selection of the transmitting MODCODs is required for this scenario in order to allow successful decoding by both user terminals and not

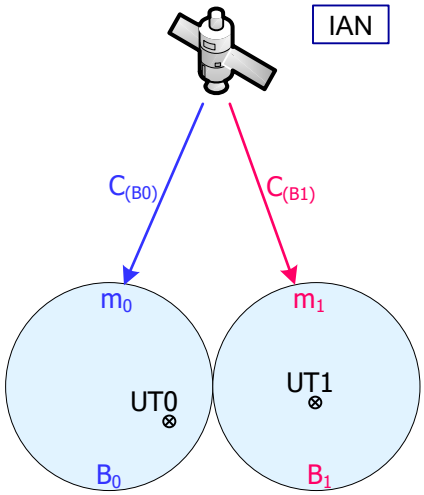

Figure 4.15: Interference as noise

to sacrifice the performance of one terminal for the performance of the other. This fact is illustrated in Figure 4.16 by the indicated MODCOD pair in each beam which is exactly the opposite in both beams. This means that from the perspective of B_0, B_1 is the strongest interferer and vice versa. This is also true for their MODCODs and this is why the MODCOD pair is not identical in both beams, but flipped.

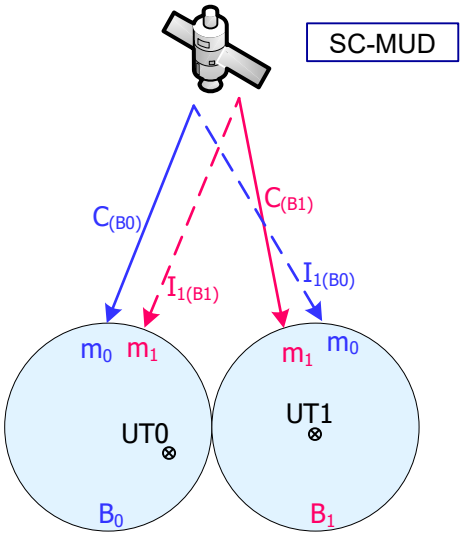

Figure 4.16: Single carrier (SC)-MUD concept, where the data transmitted by the strongest interferer are discarded

4.9.2 Reception Mode for Multiple Beams Per User

This section introduces a transmission mode applicable to a multi carrier per user transmission scenario.

Multiple Access Channel Multi-User Detection (MAC-MUD)

Multiple access (MAC)-MUD is a reception mode that is only applicable in systems where the data transmission to a single user terminal during a certain time slot is realized via two spot beams. The strongest co-channel interferer is thus borrowed by the scheduler to provide data to a single user terminal via two carriers. This implies that the user terminal has to fully decode the data provided by both carriers, the main carrier by the dedicated spot beam and its strongest interferer and recombine their data. The MODCOD pairs assigned by the scheduler during a transmission time slot are user terminal specific and therefore independent of any other user terminal. For this reason, the indicated MODCOD pairs for both user terminals, shown in Figure 4.17, are different and depend only on the interference, impairment and C/N conditions on ground of the individual user terminal.

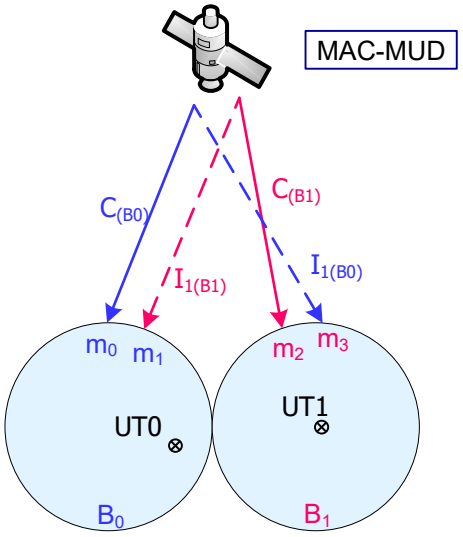

Figure 4.17: Multiple access channel (MAC)-MUD concept, where the data transmitted by the strongest interferer are decoded as well

4.10 Capacity Regions

Identifying the capacity region or optimal rates is important to determine the limits of a technique where reliable transmission is feasible. In contrast to the achievable capacity of the user uplink provided by [47], [48], this section is dedicated to examine the achievable rate regions for the introduced data transmission and reception concepts in the user downlink. For this purpose a memoryless interference channel with two

user pairs is assumed.
Let M0 and M1 be the messages to be transmitted by the individual user, X_0 and X_1 the transmitted and Y the received information. The actual achievable rate by the two users is hence denoted as R_0 and R_1, respectively.

4.10.1 IAN Capacity Region

This scenario assumes that the present co-channel interference is treated as noise [6].

User 0 is able to decode the message X_0 successfully if the rate R_0 satisfies the condition in (4.7), as illustrated in Figure 4.18:

$$R_0 < I(X_0; Y). \tag{4.7}$$

The term I denotes the mutual information, representing the amount of information shared between two random variables X_0 and Y. In other words, if X_0 and Y are independent, then $I(X_0; Y) = 0$. The rates of the remaining CCI carriers in the system do not affect R_0 since they are treated as noise in this scenario.

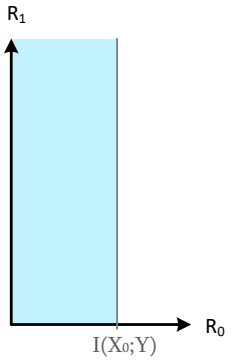

Figure 4.18: IAN capacity region [6]

4.10.2 MAC Capacity Region

In the case of the MAC-MUD scenario, in literature also denoted as simultaneous decoding (SD) [9], [7], [6], the channel configuration is represented by a multiple access channel (MAC) [46].

As explained in [46] a multiple access channel consisting of two senders and a single receiver with the alphabets X_0, X_1 and Y and the transition matrix $p\,(y|x_0,x_1)$ can be assumed. The achievable capacity region in this case is defined as the closure of the convex hull of all achievable rate pairs (R_0, R_1) that satisfy the conditions (4.8), (4.9), (4.10) for some joint distribution $p_0(x_0)p_1(x_1)$ on X_0X_1:

$$R_0 < I\left(X_0;Y|X_1\right) \tag{4.8}$$

$$R_1 < I\left(X_1;Y|X_0\right) \tag{4.9}$$

$$R_0 + R_1 < I\left(X_0,X_1;Y\right) \tag{4.10}$$

The MAC capacity region obtained by the conditions listed before is illustrated in Figure 4.19.

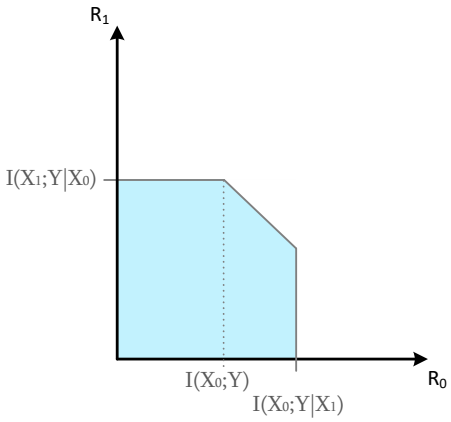

Figure 4.19: MAC capacity region [6]

At this point, it needs to be noted that this is the ideal capacity region for the case that there is a perfect AWGN channel with no additional interferers in the systems. The additional interferers contribute to the noise in the system since they are not detected by the receiver. Considering this situation, the noise on the channel is not pure AWGN anymore.

4.10.3 SC-MUD Capacity Region

The capacity region of the SC-MUD concept, in literature also referred to as SND (simultaneous non-unique decoding) [9], [6], [7], is provided in this section.

According to [9] the capacity region of the SC-MUD mode, shown in Figure 4.20, can be determined as follows:

$$R_0 \leq \max(I_A,I_B) \tag{4.11}$$

$$I_A = I(X_0;Y) \tag{4.12}$$

$$I_B = \begin{cases} I_C, & R_1 < I(X_1;Y|X_0) \\ 0, & R_1 \geq I(X_1;Y|X_0) \end{cases} \tag{4.13}$$

$$I_C = \min(\, I(X_0;Y|X_1),\; I(X_0,X_1;Y) - R_1 \,) \tag{4.14}$$

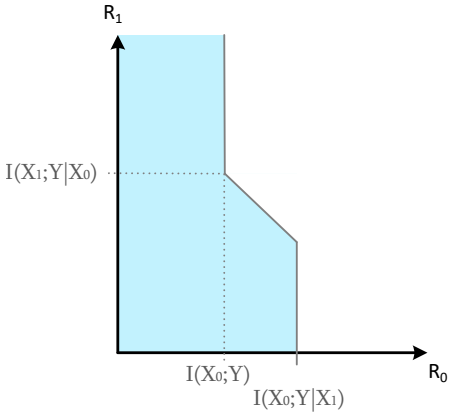

Figure 4.20: SC-MUD capacity region [6]

Considering the joint achievable rate for the user terminal 0 and user terminal 1, the following can be achieved [7]. The result of optimum scheduling is a capacity region that includes the IAN and MAC region in terms of rate, meaning that any rate pair (R_0, R_1) belonging to the IAN and MAC region can be achieved by the SC-MUD region [9].

Based on this aspect the joint achievable rate with SC-MUD combining the rates of IAN (a) and MAC (b) and SC-MUD (c) for each of both users, leads to an optimum case in terms of capacity shown in Figure 4.21.

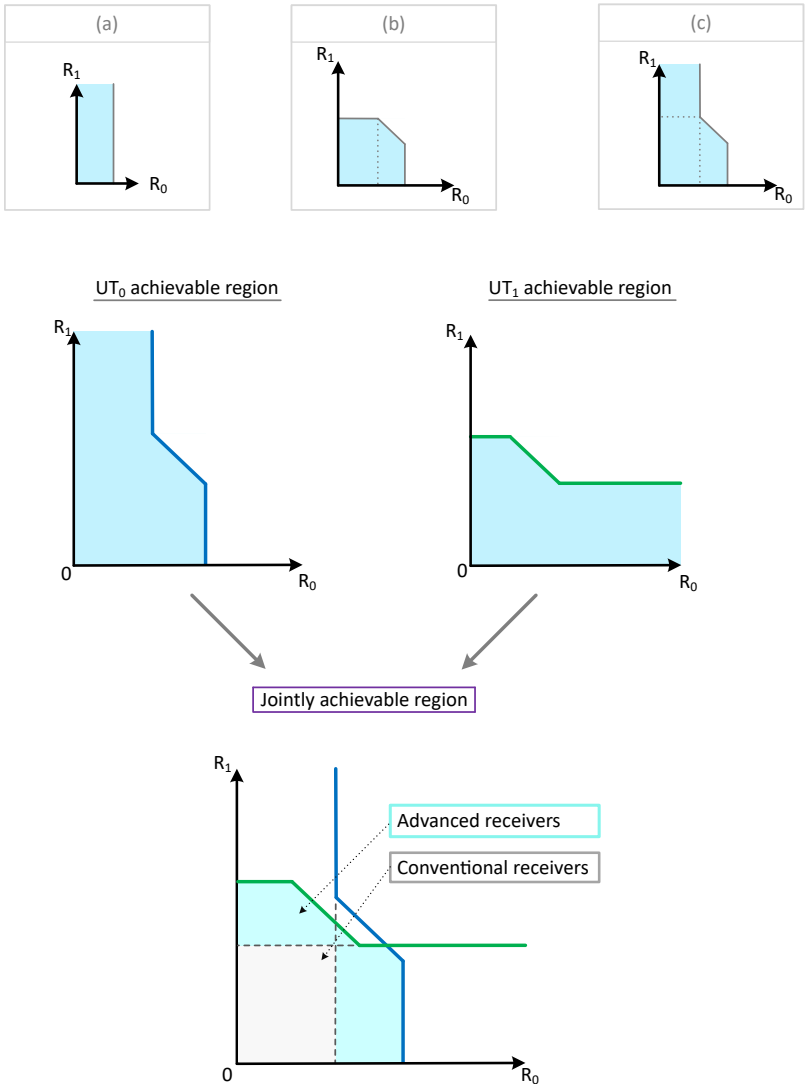

Figure 4.21: Joint achievable capacity region [7] for the individual user with (a) IAN, (b) MAC and (c) SC-MUD region

4.11 SC-MUD Gain

The achievable gain of SC-MUD [8] compared to the theoretical single carrier (SC) performance is demonstrated by means of an example shown in Figure 4.22. In this example we assume the interference scenario ID 2 with $C/I_1 = 2$ dB and a MODCOD pair consisting of QPSK 1/2 for UT_0 and 8PSK 3/4 for UT_1. In a SC-MUD scenario the individual information is transmitted via two dedicated carriers to two user terminals. Nevertheless, MUD is executed by them until their dedicated carrier is successfully detected, which causes the main carrier and strongest interferer to be flipped in both cases. For this reason the scheduler aims to optimize the achievable

joint throughput of both carriers, while the data in each of the two carriers are independent from the other and this is also true for the local atmospheric attenuation and the contour loss at the individual user terminal. Additionally, this optimization claims to be done in a fair way in order that the throughput of one terminal is not sacrificed for the throughput of the other.

Despite the fact that individual data transmission happens in SC-MUD, both user terminals still could benefit from each other when applying MAC-MUD at the receiver under certain conditions.

These conditions will be examined by means of the sample in Figure 4.22 that shows the critical C/N values for the individual carrier where quasi error-free (QEF) performance with FER = 10^{-5} is reached. In addition to the C/N, also the SNIR form the perspective of UT_0 and the perspective of UT_1 is shown in the graph. Table 4.1 provides a carrier-specific overview to put the SC-MUD performance in relation to the single carrier (SC) performance.

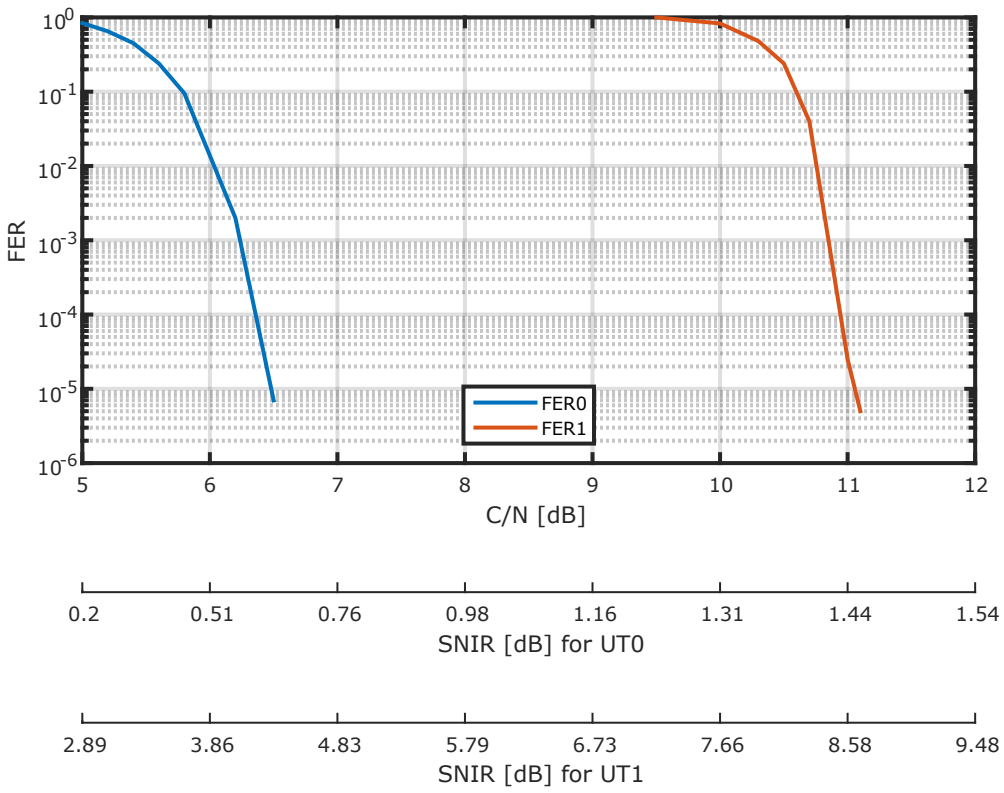

Figure 4.22: SC-MUD example with SNIR from perspective of UT_0 and UT_1, C/I_1 = 2 dB, MODCOD pair QPSK 1/2 + 8PSK 3/4, from the perspective of UT_0 [8]

User	MODCOD	Spectral efficiency [bit/s/Hz]	SC SNR [dB] QEF	MUD SNR [dB] QEF	SNIR [dB] at QEF SNR
UT_0	QPSK 1/2	0.89	1	6.5	0.64
UT_1	8PSK 3/4	2.2	8.2	11.1	8.7

Table 4.1: SC-MUD performance table of QPSK 1/2 and 8PSK 3/4, QEF at FER = 10^{-5}

On closer inspection of the performance shown in Figure 4.22 and Table 4.1, it can be noticed that the SC QEF performance of UT_0 is improved by the application of SC-MUD, since the carrier reaches FER = 10^{-5} at 0.64 dB SNIR instead of 1 dB, measured in the single carrier mode. As in [8], this effect can be explained by the fact that in SC-MUD, from the perspective of UT_0, the strongest interferer, which is dedicated to UT_1 and is not yet decoded (FER=1), still already contributes to the detection process of UT_0 . The achieved gain between the IAN and SC-MUD mode is here denoted as MUD gain g_{MUD}. Over 300 similar test cases with a SNR gap between QEF of MODCOD0 and MODCOD1, revealed a MUD gain of 0.6 dB on average, if the SNR gap was lower than 10 dB. If this condition is met, the contribution of the interferer is still significant enough for the decoding of the main carrier, despite the fact that it might not yet be fully decoded.

Let $m0$ denote the MODCOD0 in beam B_0 and $m1$ denote the MODCOD1 in beam B_1. The theoretical QEF threshold for a MODCOD $m0$ in the SC case is denoted as SNR^{m0}, the same is true for $m1$. The terms $CNI_1^5R^{m0}$ and $I_1NCI_2^5R^{m1}$ denote the SNIR from the perspective of the main carrier and the strongest interferer respectively, indicating the investigated MODCOD $m0$ or $m1$.

The condition for a present MUD gain and its effect on the SNIR can now be formulated as in (4.15) and (4.16) for UT_0, as well as (4.17) and (4.18) for UT_1:

$$g_{MUD} > 0 \quad \text{if} \quad |\, SNR^{m1} - CNI_1^5R^{m0} \,| < 10\, dB \tag{4.15}$$

$$CNI_1^5R^{m0} \geq SNR^{m0} - g_{MUD} \tag{4.16}$$

$$g_{MUD} > 0 \quad \text{if} \quad |\, SNR^{m0} - I_1NCI_2^5R^{m1} \,| < 10\, dB \tag{4.17}$$

$$I_1NC_2^5R^{m1} \geq SNR^{m1} - g_{MUD}. \tag{4.18}$$

Considering the MUD gain with 0.6 dB, the UT_1 in the introduced example requires a SNIR = 7.6 dB, which was also confirmed by simulations. UT_1 however, requires a C/N of 12.2 dB to achieve a SNIR of 7.6 dB. Such high SNIR values are only reachable

in a low interference scenario. For this reason a scenario ID 6 with $C/I_1 = 10\ dB$ has to be selected in this case by the scheduler.

For B_0 on the other hand, $C/I_1 = 2$ dB is sufficient to decode QPSK 1/2, as listed in Table 4.2. The achievable spectral efficiency in this scenario is shown in Table 4.3.

Beam	**C/N [dB]**	**C/I Scenario** $C/I_1[dB]$	**MODCOD**
B_0	6.5	2	QPSK 1/2
B_1	12.2	10	8PSK 3/4

Table 4.2: SC-MUD C/N and C/I configuration to decode QPSK 1/2 in B_0 and 8PSK 3/4 in B_1

The obtained spectral efficiency by the SC-MUD example is shown in Table 4.3.

User	**MODCOD**	**Spectral efficiency [bit/s/Hz]**
UT_0	QPSK 1/2	0.89
UT_1	8PSK 3/4	2.2
Total		3.09

Table 4.3: SC-MUD spectral efficiency of QPSK 1/2 + 8PSK 3/4

Comparing the obtained SC-MUD performance with MAC-MUD considering the C/N and C/I setting in Table 4.2 and selecting the MODCOD pairs according to the results in Section A.2, the following spectral efficiencies were obtained as shown in Table 4.4.

User	**MODCOD**	**Spectral efficiency [bit/s/Hz]**
UT_0	QPSK 1/2+QPSK 2/3	1.11
UT_1	8PSK 26/45+QPSK 2/5	1.27
Total		2.38

Table 4.4: MAC-MUD spectral efficiency

Comparing the actual total spectral efficiency achieved by SC-MUD and MAC-MUD in Table 4.3 and Table 4.4 respectively, it is clearly visible that the SC-MUD mode is the more efficient transmission technique for this example. However, the critical performance aspect for SC-MUD, as also reported by [32], is the optimum user pairing by the scheduler. The scheduling algorithm applied in the context of this analysis selects user pairs with interference conditions suitable for the current reception mode that achieves the highest possible throughput. This decision is based on transmission and reception mode specific performance tables that are introduced later in this work.

The scheduling algorithm for the SC-MUD mode can be summarized in the following 6 steps that are also illustrated in Figure 4.23.

Step 1: The scheduler first picks two user terminals in adjacent spot beams with the essential condition that the individual spot beams are each the strongest interferer for the other user terminal.

Step 2: A temporary MODCOD (QPSK 1/2) is assigned to UT_0 that is updated in the following steps.

Step 3: The scheduler assigns the MODCOD for UT_1 (MODCOD1) by selecting the highest MODCOD pair from the MUD performance table while considering the already selected MODCOD of UT_0 (MODCOD0).

Step 4: Keeping the assigned MODCOD1, the scheduler again seeks for the highest possible MODCOD0. If a higher MODCOD0 can be assigned, the scheduler continues to Step 5. Otherwise, the algorithm continues with Step 6.

Step 5: If the MODCOD0 was updated to a higher MODCOD, the MODCOD1 is again selected by the scheduler. The algorithm continues then with Step 4.

Step 6: The highest possible MODCOD pair was found by the scheduler and the MODCODs get assigned to the individual carriers.

This example represented the practical demonstration of the theory shown in Figure 4.21 that illustrates the joint achievable rates of SC-MUD. The strength of SC-MUD is the fact that the statistical information of the first interferer is utilized for the decoding of the main carrier, which leads to the fact that the receiver doesn't need to go the extra mile in order to decode also the strongest interferer, which usually requires a higher SNIR.

Due to this fact, the performance of SC-MUD will always be at least at IAN level or better.

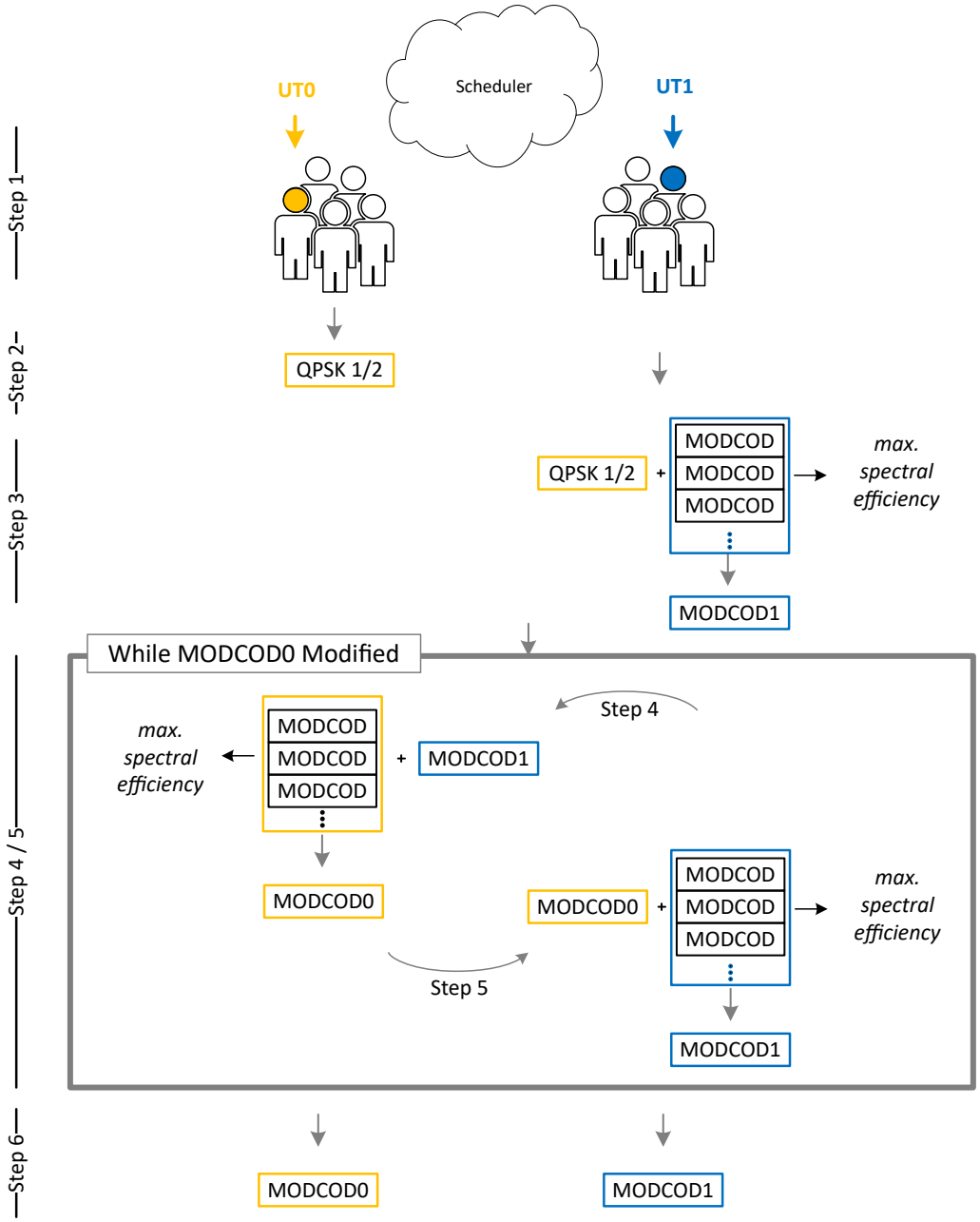

Figure 4.23: SC-MUD scheduling algorithm

CHAPTER 5

Multi-User Detection

The concept of multi-user detection deals with the recovery of information transmitted by multiple signals over a channel that mutually interfere each other. The situation of interfering simultaneous data transmission over the same medium, called multi-access communication, can be encountered in different fields of wired and wireless communication, and thus also in satellite communications [43].

When considering a multiple access channel for MUD, mutually interfering non-orthogonal signals are assumed. The receiver faces the challenge to decode the transmitted bits from the noisy superposition of the transmitted signals considering any interference scenario. Verdu [43] further explains that the demodulation is a hypothesis testing problem. The hypothesis H_i, a set of transmitted symbols on the one hand and the noisy observations by the receiver on the other have to be matched by the decoder. This process can be done by decision rules that divide the observation space into decision regions. In this context two types of probabilities are introduced. The *a priori* probabilities $p(H_i)$ denote the unconditional probability before the data are observed and the *a posteriori* probabilities $p(H_i|z)$ are conditioned on a realization, while the actual observation is represented by z. The *a posteriori* probability can be computed via the Bayes formula

$$P(H_i|z) = \frac{p(z,H_i)}{p(z)}. \tag{5.1}$$

The maximum a posteriori (MAP) rule, that selects the highest $p(H_i|z)$, represents the decision rule that leads to the minimum error probability for *a posteriori* probabilities. Nevertheless, MAP demands knowledge of *a priori* probabilities. If the *a priori* probabilities are not known, the maximum likelihood (ML) decisions can serve as alternative approach.

The general channel model for the considered HTS system is given in (5.2), where M denotes the number of strongest carriers considered. Let $b = 0$ be the main carrier with 5 additional interferers ($B = 5$) in the system. In the context of this analysis, a

total of 6 beams are therefore considered with $b = \{0,1,2,3,4,5\}$.

Then, r_t denotes the received signal by user terminal t, the parameter $h_{t,b}$ describes the channel from beam b to terminal t. Let s_b denote the transmitted symbol by beam b and ω_t the AWGN on the channel for terminal t. The received signal r can therefore be written as

$$r_t = \sum_{b=0}^{B} h_{t,b} s_b + \omega_t. \tag{5.2}$$

The channel models for the individual cases covered by this analysis, which are IAN, SC-MUD and MAC-MUD are listed in the following.

1. Interference as Noise

$$r_0 = h_{0,0} s_0 + \sum_{b=1}^{5} h_{0,b} s_b + \omega_0 \tag{5.3}$$

2. Single user detector in a Gaussian MAC channel

$$r_0 = h_{0,0} s_0 + \sum_{b=1}^{5} h_{0,b} s_b + \omega_0 \tag{5.4}$$

$$r_1 = h_{1,1} s_1 + \sum_{b=1}^{5} h_{1,b} s_b + \omega_1 \tag{5.5}$$

3. Multi-user detector in Gaussian MAC channel

$$r_0 = h_{0,0} s_0 + h_{0,1} s_1 + \sum_{b=2}^{5} h_{0,b} s_b + \omega_0 \tag{5.6}$$

5.1 The Multi-User Detector

In a system with high interference, the signal reception is significantly degraded. Interference mitigation techniques are thus applied to counteract the present interference and enable signal reception in this environment. The term interference mitigation technique though, simply describes its purpose but the ways of mitigation can be vastly different. Taking the example of MUD and precoding, the MUD technique mitigates the interferences at the receiver, while the precoding technique is applied at the gateway calculating a precoding matrix in order to cancel out the present interference before the reception.

This work focuses on the first part, MUD, where the user terminal receives a linear combination of all signals transmitted at the same frequency by different spot beams.

The strength of the interfering signals depends on the distance and the shape of the spot beam antenna pattern in the system.

The MUD technique in this case aims to extract the information of the main carrier transmitted by the assigned spot beam and the strongest interferer via joint detection. Hence, both the main carrier and the strongest interferer are detected at the same time.

This detection can be realized by an iterative process, where information of both signals is exchanged in form of log-likelihood ratios (LLRs). The exchange of soft bit information is very sensitive and is therefore the expedient technique in this case, in contrast to hard bits.

Multi-user detection is a technique that utilizes high interference levels in order to extract the transmitted information. The extraction of information is a delicate process and consequently, soft bit detection is applied. Caus et al. [9], [8] recommend two algorithms for multi-user detection purposes in the forward link, which are the algorithm for soft-input soft-output detection by Colavolpe et al. [22] and the single tree search approach by Studer et al. [26] and [27]. Both algorithms were tested but the latter was chosen to simplify the scaling of LLRs. For channels with memory where inter-symbol interference (ISI) is present, the BCJR algorithm [28] would be the suitable choice for the detector.

5.2 MUD Algorithm

Studer et al. introduce in [26] and [27] a sphere decoding approach as tool for soft detection in a multiple-input multiple-output (MIMO) system to separate interfered data steams. Due to the good performance as reported in [9] this approach was chosen and is now applied in this analysis for the purpose of detection in the user downlink.

Studer et al. transformed the MAP detection problem and computation of the intrinsic LLRs into a tree-search problem, which they call *single tree-search* (STS) approach. This approach associates the partial symbol vectors and partial Euclidean distances with the nodes of a tree, while the distance increments represent the branches. As a result, the paths from the root to a leaf correspond to individual symbol vectors.

This concept consideres coherent detection and thus assumes knowledge of the channel matrix $\mathbf{H}$ at the receiver terminal [49]. The assumed MIMO system consists of M_T transmit and $M_R \geq M_T$ receive antennas. Considering the system with

$$\mathbf{y} = \mathbf{H}\mathbf{s} + \mathbf{n}, \tag{5.7}$$

where $\mathbf{s}$ and $\mathbf{y}$ denote the transmitted, respectively received symbol vector and $\mathbf{n}$ the AWGN noise vector. As described by [27] the intrinsic LLRs are computed by

$$L_{i,b} \triangleq \log \frac{P[x_{i,b} = +1|\mathbf{y}, \mathbf{H}]}{P[x_{i,b} = -1|\mathbf{y}, \mathbf{H}]}, \tag{5.8}$$

where the index b refers to the bth bit in the binary label x of the ith item in the symbol vector $\mathbf{s}$. Applying Bayes' theorem to (5.8) results in

$$L_{i,b} = \log \left(\sum_{\mathbf{s} \in \chi_{i,b}^{(+1)}} p\left(\mathbf{y}|\mathbf{s},\mathbf{H}\right) P[\mathbf{s}] \right) - \log \left(\sum_{s \in \chi_{i,b}^{(-1)}} p\left(\mathbf{y}|\mathbf{s},\mathbf{H}\right) P[\mathbf{s}] \right), \tag{5.9}$$

where the terms $\chi_{i,b}^{(+1)}$ and $\chi_{i,b}^{(-1)}$ are sets of symbol vectors with -1, respectively +1 bit value at the indicated position i and b. The required probability density distribution $p(\mathbf{y}|\mathbf{s},\mathbf{H})$ is computed via

$$p\left(\mathbf{y}|\mathbf{s},\mathbf{H}\right) = \frac{1}{(\pi N_0) M_R} \exp\left(-\frac{\|\mathbf{y} - \mathbf{H}\mathbf{s}\|^2}{N_0} \right). \tag{5.10}$$

The term $P[s]$ in (5.9) is provided as *a priori* LLRs computed by

$$L_{i,b}^{A} \triangleq \log \frac{P[x_{i,b} = +1]}{P[x_{i,b} = -1]}, \ \forall i,b. \tag{5.11}$$

The detector is then able to compute the extrinsic LLRs based on the available intrinsic information by

$$L_{i,b}^{E} \triangleq L_{i,b} - L_{i,b}^{A}, \ \forall i,b. \tag{5.12}$$

Motivated by the considerable computational complexity of the Euclidean distance for each LLR, Studer et al. [27] utilize the max-log approximation instead, which causes a minor performance loss. This step however, enables them to transform the LLR computation problem in a weighted tree-search problem.

After QR-decomposition of $\mathbf{H}$ and left-multiplication by $\mathbf{Q^H}$, (5.7) results in

$$\tilde{\mathbf{y}} = \mathbf{R}\mathbf{s} + \mathbf{Q^H}\mathbf{n}, \tag{5.13}$$

where $\tilde{\mathbf{y}} = \mathbf{Q^H}\mathbf{y}$.

The intrinsic max-log LLRs are then computed by

$$\begin{aligned} L_{i,b}^{D} \triangleq & \min_{s \in \chi_{i,b}^{(+1)}} \left\{ \frac{1}{N_0} \|\tilde{\mathbf{y}} - \mathbf{R}\mathbf{s}\|^2 - \log P[\mathbf{s}] \right\} - \\ & \min_{s \in \chi_{i,b}^{(-1)}} \left\{ \frac{1}{N_0} \|\tilde{\mathbf{y}} - \mathbf{R}\mathbf{s}\|^2 - \log P[\mathbf{s}] \right\} \end{aligned} \tag{5.14}$$

and can be used in (5.12) by replacing $L_{i,b}$, which means that

$$L_{i,b}^{E} = L_{i,b}^{D} - L_{i,b}^{A} \tag{5.15}$$

to obtain the extrinsic max-log LLRs.

The max-log LLR (5.14) for each bit is computed by the difference of two minima, where one of them is

$$\lambda^{MAP} = \frac{1}{N_0}||\tilde{\mathbf{y}} - \mathbf{R}\mathbf{s}^{MAP}||^2 - \log P[\mathbf{s}^{MAP}], \tag{5.16}$$

which depends on the MAP solution

$$\mathbf{s}^{MAP} = \arg \min_{s \in \mathcal{O}^{M_T}} \left\{ \frac{1}{N_0}||\tilde{\mathbf{y}} - \mathbf{R}\mathbf{s}||^2 - \log P[\mathbf{s}] \right\}, \tag{5.17}$$

with $\mathcal{O}$ denoting the complex scalar constellation, while the other minimum can be written as

$$\lambda_{j,b}^{\overline{MAP}} = \min_{s \in \mathcal{X}_{i,b}^{\overline{MAP}}} \left\{ \frac{1}{N_0}||\tilde{\mathbf{y}} - \mathbf{R}\mathbf{s}||^2 - \log P[\mathbf{s}] \right\}. \tag{5.18}$$

The two minima in (5.14) essentially represent the MAP hypothesis λ^{MAP} and its counter-hypothesis $\lambda_{i,b}^{\overline{MAP}}$. For this reason (5.14) can be rewritten as

$$L_{i,b}^{D} \triangleq \begin{cases} \lambda_{i,b}^{\overline{MAP}} - \lambda^{MAP}, \; x_{i,b}^{MAP} = +1, \\ \lambda^{MAP} - \lambda_{i,b}^{\overline{MAP}}, \; x_{i,b}^{MAP} = -1. \end{cases} . \tag{5.19}$$

Let the already announced partial symbol vectors be presented as

$$\mathbf{s}^{(i)} \triangleq [s_1 ... s_{M_T}]^T. \tag{5.20}$$

The Euclidean distances, computed as

$$d(\mathbf{s}) \triangleq \frac{1}{N_0}||\tilde{\mathbf{y}} - \mathbf{R}\mathbf{s}||^2 - \log P[\mathbf{s}] \tag{5.21}$$

can be evaluated recursively as $d(\mathbf{s}) = d_1$ using the partial distances

$$d_i = d_{i+1} + e_i, \; i = M_T, ..., 1, \tag{5.22}$$

that are also associated to the nodes of the tree, where the distance increments are denoted by

$$e_i \triangleq \frac{1}{N_0}|\tilde{y}_i - \sum_{j=i}^{M_T} R_{i,j} s_j|^2 - \log P_c[\mathbf{s}^{(i)}], \tag{5.23}$$

that represent the branches of the tree. The term P_c is actually a simplification that evloves from

$$P[\mathbf{s}] = \prod_{i=1}^{M_T} P[s_i|\mathbf{s}^{(i+1)}] \tag{5.24}$$

$$P[s_{M_T}|\mathbf{s}^{(M_T+1)}] \triangleq P[s_{M_T}] \tag{5.25}$$

$$P_c[\mathbf{s}^{(i)}] \triangleq P[s_i|\mathbf{s}^{(i+1)}]. \tag{5.26}$$

The functionality of the single tree search (STS) detection algorithm is shortly summarized by the following steps detailed in [26], [27].

The STS follows the strategy to optimize the search by visiting each node at most once. In addition to that, the search of a subtree is only executed if the search leads to an update of current MAP hypothesis metric λ^{MAP} or extrinsic metrics $\lambda_{i,b}^{\overline{MAP}}$.

If a leaf in the tree has been reached, the decoder executes one of the two possible scenarios:

(a) MAP hypothesis update Once the MAP hypothesis is changed for a bit, the substituted MAP hypothesis becomes the extrinsic metric of the new counter-hypothesis instead.

(b) Extrinsic metric update If the distance exceeds the MAP hypothesis metric, the update affects only extrinsic metrics that refer to counter-hypotheses.

5.3 Joint Multi-User Detector Functionality

As described in [9] the MUD technique applied for this analysis is based on iterative joint detection of the received symbols, denoted as r, that is a superposition of two signals that fully overlap. For each signal a dedicated process chain for detection and decoding is executed in each iteration, shown in Figure 5.1.

This processing chain consists of a multi-user detector, a deinterleaver $\prod^{-1}$, the low density parity check (LDPC) decoder, invented by Gallager in 1962 [50], and an interleaver $\prod$. The information between these blocks is exchanged in form of LLRs for each bit. The deinterleaver and interleaver are required since the DVB-S2 standard [5] foresees a bit interleaver at the transmitter for modulations higher than QPSK to avoid burst errors at the decoder. This causes the need for a bit interleaver before the extrinsics are fed back to the detector for the next iteration because the received input sequence is bit interleaved.

The iterative process starts with the *a priori* information of B_0 and B_1 denoted as λ_0 and λ_1 respectively, which is set to zero. The first iteration starts with the detection of Beam0 followed by the deinterleaver and decoding of the obtained LLRs. The extrinsic information gets computed and interleaved after the decoder and the a

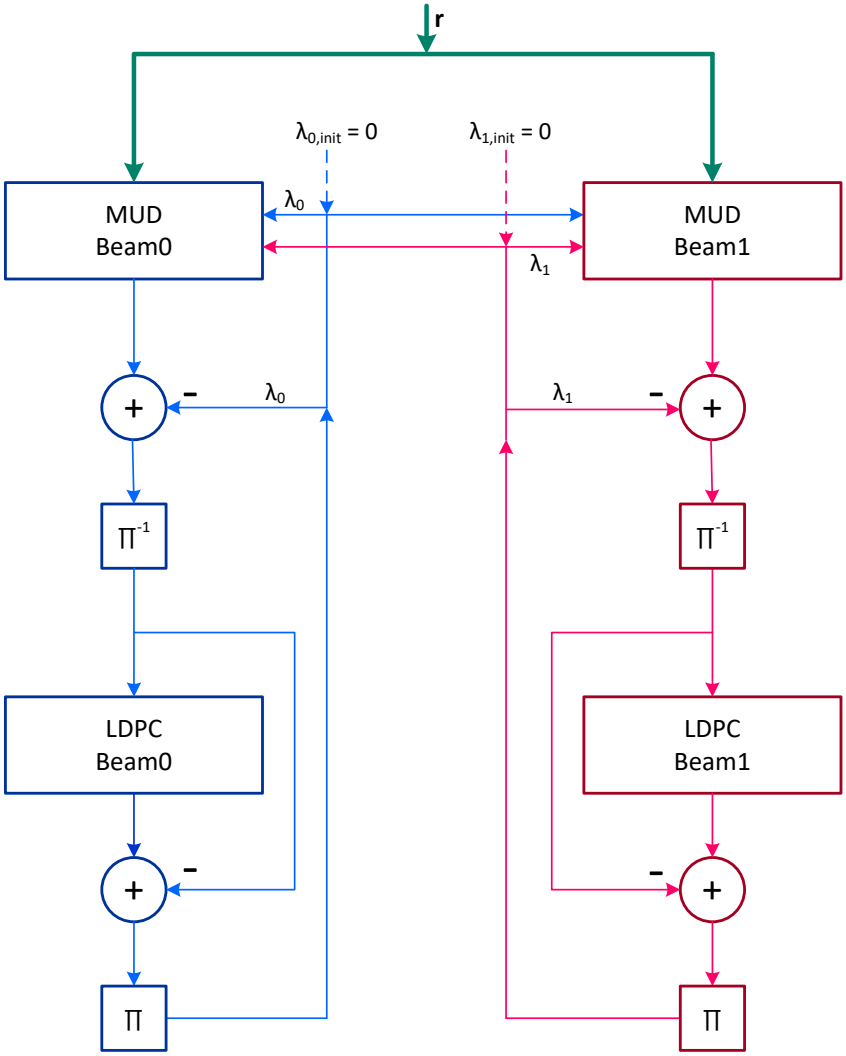

Figure 5.1: Multi-user detector concept for joint detection [9]

priori information of Beam0 (λ_0) gets updated. Then the same procedure is repeated for Beam1 resulting in the update of λ_1. By now, a full MUD iteration was executed. The iterating process is continued until either the MUD early stop criterion is fulfilled, which implies that both LDPC decoders report a valid code word, or alternatively, the maximum number of MUD iterations is reached.

The obtained LLRs, represented in the system demonstrator with 8-bit, indicate based on their sign, if the bit is 0 (in case of a negative sign) or 1 (in case of a positive LLR value). The magnitude of the individual LLR however, represents the reliability of the current soft bit information. This exchange of soft information in the joint detection process is vital, since even a carrier that is not yet decoded and has thus still a FER of 1, contributes to the detection of the second carrier in form of soft

information. The joint detection process is characterized by the iterative process, where the mutual use and subtraction of the updated carrier specific LLRs leads to an improvement of the LLR magnitudes and with that, the reliability in each process. Typical LLR distributions which are encountered during the MUD detection process are illustrated in Figure 5.2. The typical LLR distribution after the detector in the first iteration, shown in a) has a normal distribution. Most of the LLRs have a value around zero indicating a high level of uncertainty. Only few LLRs at the edge of the Gaussian distribution have a stronger tendency towards -1 or 1. The LLR distribution in b) represents a typical distribution after the LDPC decoder. The distribution nicely demonstrates the fact that the decoder adds more reliability to the LLRs. With that the number of LLRs with values around zero vanishes or becomes very small and it results in two normal distributions within each hard bit state.

The graph in c) demonstrates a behaviour that can be observed when the system is operated with an 8-bit interface, where the LLRs reach a saturation state after the LDPC decoder. This state could be reached already in the first iteration of the MUD block after the execution of the LDPC decoder but is usually observed in the second or higher iteration of the MUD block.

Considering a 8-bit LLR implementation for the joint MUD process, the LLRs have a resolution of $[-127, +127]$, where -127 represents a reliable bit with state 0 and +127 the state 1.

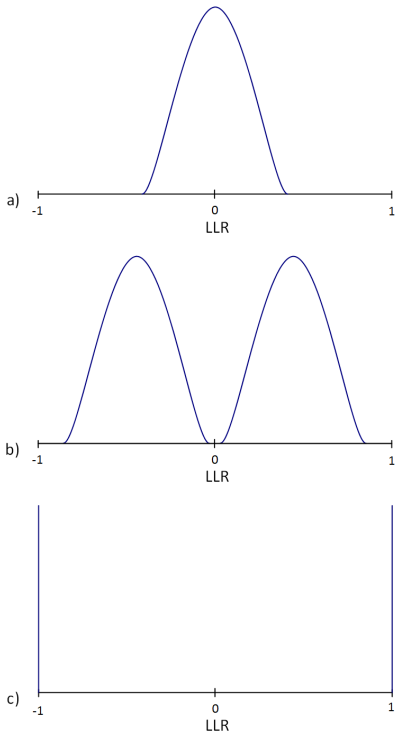

Figure 5.2: Log-likelihood ratios a) after the detector, b) after the decoder, c) saturated

CHAPTER 6

Software Framework

This chapter provides a general software architecture overview of the system demonstrator. It lists the components of the demonstrator as well as the effects that are considered for this MUD study. The software demonstrator is written in C++ and is based on the JOANNEUM RESEARCH proprietary software framework SpaceComm-SIMU. This software framework was utilized for the purpose of this work. In the course of this work, the framework was extended supporting the conditions required for MUD. More specifically, existing software modules, such as the decoder and the synchronization plus parameter estimation, were used but also some software modules were enhanced or new MUD specific modules were added to the framework in order to enable an environment suitable for MUD and support its functionality.

In the following, the general software demonstrator setup used for MUD performance analysis is explained.

6.1 Implementation Targets

The software implementation followed two main goals, which are to increase the processing speed on the one hand and to increase the TRL of the system demonstrator on the other. The exact definition of the TRL usually varies between companies and industry sectors. Since this work was done in the course of a project funded by the European Space Agency, the project's readiness level refers to their applied TRL definition as it is provided in Figure 6.1.

This work intends to enhance the current TRL 2 level for the operational capability of MUD at a user terminal on ground to TRL 3. The target is to analyze the MUD behaviour in a software based system demonstrator that creates a realistic environment of a full satellite link. The technological concept of MUD can be tested and compared between various scenarios. Results of these tests then provide information on the feasibility of further steps and hardware capability.

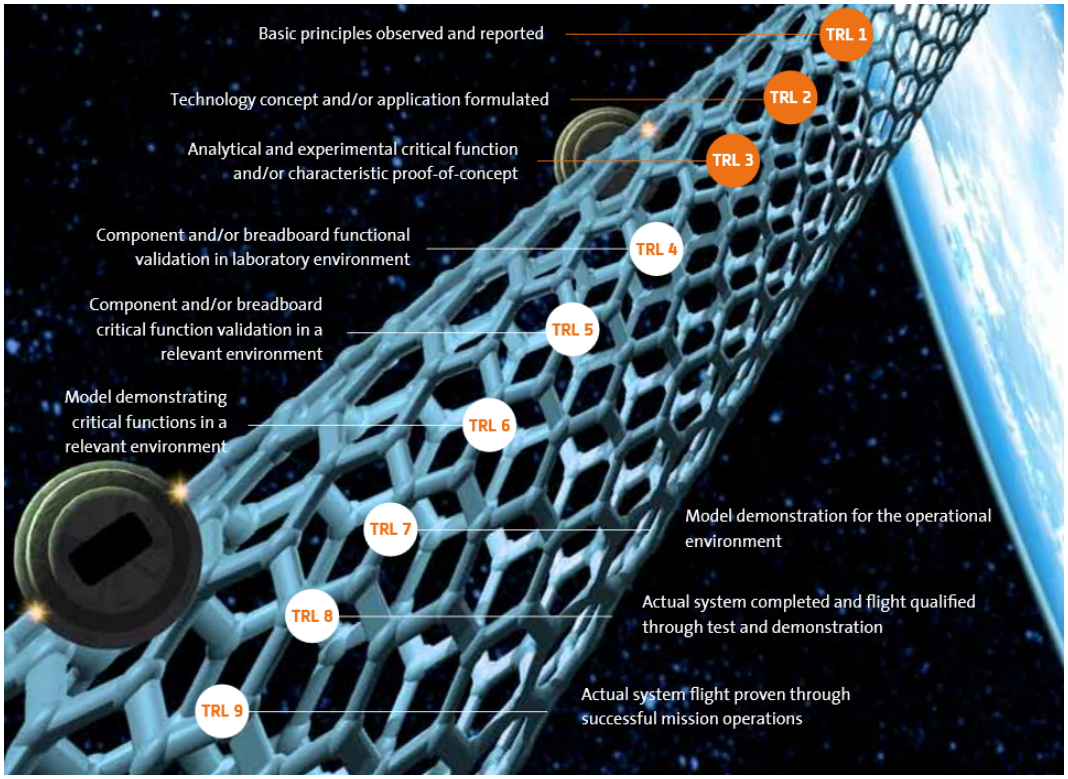

Figure 6.1: Technology readiness level (TRL), as specified by the European Cooperation for Space Standardization [10]

6.2 Software Architecture

The SpaceCommSIMU software framework by JOANNEUM RESEARCH is based on a modular software concept providing flexibility and with that the applicability for various topics in the field of satellite communication.

Relevant scenarios for the analysis of MUD in a HTS system consider the presence of multiple carriers, operated at the same frequency, and consequently, the experienced interference by the user terminal on ground.

This fact motivates the need for the configuration and transmission of various carriers. The number of considered interferers by the system demonstrator in this analysis is limited to five, as already shown in Table 3.1 before. The detector is able to jointly detect two distinct carriers, representing the main carrier and the strongest interferer, which can be manually configured according to the selected scenario. The remaining interferers are added to the signal as pre-configured and pre-generated carriers, since they are not decoded by the receiver but treated as noise instead. This approach provides the benefit that the remaining interferers are not required to be configured for each scenario and the processing speed is kept low because data generation is only required for two carriers.

The system demonstrator is composed of a transmitter, the channel and a receive

unit, shown in Figure 6.2. A simulation can be specified in a dedicated configuration file (SimFile) that specifies the parameters of each module. The components marked in grey symbolize optional system impairments.

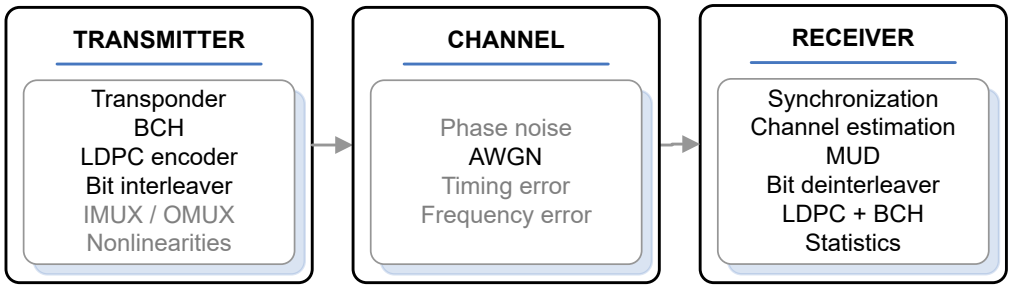

Figure 6.2: Transmit, channel and receive part of the simulator [11]

6.2.1 Configuration

A simulation file represents the application programming interface (API) to the SpaceCommSIMU framework. The user can setup a simulation by specifying the required modules for the transmit part, the channel and the receive part in the SimFile. The modular software concept allows configuration of the SpaceCommSIMU core and of individual modules. In the simulation file, the modules for the transmit part, the channel and receive part are listed together with individual parameters, such as the number of transmitted FECframes but also the transponder modulation or SNR can be specified. The simulation file is processed by the demonstrator at the beginning of the simulation to get the initial configuration of the specified scenario. A SimFile specifying a sample MUD scenario is provided in the appendix A.1.

6.2.2 Transmitter

The transmit part of the simulation contains the scheduler, two configurable transmitters, transmitter specific encoders as well as root-raised cosine (RRCos) filters. As specified by the DVB-S2X standard [2] the forward error correction (FEC) [51] is done via a concatenation of BCH [28] as outer code and LDPC as inner code. Despite of the early invention of the LDPC codes in 1962, as already mentioned, but did not gain acceptance at that time. Instead, turbo codes [52] were invented in 1993 and became the powerful coding scheme. MacKay however, re-discovered the LDPC [53] in 1997 and proved that its performance is comparable to the results achieved by turbo codes. Today, the LDPC is a well established in digital communication applications to improve the error correction capability.

The transmitter can be optionally equipped with IMUX and OMUX filters, as well as HPA nonlinearities. Additional interferers are linearly added to the transmitted signal according to the interference levels of the specified scenario.

6.2.3 Channel

All signals are transmitted over the common AWGN channel. In addition to the AWGN channel with modifiable SNR, also channel impairments such as phase noise as well as timing and frequency error can be added to the signal.

6.2.4 Receiver

Since the detection in the receiving unit is based on soft information, the bits have to be converted to hard bits, once the decoding is finished. The data analyzer evaluates the received data based on a cyclic redundancy check (CRC) and determines the performance in terms of frame error rate (FER).

If synchronization and parameter estimation is active, the amplitude and phase is provided to the MUD detector as input. Otherwise, ideally computed parameters are assumed.

The modular concept supports the use of different detector modules for the processing in order to analyze the performance discrepancies of different frequency reuse scenarios and reception techniques in individual simulations. However, at this point it needs to be mentioned that only a single detector module can be used per simulation.

6.3 Data Architecture

Throughout this framework, the data is organized in logical containers, where single or even multiple frames can be stored. These containers are structured in a header and a body. The purpose of the container header is to exchange information between the individual modules of the simulation. The container body carries the actual transmitted data that can be read, modified and written by each module. The variable size of the data containers allows storage of single FECframes, bundled frames as well as MUD structures. The structure of bundled frames consisting of FECframes is shown in Figure 6.3. Figure 6.4 demonstrates the data basis on which the detector and the decoder are operated. The detector works with bundled frames that contain the RX symbols and the extrinsic information of the LDPC as input while the LDPC exclusively operates on FECframes containing soft bits. A bundled frame (BF) contains several FECframes, as listed in Table 2.1, causing the LDPC to be executed several times per BF. The decoder is implemented with AVX2 for speed reasons, which enables the LDPC to process 32 FECframes in parallel. To solve this discrepancy in the data basis between detector and decoder, 32 BF are collected before the LDPC and their FECframes are processed sequentially in up to five iterations, in case of 32APSK. For this reason, 32 bundled frames are collected for the decoder that processes their FECframes sequentially.

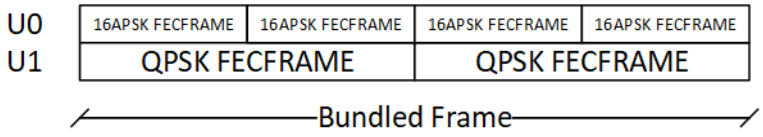

Figure 6.3: DVB-S2X concept of bundled frames (BF) for MUD, simplified version omitting pilots [12]

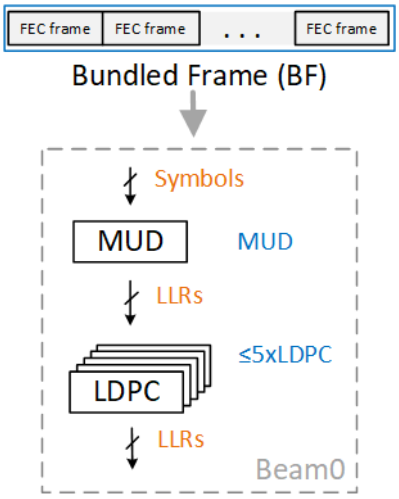

Figure 6.4: Data processing basis for MUD and LDPC [12]

6.4 System Architecture

The software is developed on Windows and compiled with the Intel compiler supporting the AVX2 command set. The demonstrator application was executed on Linux. To achieve a suitable processing speed for broad performance analysis of various MODCOD pair and interference combinations, the performance of a single computer with 4 cores was clearly not sufficient. The performance analysis in the final setup was executed on a grid of 24 computes providing 96 available cores. The grid setup enabled the achievement of a crucial processing time of approx. one hour for the computation of a single point at $FER = 10^{-6}$.

6.5 Scenario Configuration

The flexible software concept ultimately allowed to achieve the aim of supporting a single carrier simulation including additional interferers as well as a MUD scenarios. Adequate SimFile configuration was essential for this process including the use of different detectors, depending on the purpose of the application since a SimFile cannot support multiple detectors for a single scenario.

CHAPTER 7

Implementation

The development of the detector in the receiver was an iterative process. In the first iteration, the receiver was implemented as floating-point arithmetic in order to achieve high precision and with that, the best performance in terms of spectral efficiency. The low processing speed however, requested a more performant implementation allowing multiple simulations within shorter time for a broad performance analysis. Based on this request, the interface between detector and decoder was modified to bit-accurate (8-bit), allowing to operate the decoder with AVX2. The parallel processing feature brought a significant speed improvement leaving the detector as performance bottleneck. The aim to further reduce the decoder's processing time lead to the final successive interference cancellation (SIC) approach that was embedded into the MUD procedure. The details on these receiver versions are given in the course of this section.

7.1 Low-Complexity MUD Implementation

Implementing an interference mitigation technique to the receiving user terminal adds a lot of complexity to the receiver unit and calls for hardware-specific requirements to be fulfilled by the implementation. The aim is therefore to build a software-based system demonstrator for multi-user detection, while considering optimizations in terms of processing speed and obeying certain hardware requirements in view of a potential hardware prototype in the future. In order to achieve this aim, this process started with the implementation of a reference system based on floating-point arithmetic. Due to low processing speed results and hardware requirements to consider, it was decided to switch to an 8-bit integer interface in the first improvement phase. Having with that removed the bottleneck from the LDPC, the detector required further optimization to gain more speed which was done in a second improvement step, as shown in Figure 7.1 that lists the advantages (+), disadvantages (-) and status (•) of each implementation phase. The details on the individual speed improvement steps are outlined in the following.

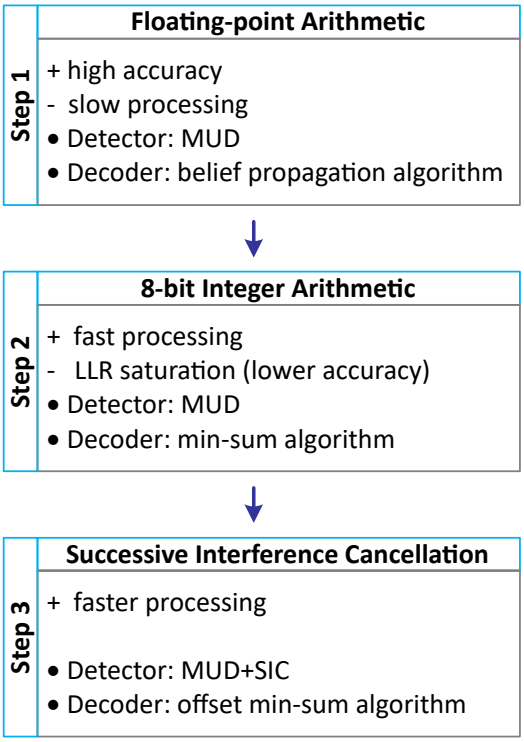

Figure 7.1: Implementation steps to increase the processing speed

7.1.1 MUD Floating-Point Arithmetic - Reference Implementation

It was decided to head for a floating-point arithmetic in the first instance in order to create a reference system and to evaluate the general MUD performance and its sensitivity to interference. The major advantage of a floating-point arithmetic is clearly the high accuracy of the achievable results, while accepting a very low processing speed. Due to this slow performance, an extensive MUD performance analysis was not feasible at this stage and it was decided to aim for a faster implementation, removing the bottleneck of the LDPC receiver that is operated with the belief propagation algorithm [50].

Along with the processing also the consideration of hardware requirements was a driving factor that called for an 8-bit integer arithmetic, which also allowed the use of the min-sum algorithm [54] for the LDPC.

7.1.2 MUD 8-bit Integer Arithmetic

The first version of the detector and decoder processing chain was implemented in floating-point arithmetic in order to verify the demonstrator performance. The main advantages of the float implementation are the high accuracy of the calculations and the data range for the algorithmic computation. Besides the strong benefits, there is a major disadvantage of this implementation, which is the processing speed. Since a reasonable processing speed is definitely a requirement in order to investigate

different effects, this was the driving factor for a new implementation based on a 8-bit interface between the MUD and LDPC blocks. The 8-bit interface, shown in Figure 7.2, enables the LDPC to be operated with the AVX2 command set improving the processing speed of this block significantly. Due to this modification the joint detector, processing becomes the bottleneck for the processing speed. The 8-bit implementation also brings another drawback which is the heavily limited data range that often leads to saturation effects.

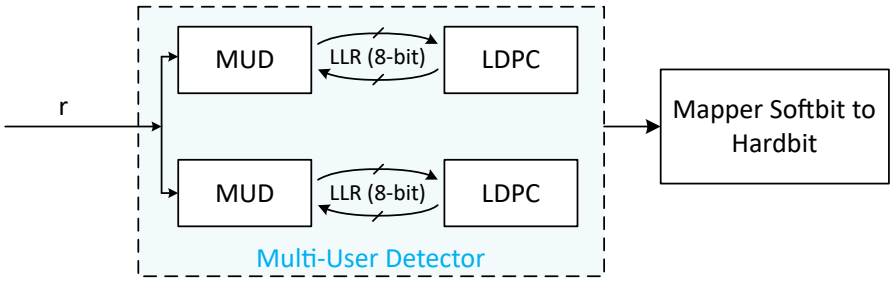

Figure 7.2: 8-bit interface between detector and decoder [12]

The LLRs exhcanged by the detector and decoder are much faster saturated than in the float implementation, causing the loss of some sensitivity in the MUD detector.

This raises the question why it is still relevant aiming for an 8-bit implementation despite these mentioned drawbacks.

The MUD technique is an algorithm intended for execution at the user terminal that receives the signal on ground. User terminals do not come with unlimited computational power and are strictly cost-limited for obvious market reasons. Off-the-shelf receivers are equipped with field programmable gate arrays (FPGAs) and application-specific integrated circuits (ASICs) that do not offer floating-point precision, as a CPU does. These devices are optimized for power and cost efficiency, while offering limited computational precision.

The process of developing algorithms for a hardware device usually starts with a high performing algorithm with floating-point precision. This algorithm is then implemented with limited precision in order to build a model for the hardware, investigating the effects that occur due to limited precision. The next step would be a hardware implementation and a performance evaluation based on the software model.

This work however, rather focuses on the first two activities since the hardware implementation and its performance evaluation is beyond the scope of this work.

7.1.3 MUD Enhanced by Successive Interference Cancellation

The MUD enhanced by successive interference cancellation (MUD+SIC) approach in Figure 7.3 is an attempt to speed up the processing time. MUD is a symbol based algorithm and the MUD+SIC approach benefits from this fact. This approach describes the principle where MUD is executed as long as none of both symbols (the symbol from B_0 and the time-wise fully overlapping symbol of B_1) is fully decoded. In the context of MUD+SIC this means that the LLRs are not saturated. Once all the soft bits of a single symbol for one of both signals are detected with highest certainty (all LLRs are saturated), this symbol is flagged and consequently not any longer considered for MUD, as demonstrated in Figure 7.4.

The detected bits are converted to hard bits, mapped to a symbol and this information is subtracted from the originally received symbol. If the detected symbol originated from the main carrier, the remaining signal is amplified by the C/I_1 level and the remaining information is also mapped to a symbol having conditions comparable to a single carrier mode since the remaining interferers are relatively small. For the impaired system, the impairments are of course also in the MUD+SIC performance notable as degradation.

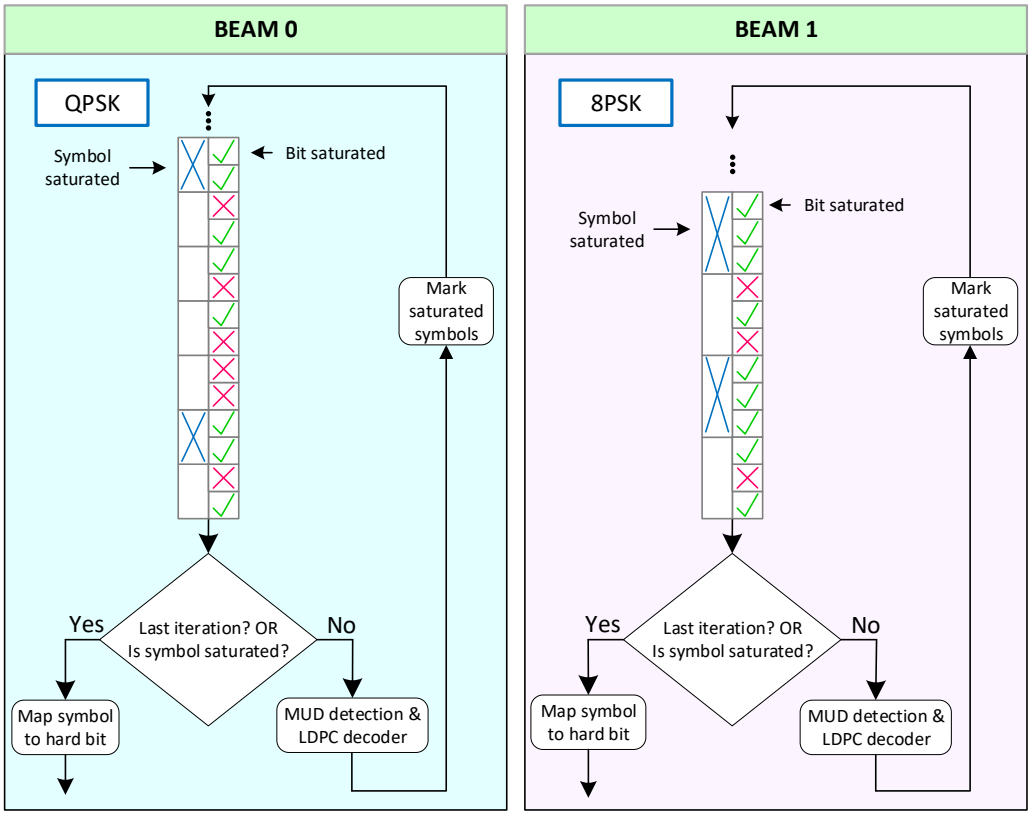

Figure 7.3: Successive interference cancellation (SIC) block diagram, based on [12]

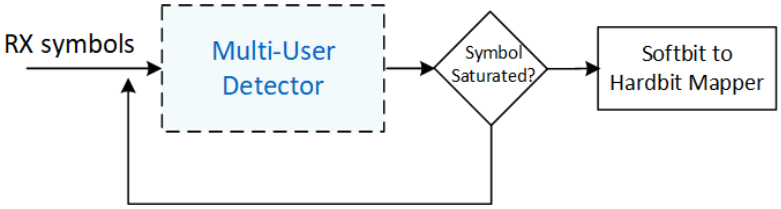

Figure 7.4: In the MUD+SIC concept, the mutli-user detection is only mandatory in the first iteration and is then only employed, once the LLRs are not saturated [12]

Certainly not every symbol pair that was transmitted at the same time instant by the main carrier and strongest interferer will enter the MUD+SIC mode. Nevertheless, with each MUD iteration it becomes more likely that additional symbols become flagged and excluded from the MUD process. This principle results in the situation that with each iteration the number of bits to be investigated decreases, leading to shorter processing times.

7.2 MUD Data Structure

MUD is executed on the unit of DVB-S2x bundled frames (BF) since they provide the mandatory constant frame length for this process. The MUD container, shown in 7.5, represents a MUD-specific data structure that was introduced to manage the data within the joint detection process. A MUDcontainer starts with the sequence of received complex symbols, concatenates then the LLRs of the main carrier, transmitted by B_0, the LLRs of the first interferer, transmitted by B_1, and has a field for temporary storage of the detector output which can be used by the individual beams. Concatenated to this data sequence are the resulting LLRs after the detector for B_0 and B_1 respectively, to determine the extrinsics after the decoder. The decoder reads the resulting LLRs and updates this field with its own LLR results, since this information is used as final result, once the early stop criterion becomes valid.

The structure of a single MUDcontainer is illustrated in Figure 7.5, where the length is indicated as a function of the BF length N and the modulation order $[bit/symbol]$:

- RX ($2 \cdot$ BF length (real and imaginary part))
- LLR0 (modulation order $\cdot$ BF length)
- LLR1 (modulation order $\cdot$ BF length)
- MUD_{output} (max(LLR0 length, LLR1 length))
- $LLR0_{result}$ (LLR0 length)
- $LLR1_{result}$ (LLR1 length)

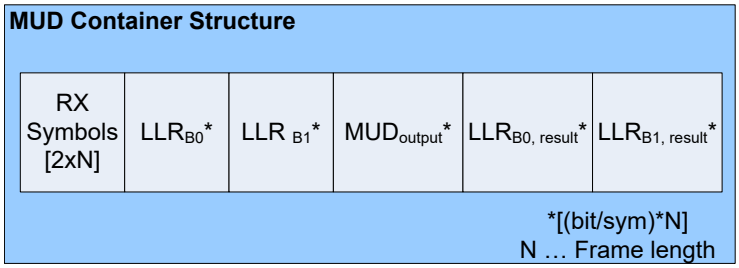

Figure 7.5: Data structure for the handling of the internal data in the joint detection and decoding process, denoted as MUDcontainer

7.2.1 MUD AVX2 Interface Management

Utilizing a decoder based on AVX2 for faster processing, required the modification of the interface. The major benefit of AVX2 is the fact that 32 values can be processed in parallel. For this reason the interface management in Figure 7.6 was implemented. The contrasting demand between detector and decoder is handled in a way that the demonstrator generates a new FECframe (abbreviated in Figure 7.6 with FF) in the transmit part in each iteration.

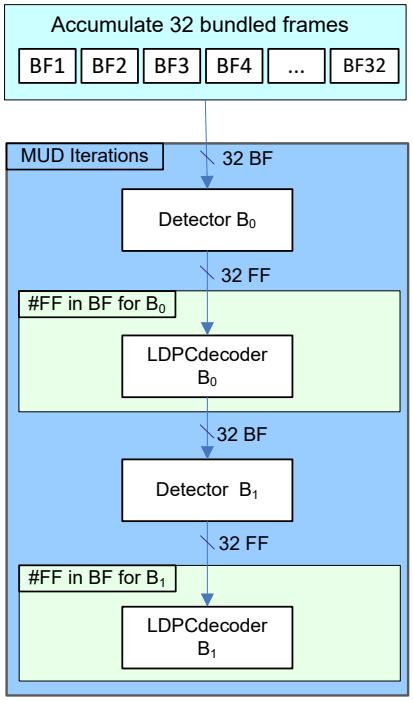

Figure 7.6: MUD interface description

The FECframes are grouped to DVB-S2X BFs using the specific transponder settings and get stored in a MUDcontainer structure for easier data handling. A

module at the beginning of the receive part collects the incoming bundled frames and once 32 BFs are collected and concatenated together to a structure shown in Figure 7.7, the MUD processing is started. The detector operates on BF and processes the 32 BF sequentially while the LDPC processes 32 FF in parallel. For this reason the decoder module of a single user is invoked for each FF contained in the bundle, where the number of FF in a BF is determined by the modulation used by the specific beam.

The same procedure is repeated for the decoding and detection of the data transmitted by the beam representing the strongest interferer.

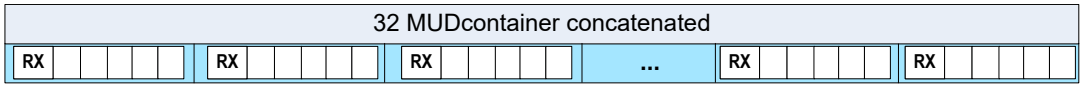

Figure 7.7: 32 MUD data structures (here denoted as MUD bundled frames) concatenated for further processing

7.2.2 MUD Memory Consumption

The worst case memory consumption for MUD is estimated based on the following assumptions:

- Normal frames
- 32APSK modulation
- MAC-MUD

Based on the MUD container memory consumption scenario in Table 7.1 and considering an implementation requiring one byte per value and 32 MUD frames in parallel for AVX2 processing, results in a total memory requirement of $2.4 Mbyte \cdot 32 = 76.7 Mbyte$ per MUD container.

Parameters	Amount
Received symbols	64800 (complex, consisting of 2 values) $= 2 \cdot 64800$
LLRs	$3 \cdot 5 \cdot 64800$
LLRa	$5 \cdot 64800$
LLRs for the final result	$3 \cdot 5 \cdot 64800$
Total	$37 \cdot 64800 = 2.4$ million floats

Table 7.1: Worst case memory consumption for a single MUD container

7.3 Early Stop Criterion

When optimizing the processing speed, avoiding unnecessary iterations and thus, reducing the average amount of iterations is of utmost importance. The term "unnecessary" in this context denotes iterations that do not result in an information gain, which calls for the introduction of an early stop criterion [55]. The implementation of an early stop criterion allows aborting the execution before the specified number of iterations has been reached under the condition that a certain condition is met. Since the use of an early stop criterion for the LDPC is well established, a similar criterion is desirable for the MUD process.

In this work, the LDPC early stop criterion is based on the parity check constraints [56]. The early stop criterion is met, if the syndrome is zero and thus, a valid code word has been found. If this condition is met by the LDPC, the iterative process is safely aborted even if the specified number of iterations is not yet reached.

Aiming to diminish also the processing time of the multi-user detector, the early stop criterion concept of the LDPC decoder was used as indicator for the introduced MUD early stop criterion. Utilizing the information provided by the early stop criterion is also essential information for the detection process since further iterations do not provide more information, once a valid code word was already identified. A single MUD iteration includes the execution of both decoders and therefore the MUD early stop criterion can only be fulfilled if both decoders independently report that their early stop criterion was met. In this case the MUD iterative processing can be aborted since further iterations will not lead to an information gain and the soft bits can be converted to hard bits for further processing.

If only one of the decoders report the detection of a valid code word, the MUD iteration continues since the other detector still requires more information to detect the signal and therefore an early stop of the MUD iterative process is not allowed under these circumstances.

7.4 Processing Performance

The performance of the MUD system demonstrator is evaluated comparing the three implementation stages. The actual performance is assessed in terms of frame error rate, the achieved system processing speed [frames/s] and the number of MUD and LDPC iterations. After the evaluation results the performance critical parameters are identified.

7.4.1 Frame Error Rate (FER) Performance

Before improving the processing speed, a reference implementation based on floating point LLRs using the belief propagation (BP) LDPC [50] was preferred to quantify the performance of the following speed optimized implementations. With the switch to the 8-bit integer arithmetic as interface between detector and decoder, the decoder was replaced by a decoder operating on an AVX2 construction set using the min-sum (MS) algorithm [57]. Since the BP and min-sum algorithm are not identical in the

performance, a degradation in the order of approx. 0.1 dB was sacrificed for the speed gain that was achieved by this switch caused by the lower complexity and the fact that the min-sum algorithm is hardware-efficient [58]. The introduction of the MUD+SIC concept actually does not affect the FER performance but it was introduced together with an LDPC upgrade to offset min-sum [54] which reduced the degraded performance w.r.t. to BP. This effect is also visible in the FER performance comparison shown in Figure 7.8.

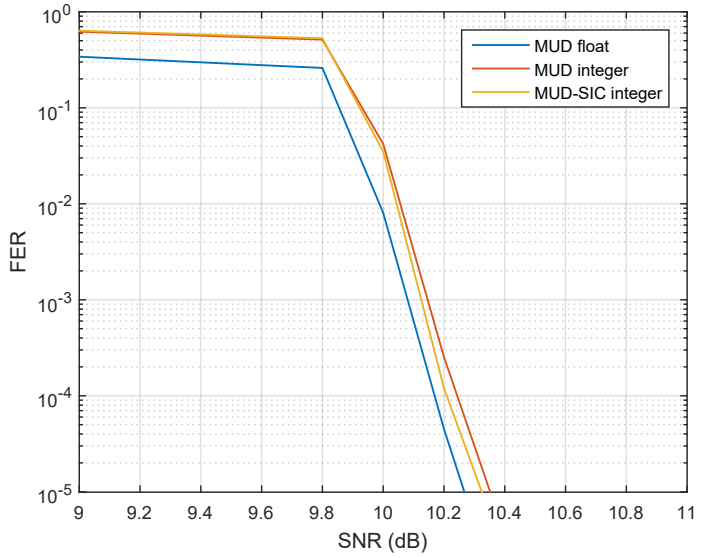

Figure 7.8: FER performance analysis for different implementation levels comparing the floating-point interface with the 8-bit interface and the 8-bit MUD+SIC approach [12]

7.4.2 Performance Speed

When analyzing the processing speed of a joint multi-user detection it is necessary to remember that both carriers do not necessarily need to reach the FER waterfall region at the same time. The processing speed in general depends on the selected MODCOD and frame length since higher modulations and longer frames are more complex and therefore require increased processing time. In general, the speed increases with lower FER. For a scenario where both carriers are not detected in the same SNR range, this means that the processing speed increases moderately until the first carrier was detected successfully. The maximum processing speed is reached, once both carriers are successfully detected by the joint detection algorithm.

The processing speed comparison of the individual implementation levels is shown in Table 7.2. The carrier-specific processing speed performance of the implementation variants is compared at FER $= 10^{-5}$ with a single 4-core computer. The results of boths carriers clearly demonstrate the significant speed gain due to the switch of

the 8-bit interface. As expected, the second speed improvement by the introduction of MUD+SIC is less impressive but shows that excluding reliable symbols from redundant MUD processing brought an valuable additional speed gain.

Based on the speed processing results, it was decided to select the MUD+SIC method using offset min-sum for the MUD performance tests. For this reason the reference float and 8-bit implementation will not be considered for the iteration performance analysis.

Performance analysis	Carrier of Beam 0		Carrier of Beam 1	
	Processing speed [frames/s]	Channel throughput [Mbit/s]	Processing speed [frames/s]	Channel throughput [Mbit/s]
MUD float	4.6	0.8	60.0	1.0
MUD integer	83.1	1.4	273.2	4.4
MUD+SIC integer	111.4	1.8	301.7	4.9

Table 7.2: Beam-specific processing speed comparison of the different implementation variants [12]

7.4.3 Number of Iterations

A single joint multi-user detection iteration calls the detector and decoder twice, once for each carrier. The processing speed is therefore largely determined by the number of iterations of the detector and decoder. In literature the maximum number of detector iterations varies between 2 and 50, as in [9] and [31] respectively, whereas the number of maximum LDPC iterations per FECframe was set to 200 to be more robust against error floors at $FER = 10^{-6}$, as recommended by [57]. This fact motivates the analysis of the actual required number of iterations for detector and decoder operated with early stop. For this purpose, the detector iterations were analyzed for different numbers of maximum iterations. The result, illustrated in Figure 7.9, compares the combined FER of both carriers performance (to the left) with the number of average iterations (to the right). It can be concluded that reducing the number of MUD iterations degrades the FER performance since only in few cases the full number of MUD iterations is apparently required to decode the carrier. Nevertheless, the performance degradation is in a range of less than 0.1 dB, which is minor.

The number of required LDPC iterations is evaluated based on three scenarios with different MODCOD pairs:

(a) QPSK 1/2+ 8PSK 3/4 (black)

(b) QPSK 2/3 + 16APSK 8/9 (magenta)

(c) QPSK 2/3 + 32APSK 8/9 (blue)

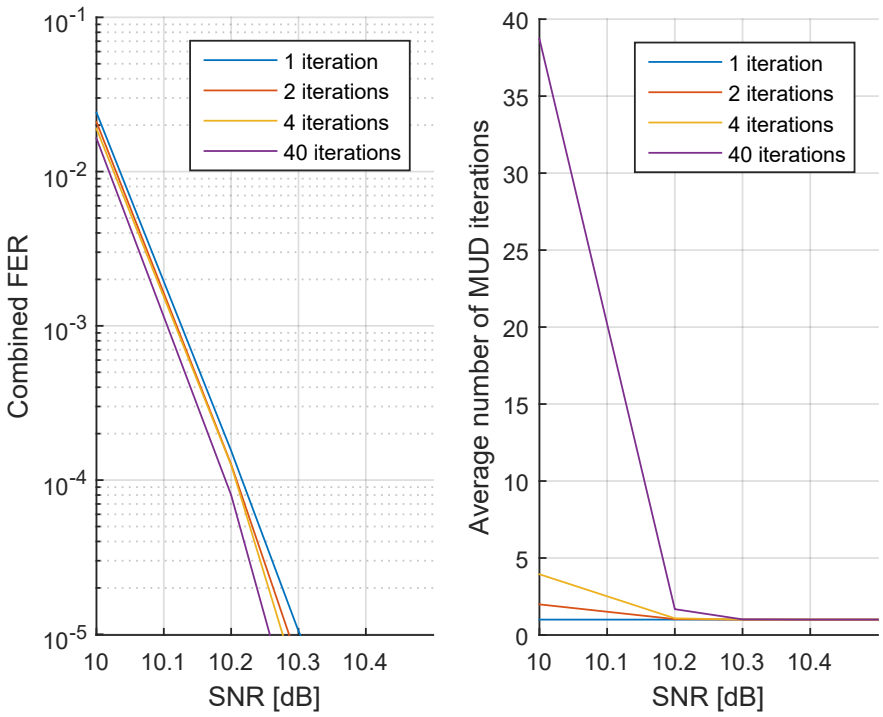

Figure 7.9: FER performance analysis for different numbers of MUD iterations [12]

Selecting a maximum number of 200 iterations per FECframes with active early stop criterion, the three examples very well demonstrate the total number of LDPC iterations per single MUD iteration on average. With the introduced setting and the number of FECframes in a bundled frame per modulation as shown in Figure 7.10, the maximum number of iterations per MUD iterations for each scenario is detailed in Table 7.3.

The obtained results show that the maximum number of iterations is only achieved at a high FER of 1. The number of iterations however, drops together with the FER because the LLRs get more reliable. The flat zone in the FER performance of the black scenario configuration is caused by the fact that the combined FER is illustrated in the chart and both carriers are detected at different SNR values.

At a FER of 10^{-5} it is interesting to see that all three scenarios, independent of their maximum number of iterations per MUD iteration, are well below 200 iterations.

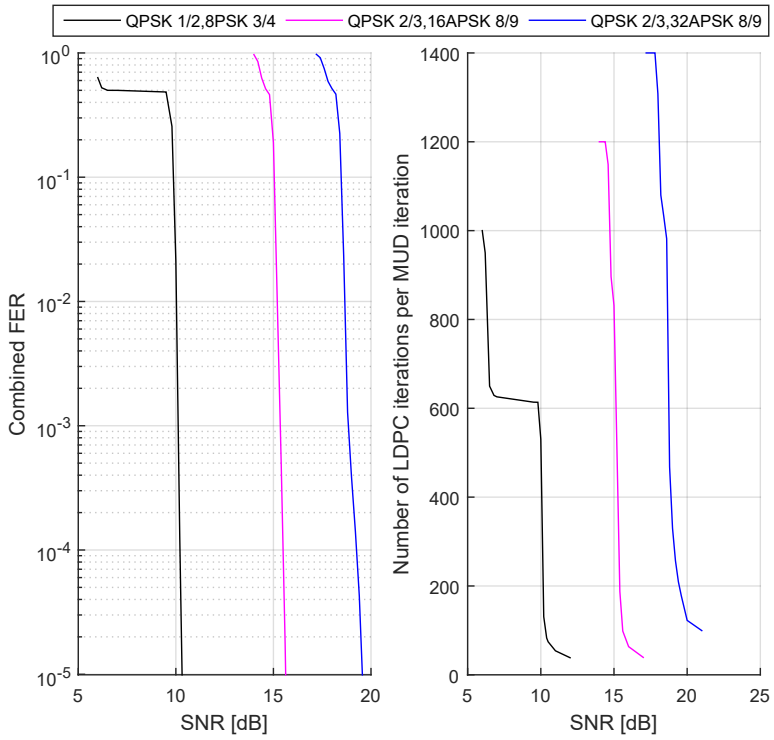

Figure 7.10: FER performance analysis for different numbers of LDPC iterations [12]

Scenario	MODCOD pair	Number of FECframes	LDPC Iterations per FECframes	Total Number of LDPC Iterations
a	QPSK + 8PSK	2 + 3	200	1000
b	QPSK + 16APSK	2 + 4	200	1200
c	QPSK + 32APSK	2 + 5	200	1400

Table 7.3: Total number of LDPC iterations for the assumed scenarios

Based on these findings it can be concluded that the processing speed is especially in the region of interest at FER $= 10^{-5}$ and lower, very fast compared to high FER rates of FER $= 1$ and does not significantly depend on the selected MODCOD pair.

7.4.4 Critical Performance Parameters

The following parameters have been identified as the leading factors that have a major impact on the system performance in terms of processing speed:

- Number of iterations (MUD, LDPC)
- Early stop active (MUD, LDPC)
- Frame length (short, normal)
- Modulation (B_0, B_1)
- MODCOD pair (QEF FER of B_0 and B_1)
- MUD algorithm (float, 8-bit)
- Number of cores (single computer, grid)

Summarizing, it can be said that the number of iterations of MUD and, consequently also the LDPC, does not only affect the processing speed but also the achieved FER performance.

Another aspect that influences the processing speed is the frame length and the chosen modulation. It can be observed that processing of normal frames is significantly slower than short frames due to the increased number of symbols. High order modulations such as 16APSK for example further slow down the processing.

MUD is characterized by the fact that information is gathered from interfering signals. Assuming a MODCOD pair with significantly different QEF performance transmitted by B_0 and B_1, where B_1 transmits a higher order modulation MODCOD, the detection and decoding of the carrier transmitted by B_0 requires significantly more processing time than the one transmitted by B_1. This fact can be explained by the available amount of reliable information in the system. At the beginning of the MUD process, it takes a longer time to determine reliable LLRs. Once one of both signals is fully decoded, the process for the second carrier is noticeably increased.

Of course not only the input and parameter setting for an algorithm but also the implemented version of the algorithm as such, makes a difference in this respect. The MUD algorithm operating on floating-point, while providing higher precision, is many times slower than its 8-bit counterpart, since parallel processing is not supported for this data type. Ultimately, also the hardware is an important factor in terms of processing speed, since a higher number of cores is always favoured but represents due to cost reasons obviously not the first step in the speed optimization process.

CHAPTER 8

Impairments

The effects that cause notable impairments in the system performance [13] such as nonlinearities in the satellite and the phase noise contributions by the user terminal radio frequency front-end are the topic of this section. Especially for modulations higher than QPSK the impact on the receiver performance becomes significant. Synchronization with parameter estimation adds only a small constant performance offset and due to the importance of the parameter estimation for the detector, this topic is shortly discussed in this chapter as well.

Signal attenuation caused by tropospheric events and especially rain [59], which contributes most in this frequency range, are considered only for scenarios with active ACM.

8.1 Synchronization and Parameter Estimation

Synchronization and parameter estimation [60], [61] are of utmost importance in a satellite communication system, and especially for multiple user application [62]. The amplitude and phase parameter estimations for each of the carriers to be detected are crucial inputs for the multi-user detector in the receiving unit. In [13] the synchronization and parameter estimation process is detailed for DVB-S2(X) applications, operating on the superframe format.

As outlined by [13], clock and carrier frequency errors are impairments that are induced by the receiver equipment. Instabilities of the oscillator lead to clock frequency errors that are provided to the demodulator sampling clock in the receiver. The precision of the oscillator is usually in direct relation with its cost. The major cause for carrier frequency errors is the LNB oscillator instability of the receiver. These two errors are compensated by the synchronization implemented in the receiver terminal that generates a constant but small performance impairment, irrespective of the presence of an error that needs to be corrected. Given that a present error is within the correctable range of the synchronization, the impairment is typically in the range of 0.1 to 0.2 dB.

The synchronization process is started by a coarse frequency recovery, where large frequency offsets have to be recovered with a non data aided (NDA) algorithm, e.g. quadri-correlator [63] or [64], before the matched filter (MF). After that the initial acquisition is executed that operates on superframe symbol sequences SOSF, pilot fields, PLH and P2, as defined in the DVB-S2X standard. First, the frame and time synchronization [65] is done in a correlation process utilizing the orthogonality of the WH codes in the SOSF field of the individual carriers.

The residual frequency error after the quadri-correlator is then compensated using a feedforward algorithm, like [66], [67] and [68] or the approach by [68] and [69] at very low SNR levels. Once the impairments are compensated, the carrier phase and signal amplitude can be computed. These estimates are then provided as input to the multi-user detector. Once the acquisition is completed, persisting residual carrier phase and timing errors need to be compensated throughout the frame. At this point data aided (DA) algorithms can be applied for joint detection of both parameters.

The amplitude and phase parameter estimations for each of the carriers to be detected are crucial inputs for the multi-user detector in the receiving unit. If the synchronization is not active, the ideal values can be used by the system demonstrator instead. The quantization of performance degradation induced by the estimation of both channel parameters was tested comparing the performance obtained with estimated and ideal channel excluding additional interferers in the system. The performance comparison result, quantifying the degradation is addressed in Chapter 9.2.2.

Especially for applications that rely on reliable SNR estimates, like ACM that adapts of the link in form of a MODCOD switch is executed, it is required to be able to detect when the SNR level is decreasing. DVB-S2(X), for instance, is able to switch the modulation scheme on a frame-by-frame basis. SNR estimation methods [70] are therefore required in this case.

8.2 Nonlinearities

The typical transfer characteristic of a travelling wave tube amplifier (TWTA) onboard of a satellite [5], shown in Figure 8.1, provides the output power and phase as a function of the input power. Aiming to avoid nonlinearities the operation point is required to be selected in the linear region of the curve requesting an adequate input and output power back-off (IBO, resp. OBO).

In the following the total degradation (TD) and OBO, as a function of the IBO, is provided for the single carrier case considering the modulations QPSK, 8PSK, 16APSK and 32APSK in Figure 8.2, Figure 8.3, Figure 8.4 and Figure 8.5.

The measurement of the TD allows the identification of the IBO and OBO that minimize the total degradation and are thus the optimum setting for the specific MODCOD or MODCOD pair in case of MUD.

The total degradation can be determined as

$$TD\,[dB] = OBO\,[dB] + Loss\,[dB]. \tag{8.1}$$

The loss in this case denotes the degradation with respect to the unimpaired (ideal) performance.

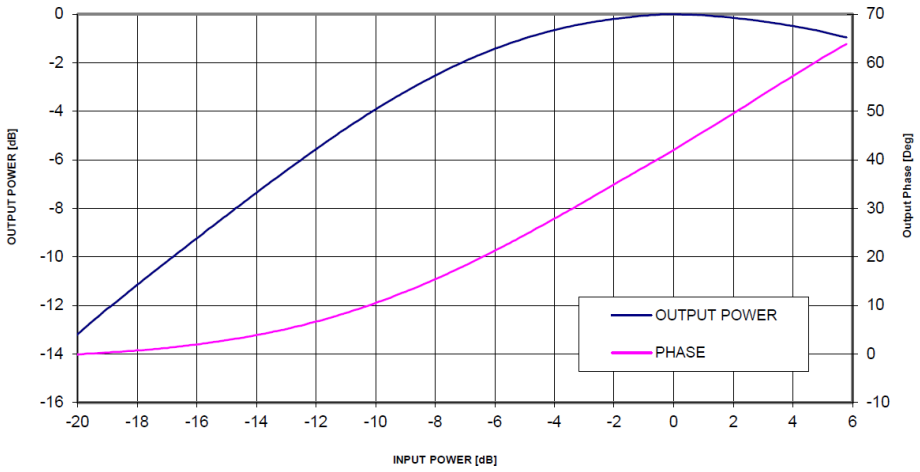

Figure 8.1: Ka-band travelling wave tube amplifier (TWTA) amplitude and phase response model of the single carrier transfer characteristics [5]

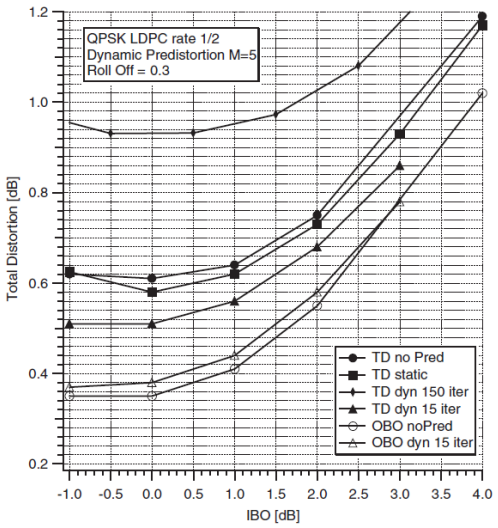

Figure 8.2: Total degradation performance for QPSK [13]

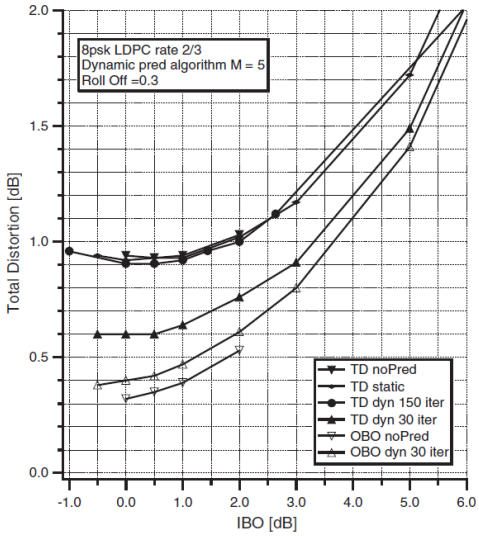

Figure 8.3: Total degradation performance for 8PSK [13]

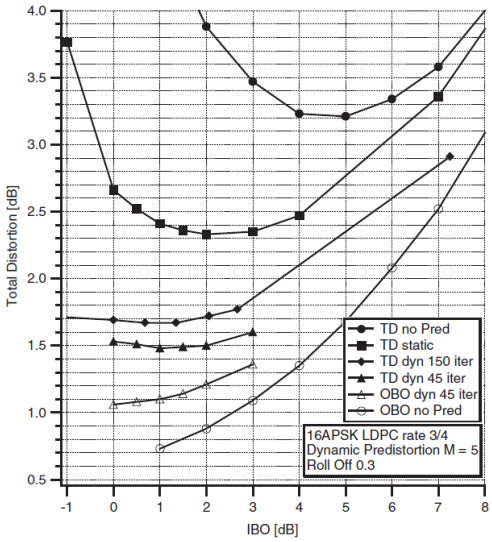

Figure 8.4: Total degradation performance for 16APSK [13]

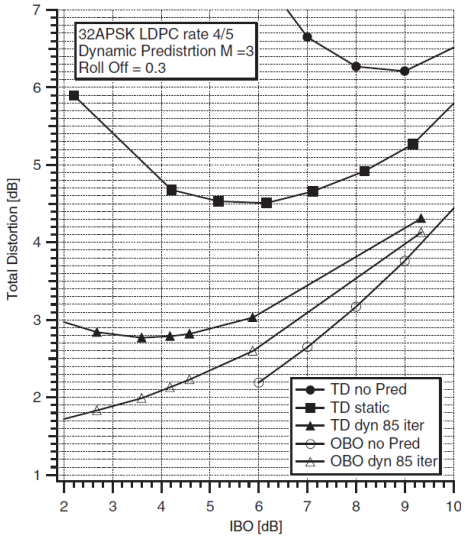

Figure 8.5: Total degradation performance for 32APSK [13]

Similar charts were generated for MUD MODCOD pairs in order to assess the effect of nonlinearities on them and compute the TD. The obtained MUD TD curves for 8PSK and 16APSK are shown in Figure 8.6 and Figure 8.7, with their respective numerical results provided in Table 8.1 and Table 8.2.

For the purpose of the MUD performance analysis considering impairments, an OBO of 1.45 dB suitable for 16APSK was chosen. The total degradation (TD) chart for 32APSK was shown here for the sake of completeness, but this modulation was excluded from the analysis, as already mentioned, since linear pre-distortion would be required in this case.

The test with MUD setup also revealed that not all MODCOD pairs are suitable to generate total degradation curves, since some do not drop in FER despite the selection of high IBO. Comparing for instance the performance of the following two MODCOD pairs:

(a) QPSK 3/5 + 16APSK 4/5

(b) QPSK 1/2 + 16APSK 4/5

The first pair (a) reaches low FER with IBO = -6 dB but not at -4 dB. The increase of SNR does not further decrease the FER since the performance is interference limited. For the second MODCOD pair (b) however, a total degradation performance can be computed up to an IBO of -1 dB. This finding leads to the conclusion that impairment specific MODCOD pairs need to be selected based on their spectral efficiency.

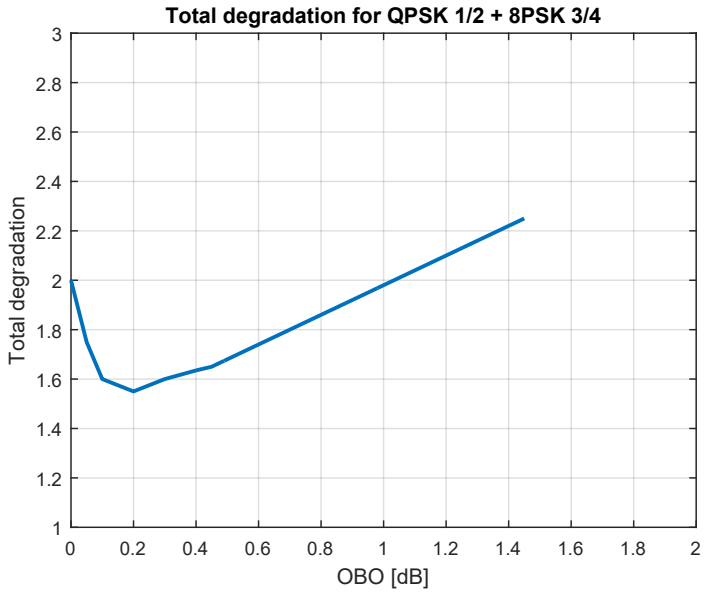

Figure 8.6: MUD total degradation (TD) performance for QPSK + 8PSK

Ideal SNR @FER 10^{-2} **[dB]**	**IBO [dB]**	**SNR@FER** 10^{-2} **[dB]**	**OBO [dB]**	**loss [dB]**	**TD**
10.3	-6	11.1	1.45	0.8	2.25
10.3	-3.2	11.5	0.45	1.2	1.65
10.3	-3	11.55	0.4	1.25	1.635
10.3	-2.7	11.6	0.3	1.3	1.6
10.3	-2	11.65	0.2	1.35	1.55
10.3	-1	11.8	0.1	1.5	1.6
10.3	-0.5	12	0.05	1.7	1.75
10.3	0	12.3	0	2	2

Table 8.1: MUD total degradation (TD) numerical results for QPSK + 8PSK

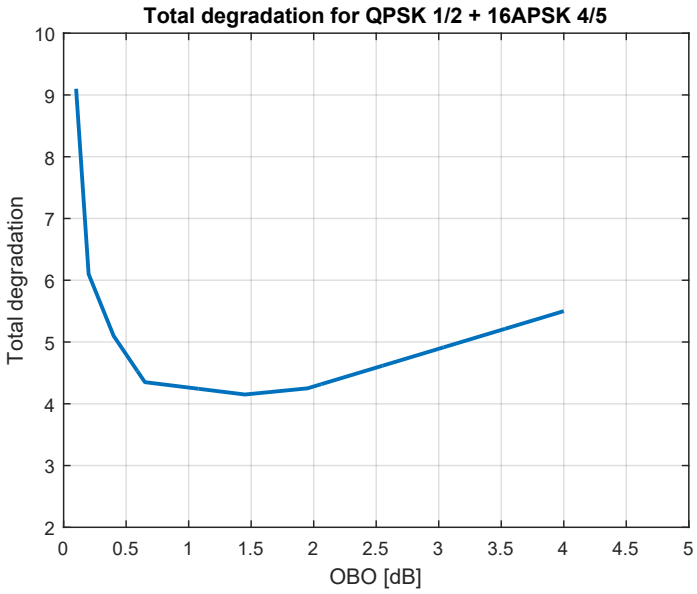

Figure 8.7: MUD total degradation (TD) performance for QPSK + 16APSK

Ideal SNR @FER 10^{-2} **[dB]**	**IBO [dB]**	**SNR@FER** 10^{-2} **[dB]**	**OBO [dB]**	**loss [dB]**	**TD**
13	-10	14.5	4	1.5	5.5
13	-7	15.3	1.95	2.3	4.25
13	-6	15.7	1.45	2.7	4.15
13	-4	16.7	0.65	3.7	4.35
13	-3	17.7	0.4	4.7	5.1
13	-2	18.9	0.2	5.9	6.1
13	-1	22	0.1	9	9.1

Table 8.2: MUD total degradation (TD) numerical results for QPSK + 16APSK

8.3 Phase Noise

The radio frequency (RF) front end of the receiver is the main contribution to phase noise. Similar as the situation with the clock frequency and carrier frequency error, also the phase noise contribution is usually directly linked with the hardware cost, since low cost LNB RF oscillator usually show a significant increase in phase noise compared to high precision equipment [13]. For impairment analysis including phase noise, the VSAT-P2 phase noise mask [14] in Table 8.3 is applied.

Mask	10 Hz	100 Hz	1 kHz	10 kHz	100 kHz	1 MHz	10 MHz	≥50 MHz
VSAT-P2 mask SSB [dBc/Hz]	-32.93	-61.96	-78.73	-88.73	-94.83	-105.74	-115.74	-117.74

Table 8.3: VSAT-P2 [14] phase noise mask [dBc/Hz]

8.4 Input and Output Multiplexer

The input multiplexer (IMUX) and the output multiplexer (OMUX) are two filters installed on board of the satellite that define the transponder bandwidth, the transponder spacing and therefore indicate the center frequency distance of adjacent transponders [14].

Their filter characteristics that are considered for a realistic MUD performance are provided in Figures 8.8 and 8.9 for the IMUX and Figures 8.10 and 8.11 for the OMUX.

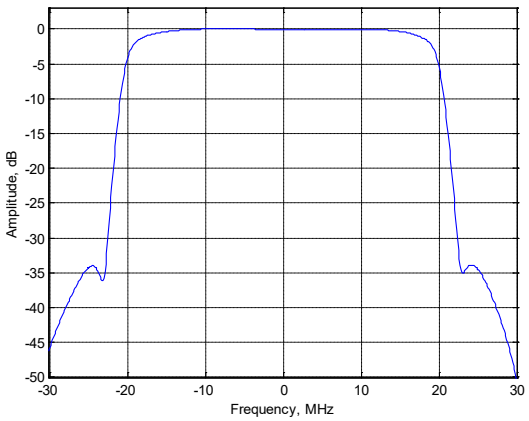

Figure 8.8: IMUX amplitude mask [14]

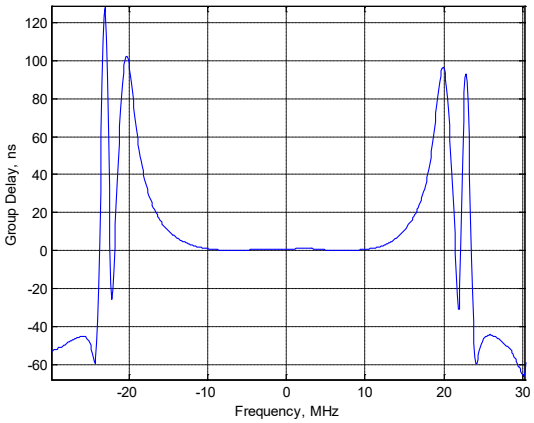

Figure 8.9: IMUX group delay mask [14]

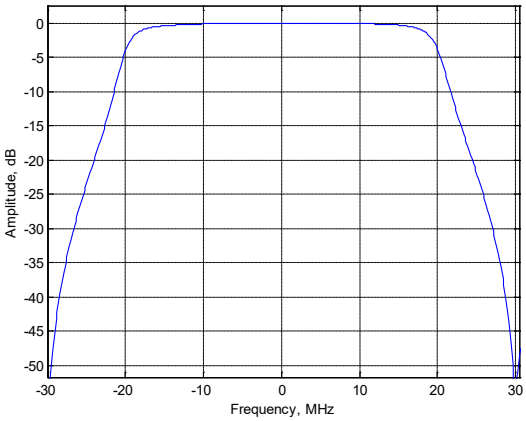

Figure 8.10: OMUX amplitude mask [14]

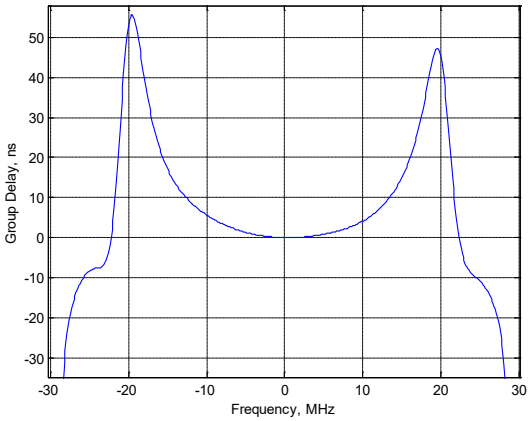

Figure 8.11: OMUX group delay mask [14]

8.5 Tropospheric Attenuation

Assuming a Ka-band user downlink in a HTS system, the strongest contribution to the tropospheric attenuation in this frequency range of 20 GHz is caused by rain. Models provided by the International Telecommunication (ITU) were used to calculate location specific rain attenuation statistics.

The model for the computation of a location specific rain attenuation statistics is provided by the ITU Recommendation ITU-R P.618 [17]. This model is dedicated to the computation of slant path long term rain attenuation statistic for a frequency range up to 55 GHz and requires a set of input parameters, listed in Table 8.4.

Parameter	**Description**
$R_{0.01}$	Location specific point rainfall rate [mm/h] for 0.01% of an average year
h_s	Station height [km] above mean sea level
Θ	Elevation angle [deg]
ϕ	Latitude of the station [deg]
f	Frequency [GHz]
R_e	Earth's effective radius (8500km)

Table 8.4: Input parameters for the computation of the location specific rain attenuation [17]

The station height of a UT above mean seal level is an essential input parameter for the computation of the rain attenuation complementary cumulative distribution function (CCDF). Therefore, to determine the station heights of random UT positions in the coverage area, the numerical map provided by the Recommendation

ITU-R P.1511 [71] were utilized. Similarly, also the location specific rain rate is determined from the data provided by the Recommendation ITU-R P.837 [72], as well as the rain height at the location of interest, which is another parameter that is computed within the model, is obtained from the ITU Recommendation ITU-R P.839 [73].

Once the required parameters are determined, the rain attenuation can be computed in a step-by-step procedure starting with the slant path length below the rain height, which is then converted to the horizontal projection for further steps. Then the specific rain attenuation is computed based on frequency-dependent coefficients. After the effective path length is known, it can be used to calculate the attenuation at a certain location that is exceeded for a certain percentage of time. This method consequently provides attenuation values for the CCDF percentages in the range from 0.001% to 5% of the year. For such applications percentages beyond 5% are in practice considered as 0 dB attenuation.

CHAPTER 9

Performance Results

This chapter adresses the MUD performance starting with a spectral efficiency performance study of MAC-MUD that resulted in interference-specific performance tables for short and normal frames, as specified in [2]. In addition to that, the MUD sensitivity is evaluated w.r.t. different factors such as the number of iterations, the interference levels as well as the degradation due to channel estimation imprecisions. Since various combinations of transmission and reception techniques are applicable at FR-2, different scheduling approaches were investigated and finally, the peak performance for MAC-MUD as well as the average system performance results w.r.t. average spectral efficiency and average system throughput are presented.

9.1 MUD Achievable Spectral Efficiencies

For the selected interference scenarios in FR-2 (see Table 3.1) all possible MODCOD pairs covering QPSK, 8PSK and 16APSK were examined in order to obtain the interference scenario specific spectral efficiency envelope evaluated at FER = 10^{-5}. This analysis was made for an ideal setting assuming MAC-MUD only, first without and then including the consideration of channel impairments in order to study the performance characteristics of MUD in an interfered system. To get the full picture, this evaluation was done for short and normal frames, resulting in MAC-MUD performance tables indicating the optimum MODCOD pair that achieves the highest spectral efficiency for a given interference scenario and C/N. The parameter setting considered for this evaluation including impairments is listed in Table 9.1.

Figure 9.1 to Figure 9.6 provide the spectral efficiency performance of MUD for short frames. The shown curves represent the spectral efficiency envelope performance of the following scenarios:

a) MUD floating-point implementation, without impairments [9] (blue markers)

b) MUD 8-bit implementation, without impairments (red markers)

c) MUD 8-bit implementation, including impairments (yellow markers)

Parameter	Setting
LDPC	offset min-sum
LDPC max iterations	200
MUD max iterations	4
Early stop	active
IBO (OBO) [dB]	-6 (1.45)
Phase noise mask	VSAT_P2
Frequency error	0.001

Table 9.1: Parameter setting for the spectral efficiency performance analysis

Due to the faster processing speed, only short frames are considered for the further performance assessments in this document. The complete numerical tables of the obtained results for normal and short frames are provided in the appendix A.2.

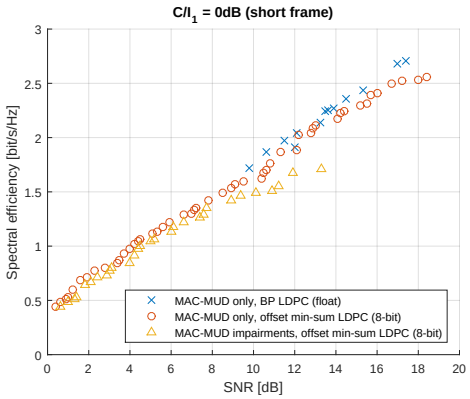

Figure 9.1: Spectral efficiency obtained for $C/I_1 = 0\,dB$, short frames [8]

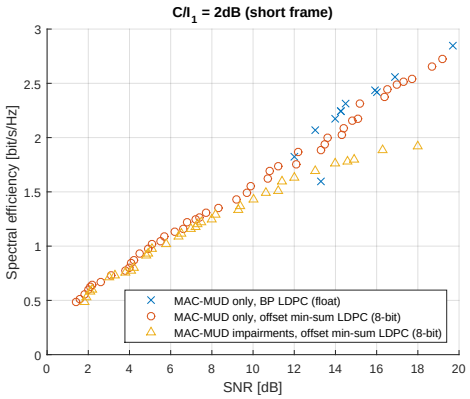

Figure 9.2: Spectral efficiency obtained for $C/I_1 = 2\,dB$, short frames [8]

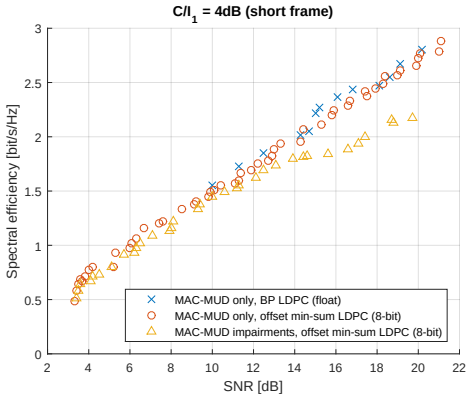

Figure 9.3: Spectral efficiency obtained for $C/I_1 = 4\,dB$, short frames [8]

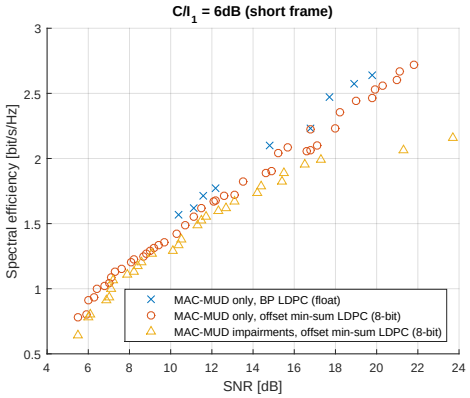

Figure 9.4: Spectral efficiency obtained for $C/I_1 = 6\,dB$, short frames [8]

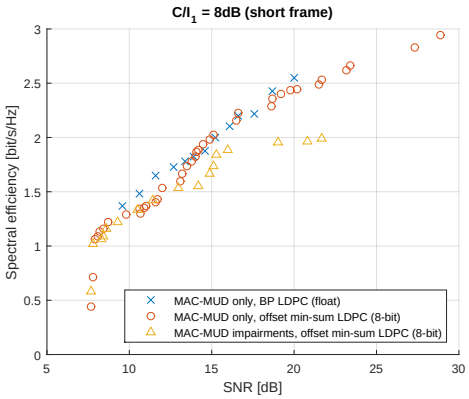

Figure 9.5: Spectral efficiency obtained for $C/I_1 = 8\,dB$, short frames [8]

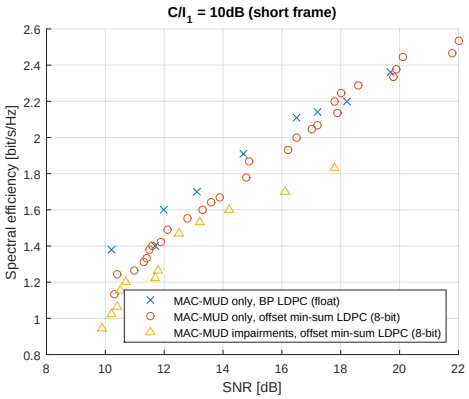

Figure 9.6: Spectral efficiency obtained for $C/I_1 = 10\,dB$, short frames [8]

To complete the picture the spectral efficiency envelope performance obtained for normal frames is shown in Figure 9.7 to Figure 9.12, comparing the MAC-MUD performance obtained by the floating-point arithmetic and BP LDPC with the performance achieved using the processing speed optimized offset min-sum implementation that is based on 8-bit. Due to the long processing time of normal frames, results with impairments are not covered by these charts. The numerical performance values for the normal frames are also provided in the appendix A.3.

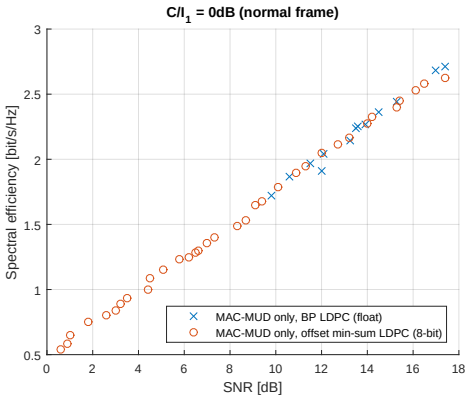

Figure 9.7: Spectral efficiency obtained for $C/I_1 = 0\,dB$, normal frames [8]

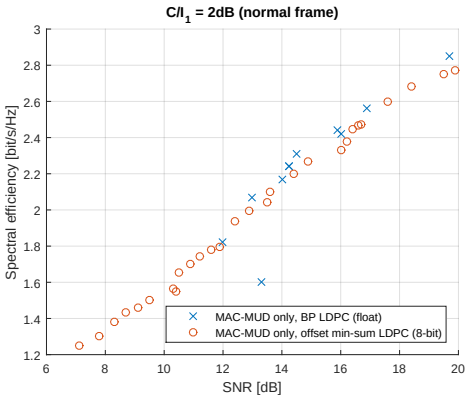

Figure 9.8: Spectral efficiency obtained for $C/I_1 = 2\,dB$, normal frames [8]

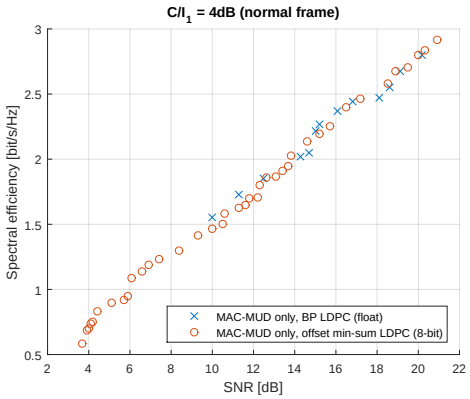

Figure 9.9: Spectral efficiency obtained for $C/I_1 = 4\,dB$, normal frames [8]

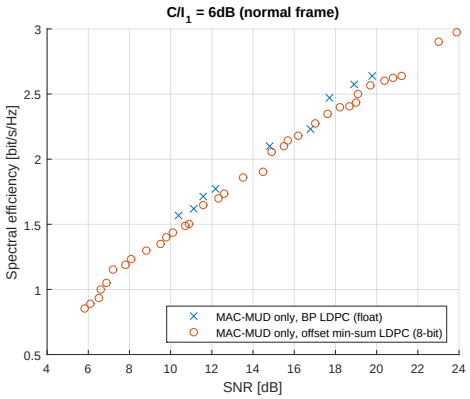

Figure 9.10: Spectral efficiency obtained for $C/I_1 = 6\,dB$, normal frames [8]

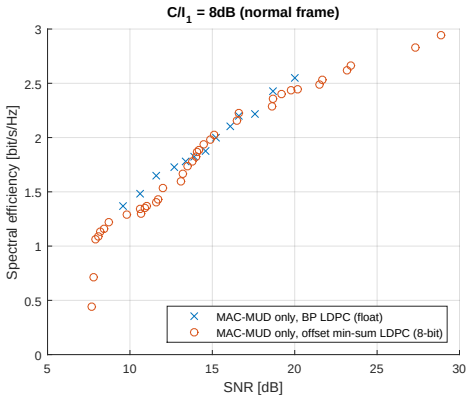

Figure 9.11: Spectral efficiency obtained for $C/I_1 = 8\,dB$, normal frames [8]

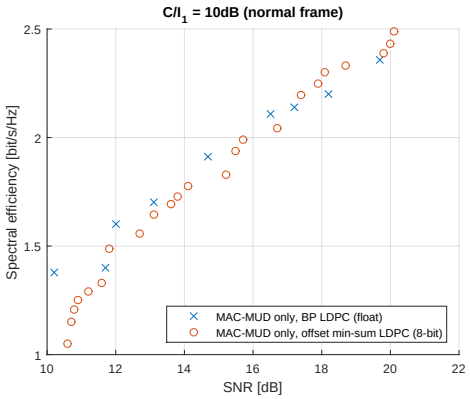

Figure 9.12: Spectral efficiency obtained for $C/I_1 = 10\,dB$, normal frames [8]

Comparing the results at a first glance, it is noticeable that the 8-bit implementation without impairments approximates the floating-point results obtained with BP LDPC. The results that include also the system impairments for short frames show comparable performance at low SNR regions, but around SNR = 10 dB they start to drop in their performance causing the curve to flatten out. This significant degradation especially at high SNR values is present since 16APSK modulation can be applied at these SNR regions and this modulation is clearly more affected in an impaired system than QPSK and 8PSK. Due to this reason, 32APSK modulations are not considered for MUD applications in the following. This leads to the fact that the impaired system is not able to reach as high spectral efficiencies as an ideal system without any impairments.

Taking a closer look on the results of short and normal frames, it is interesting to notice that the spectral efficiency pairs, which achieve comparable spectral efficiencies,

are different. This fact can lead to the situation that a MODCOD pair achieves a different spectral efficiency at FER $= 10^{-5}$ when using short frames compared to that with normal frames. In summary, it can be stated that the selected MODCOD pair as well as the interference level plus the applied impairment and C/N determine the actual performance.

9.2 MUD Performance Relevant Parameters

This section focuses on the identification of MUD performance defining parameters and their degree of influence. In the following specific effects are discussed and assessed w.r.t. their impact on the actual MUD performance.

9.2.1 MUD LLR Resolution

For the detector the floating-point implementation is considered as reference performance due to its high precision. In order to quantify the performance degradation introduced by the 8-bit interface, the performance of a specific MUD scenario is compared using both methods. The effect of the limited LLR resolution for the joint detection is shown in Figure 9.13 for an example using QPSK 1/2 in the main carrier and 8PSK 3/4 in the strongest interferer with the interference scenario characterized by $C/I_1 = 2$ dB.

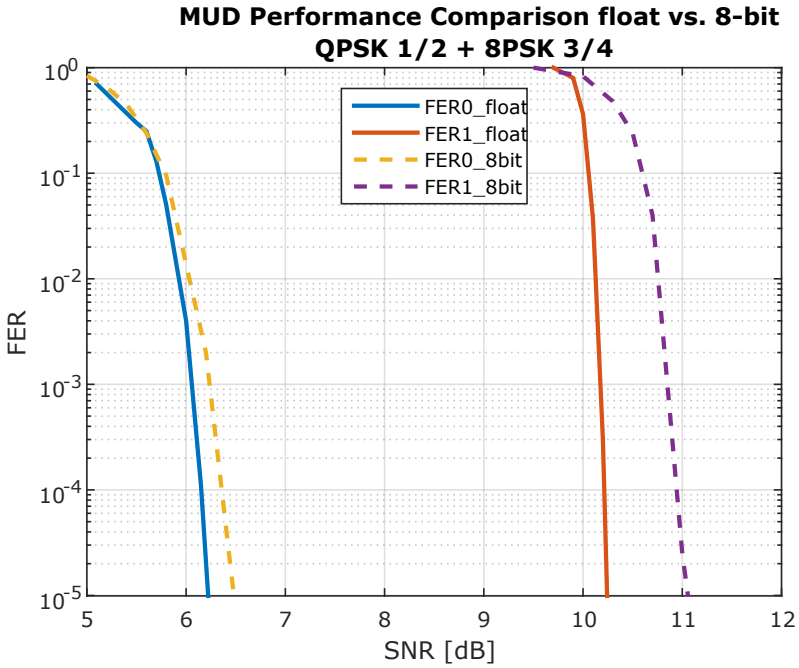

Figure 9.13: FER performance degradation due to the limited LLR resolution used for the detection and decoding process, at $C/I_1 = 2\,dB$ and QPSK 1/2 + 8PSK 3/4

Considering the floating-point arithmetic as reference, the limited 8-bit interface (dashed curves) lead to a notable performance degradation. In the presented example the degradation is in the range of 0.3 dB for B_0 and 0.8 dB for B_1. This degradation however, is not constant and depends as well on the performance of the applied LDPC algorithm. In the shown example, the min-sum LDPC decoder was used. Due to this performance change, new MODCOD pairs needed to be selected for the MUD performance analysis.

This example demonstrates the trade-off between the MUD performance in terms of FER and the MUD performance in terms of processing speed. Focusing on the processing speed, which is an essential requirement for a prototype implementation of MUD, the LDPC decoder was substituted by a LDPC decoder that uses an offset min-sum algorithm, which potentially improves the FER performance of individual MODCODs.

9.2.2 Precision of the Channel State Estimation

The amplitude and phase are important parameters for the detector performance. For this reason the precision of channel estimation applied to the user terminal is investigated by means of a sample scenario. To analyze the performance sensitivity to the channel estimation, the estimated results were compared to the results obtained using the ideal channel information while omitting additional interferers in the system. The results in Figure 9.14, using again the sample scenario with QPSK and 8PSK at $C/I_1 = 2$ dB, agree that the channel estimation causes a performance degradation of less than 0.2 dB.

The effect on the information of B_0 is notably stronger since the SNR is lower and the detection and accuracy of the channel is more critical than for B_1.

9.2.3 Additional Interferers Treated as Noise

The effect of additional interferers in the system on the FER performance is shown by an example using the MODCOD pair QPSK and 8PSK and the interference scenario $C/I_1 = 2$ dB. Figure 9.15 shows the obtained performance considering ideal channel estimates in order to isolate the degradation due to the additional interference in the system that is treated as noise.

The performance is degraded because the actual SNIR values that determine the detection performance are decreased due to the additional interference in the system.

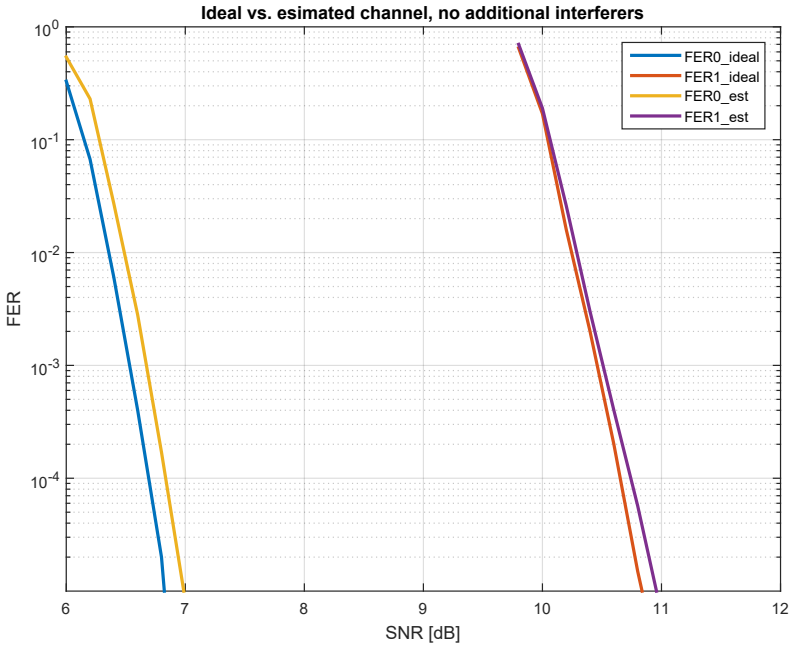

Figure 9.14: The effect of the ideal vs. estimated channel state estimate on the FER performance, at $C/I_1 = 2\,dB$, QPSK 1/2 + 8PSK 3/4

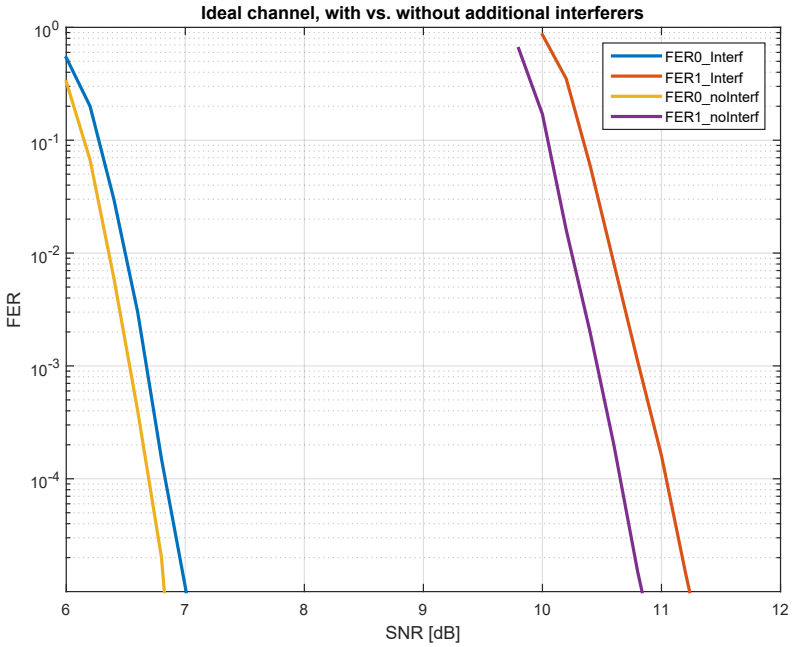

Figure 9.15: FER performance with ideal channel estimates compared to performance considering additional interferers in the system as noise, at $C/I_1 = 2\ dB$, QPSK 1/2 + 8PSK 3/4

9.2.4 System Impairments

The examples shown in Figure 9.16 and Figure 9.17 demonstrate the effect of system impairments on the FER performance for the MODCOD pair QPSK 1/2 + 8PSK 3/4 and QPSK 1/2 + 16APSK 2/3, respectively. The effect of system impairments is MODCOD-specific and thus the impairment shown in the examples is not constant for all scenarios. In general, it can be stated however, that MODCOD pairs with higher modulation schemes are more affected by the introduced system impairments than those MODCOD pairs that consist of lower modulation orders.

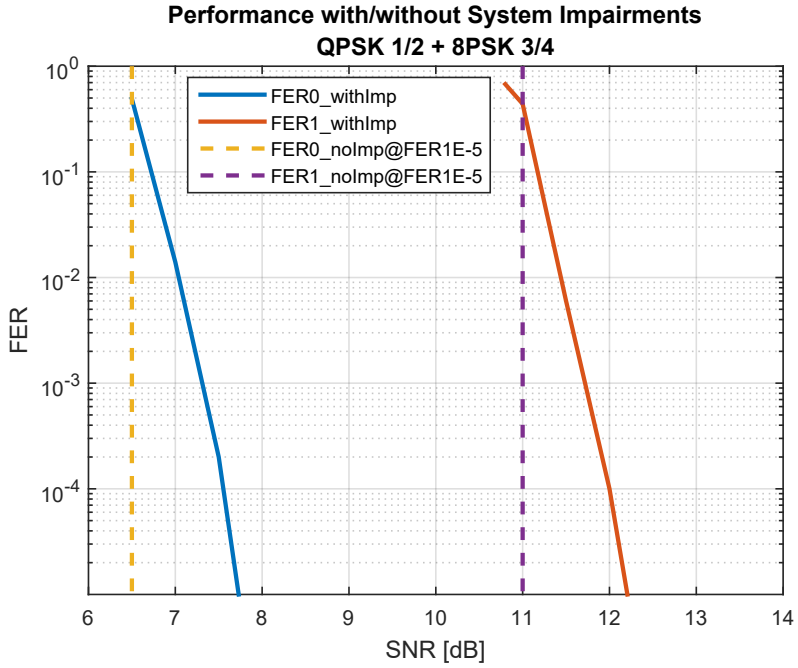

Figure 9.16: FER performance with and without system impairments at $C/I_1 = 2\ dB$, QPSK 1/2 + 8PSK 3/4

9.2.5 The Effect of MUD Iterations on the MUD Performance

The selected number of MUD iterations is relevant for the processing speed, and for that, the assessment of the achievable performance gain obtained by a higher number of iterations is of interest as well. For this purpose, the number of MUD iterations was compared, while keeping the number of LDPC iterations constant to a number of 200. The obtained result in Figure 9.18 very well demonstrates that the overall performance difference is not significant, but at very low FER levels (10^{-5} and lower) an error floor potentially emerges for a low number of MUD iterations.

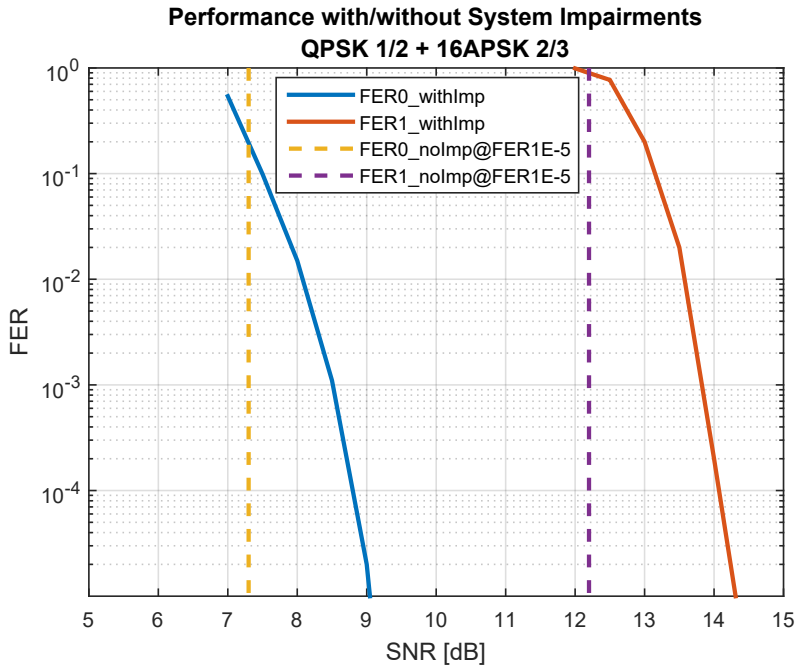

Figure 9.17: FER performance with and without system impairments at $C/I_1 = 2\ dB$, QPSK 1/2 + 16APSK 2/3

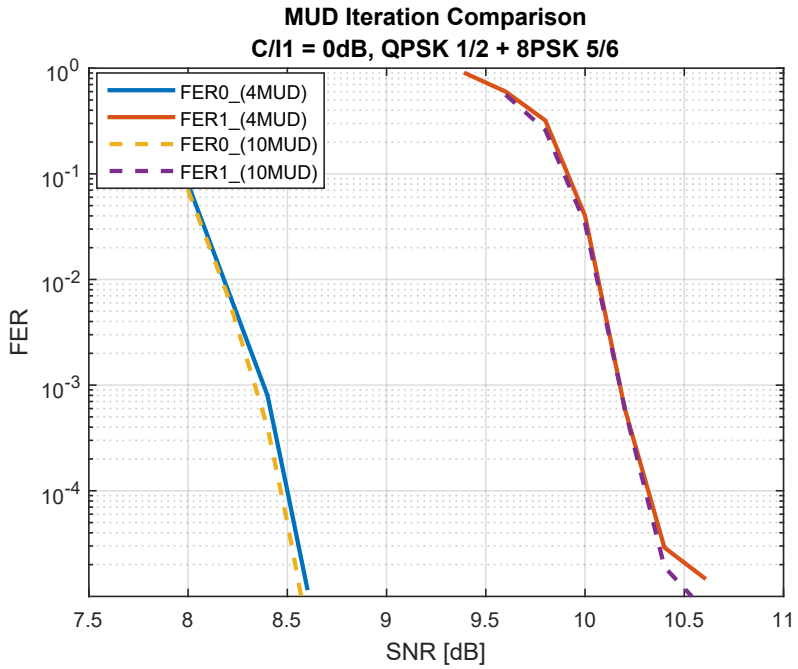

Figure 9.18: The effect of max. MUD iterations on the FER performance, with 200 LDPC iterations

9.2.6 The Effect of LPDC Iterations on the MUD Performance

A single MUD iteration for the joint detection and decoding of two signals involves the execution of the detector and the specified number of iterations for the LDPC for each carrier, in this case twice.

Certainly, the number of LDPC iterations does not only influence the processing speed, but also the performance in terms of FER. The effect of LDPC iterations on the MUD performance was analyzed. Figure 9.19 compares the performance obtained for 200 and 50 LDPC iterations. Especially at very low FER rates (10^{-5} and lower) the benefit of a higher number of iterations becomes noticeable. This analysis was executed for a constant number of 10 MUD iterations.

The LDPC iteration performance analysis shown in Figure 9.19, reveals the dependency between processing speed and selected MODCOD pair. The remarkable information obtained by the LDPC iteration comparison is the fact that at low FER the overall number of LDPC iterations is below 200 iterations, independent of the MODOCD pair. This finding is beneficial in terms of speed optimization, since the low FER region is the region of interest where the demonstrator spends the most time.

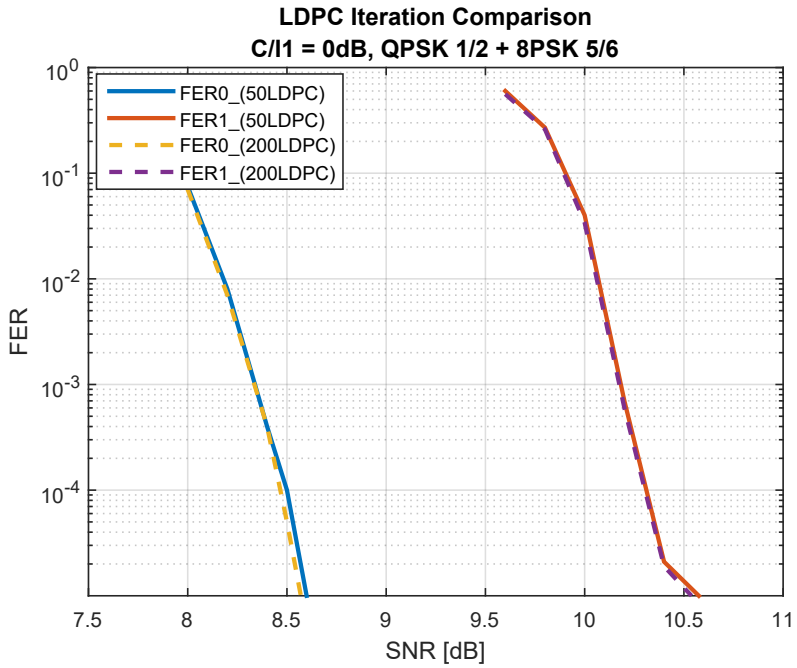

Figure 9.19: The effect of max. LDPC iterations on the FER performance, with 10 MUD iterations

9.3 Information Flow and Reception Techniques

The multi-spot beam setup and the receiver capabilities allow the comparison of different scenarios using the system demonstrator. The applicable information flow and reception techniques are addressed in this section. The scheduler is the crucial component for this functionality that aims to optimize the performance on a frame basis. For the sake of clarity, it needs to be stressed again that a dynamic switching of the colouring scheme by the scheduler is not possible.

9.3.1 Information Flow

The information flows considered in this work are:

- Single beam per user:
  Data is provided to a single user via a single beam for 100% of the time.
- Multi beam per user:
  Data is provided to a single user via two beams for 50% of the time.

9.3.2 Reception Techniques

The applicable reception techniques are discussed in the following.

Interference as Noise (IAN)

Treating the present interference as noise is the most basic technique that does not require any complexity in the receiver, but provides in return the worst performance when strong interferences are present.

This technique is usually applied in FR-4 systems since the interference levels are low in relation to FR-2. Theoretically, this method can be also applied in a 2-colouring system but the strong interferences cause a significant performance degradation.
For this reception technique an information flow with single beam per user is required.

MAC-MUD

Here, a reception technique is discussed that is only applicable for receivers equipped with MUD capabilities. For the multi-access MUD concept a single user is served by two beams, the dedicated beam and its strongest interferer at the same colour. The user terminal receives the combined signal r and detects C, the main carrier, transmitted by its dedicated beam and I_1, the signal transmitted by the strongest interferer. Where C has the MODCOD m_0 and I_1 has the MODCOD m_1. The user in B_0 receives information using this information flow for 50% of the time.

The MODCOD sets m_0 and m_1 are selected based on the position of the user that is served during this time slot. This denotes that the MODCOD pair for one user is most likely very different from the setting of the other, since it depends not only on the user position and thus, the interference levels but also on the local tropospheric conditions.

This technique is only applicable for a FR-2 scenario assuming a multibeam per user information flow.

Single Carrier MUD (SC-MUD)

The single carrier MUD reception technique is an alternative reception technique feasible in a single beam per user information flow that is operated in a FR-2 setting. For this technique, it is assumed that the receiver terminal is capable of MUD but the information is only transmitted via the dedicated single beam. The purpose of this scenario is to determine, whether there is a performance gain observable for the user if the received signal is treated as MUD and the information of the strongest interferer could be used to detect the wanted carrier. The strongest interferer in this setting does not provide useful data for the user, so MUD is only executed until the signal transmitted by the own beam is successfully decoded. The MUD algorithm is aborted after successful decoding and the information provided by the undetected interferer is discarded.

The scheduling of the MODCOD pairs in this case is of utmost importance in order to provide a fair throughput to all users in the system.

9.4 MUD Peak Performance

The MUD peak performance denotes the maximum instantaneous performance that is achievable with MUD at a certain C/N. The peak performance of MUD was analyzed in terms of achievable spectral efficiency and throughput. The obtained results are shown in Figures 9.20 and 9.21, respectively.

Comparing the achievable performance obtained with MUD in a FR-2 system with the performance in a traditional FR-4 system, shows that the application of MUD in the receiver is able to basically double the peak performance for a single user terminal by utilizing two beams for data transmission.

This instantaneous gain in throughput represents a tool for the satellite operator that allows to introduce more flexibility in a satellite system [30]. A flexible assignment and re-allocation of resources is especially of importance in situations with a highly imbalanced traffic demand. Such a scenario for instance is present if there is an event or a city covered by a single spot beam, denoted as hot spot, and the surrounding beams service predominantly rural areas with a low traffic demand. In this case, the adjacent spot beams can be utilized to add more system capacity to the spot beam with a high traffic demand.

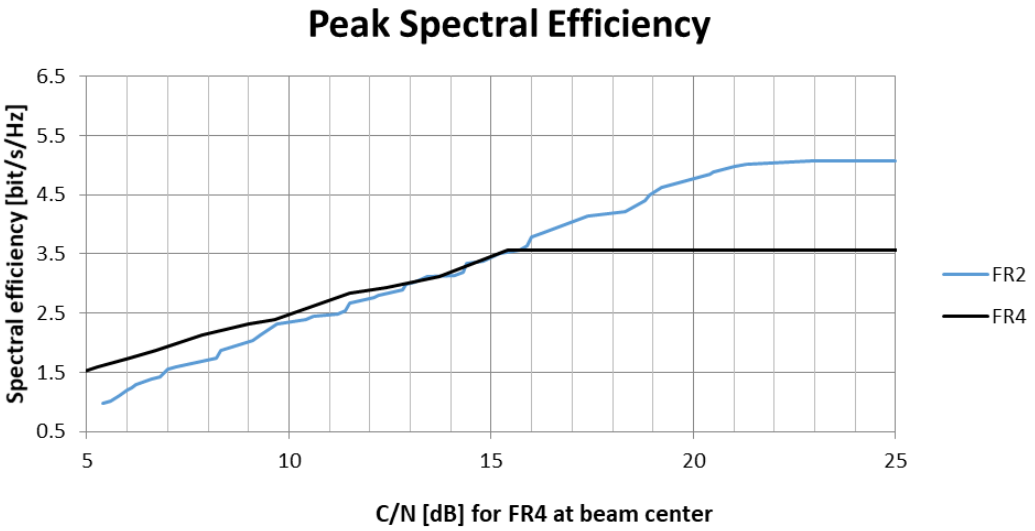

Figure 9.20: Spectral efficiency peak performance using MUD [8]

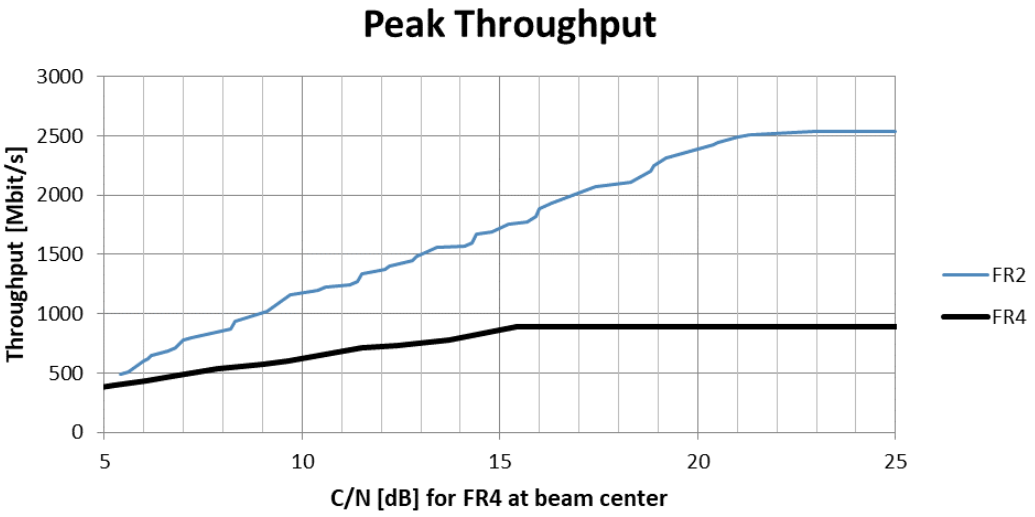

Figure 9.21: Throughput peak performance using MUD [8]

This flexibility benefit gained by the application of MUD is illustrated in the Figures 9.22 and 9.23, where in a balanced traffic demand the capcity between the beams is averaged while in an imbalanced scenario the beam with higher data traffic demand steals the capacity from the other beam.

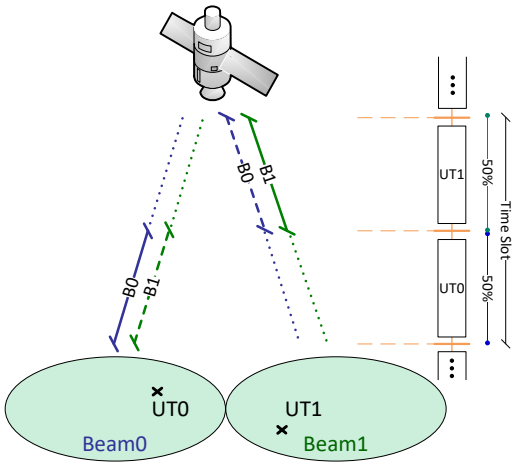

Figure 9.22: Balanced traffic resulting in averaged capacity

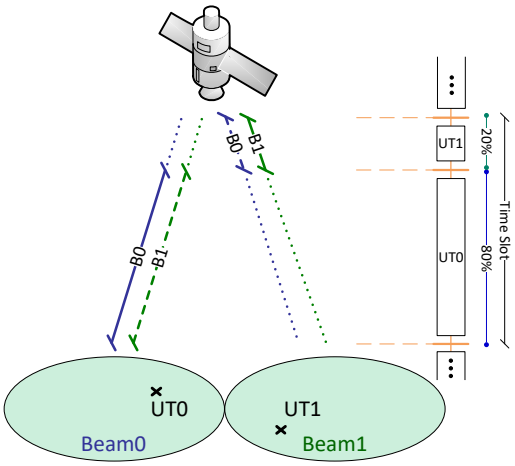

Figure 9.23: Imbalanced traffic where one beam steals capacity from the other beam

Unfortunately, the traffic demand is rarely balanced. For this reason MUD could be a useful method to cover traffic peaks and is therefore of interest for satellite operators.

9.5 MUD Interference Sensitivity

Before investigating the system performance using MUD, it is interesting to determine the interference sensitivity level of this method. In other words, this section examines the interference levels, where MUD performs best. For this reason, the MUD performance of MAC-MUD and SC-MUD is evaluated and compared at different interference ranges following [15].

The performance is evaluated at the C/N levels of 20 dB, 15 dB and 10 dB, provided by the Tables 9.2, 9.3 and 9.4, respectively. The test case IDs gradually limit the interference scenario range of the originally specified scenarios in Table 3.1 in order to isolate and demonstrate specific sensitivities. The scenarios of an individual test are randomly drawn from the uniformly distributed set of interference scenarios indicated. The 10^7 runs per test case allowed to determine the achievable availability and throughput comparing MAC-MUD with SC-MUD. The availability in this context is defined as the percentage of runs, where a valid MODCOD pair was identified and assigned to U_0 and U_1, considering the specified conditions.

		MAC-MUD		SC-MUD	
Test ID	**Interference scenario ID range for scheduling**	**Availability [%]**	**Throughput [Mbit/s]**	**Availability [%]**	**Throughput [Mbit/s]**
A	1 to 6	99.89	714.9	99.98	577.4
B	1 to 5	99.95	728.6	99.98	529.4
C	1 to 4	99.97	738.4	99.98	467.8
D	1 to 3	99.97	737.2	99.98	407.1
E	1 to 2	99.97	726.3	99.97	346.9
F	1 to 1	99.98	711.9	99.97	277.8
G	2 to 2	99.97	740.8	99.98	416.0
H	3 to 3	99.97	755.1	99.98	527.1
I	4 to 4	99.93	739.9	99.99	649.4
J	5 to 5	99.88	675.8	99.99	775.4
K	6 to 6	99.59	662.7	99.99	817.1

Table 9.2: MUD sensitivity analysis at C/N = 20 dB comparing MAC-MUD and SC-MUD performance [15]

		MAC-MUD		SC-MUD	
Test ID	**Interference scenario ID range for scheduling**	**Availability [%]**	**Throughput [Mbit/s]**	**Availability [%]**	**Throughput [Mbit/s]**
A	1 to 6	80.22	549.3	99.92	519.1
B	1 to 5	98.96	560.8	99.92	473.9
C	1 to 4	99.70	574.4	99.92	423.7
D	1 to 3	99.86	589.9	99.92	369.7
E	1 to 2	99.89	593.0	99.91	319.0
F	1 to 1	99.91	609.6	99.89	277.2
G	2 to 2	99.89	576.4	99.93	360.7
H	3 to 3	92.18	578.7	99.95	471.2
I	4 to 4	99.20	527.4	99.95	585.6
J	5 to 5	95.99	506.8	99.95	674.4
K	6 to 6	16.00	393.5	99.95	744.7

Table 9.3: MUD sensitivity analysis at C/N = 15 dB comparing MAC-MUD and SC-MUD performance [15]

		MAC-MUD		SC-MUD	
Test ID	**Interference scenario ID range for scheduling**	**Availability [%]**	**Throughput [Mbit/s]**	**Availability [%]**	**Throughput [Mbit/s]**
A	1 to 6	24.82	358.3	99.24	394.6
B	1 to 5	35.34	364.1	99.23	367.5
C	1 to 4	54.50	369.8	99.22	337.3
D	1 to 3	96.64	368.6	99.20	304.5
E	1 to 2	98.63	388.5	99.17	273.0
F	1 to 1	99.22	416.6	98.62	242.7
G	2 to 2	98.04	361.3	99.72	303.2
H	3 to 3	99.79	315.4	99.81	369.6
I	4 to 4	0	0	99.84	435.7
J	5 to 5	0	0	99.85	478.4
K	6 to 6	0	0	99.99	520.4

Table 9.4: MUD sensitivity analysis at C/N = 10 dB comparing MAC-MUD and SC-MUD performance [15]

The obtained results confirm that the MAC-MUD approach does not perform very well under circumstances with low interference levels. For this reason, interference scenario 6 with an C/I_1 of 10 dB achieves the lowest performance and, as shown by Table 9.4, does not work at low C/N ranges, e.g. during a rain event due to the low SNIR levels of the strongest interferer. The comparison of MAC-MUD with SC-MUD shows that MAC-MUD starts to outperform SC-MUD in terms of throughput at C/N levels of 15 dB and higher. In general the best performance can be achieved in scenarios with high interference levels, such as scenario 1 with $C/I_1 = 0\ dB$. This can be again explained by strong SNIR levels, as demonstrated in Figure 3.5 to Figure 3.8.

Inspecting the obtained availability and throughput results for MAC-MUD at C/N = 20 dB in Figure 9.24 and Figure 9.25, respectively, the low variation in the availability result is noticeable. The throughput variation becomes low at 20 dB C/N and beyond that, the tests E and F that both perform better at low C/N values, start to saturate. Since the aim of an interference mitigation technique is the applicability at a wide range of scenarios and the fact that the consideration of scenario 6 for scheduling does not cause a significant performance drop together with the minor variation in the results lead to the decision to use the full set of interference scenarios for the scheduler.

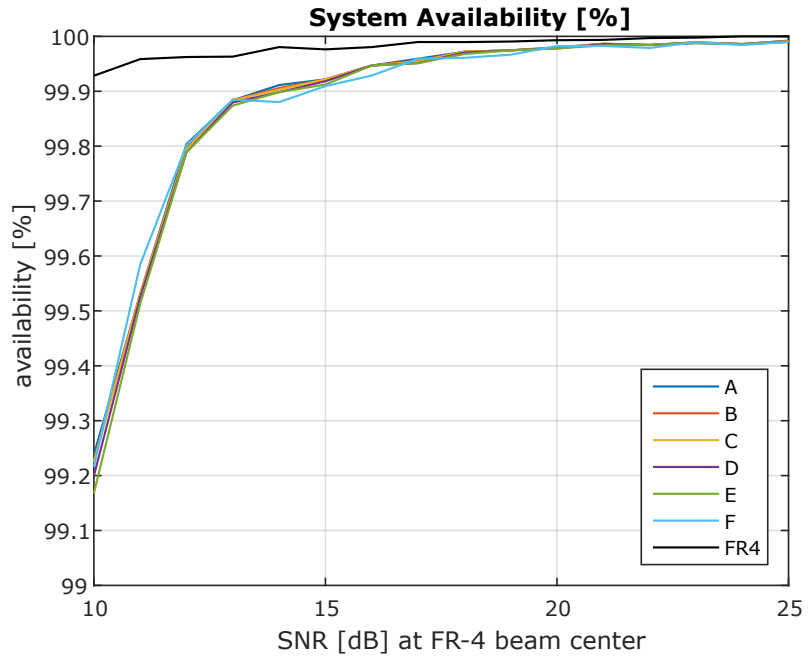

Figure 9.24: Availability performance [15]

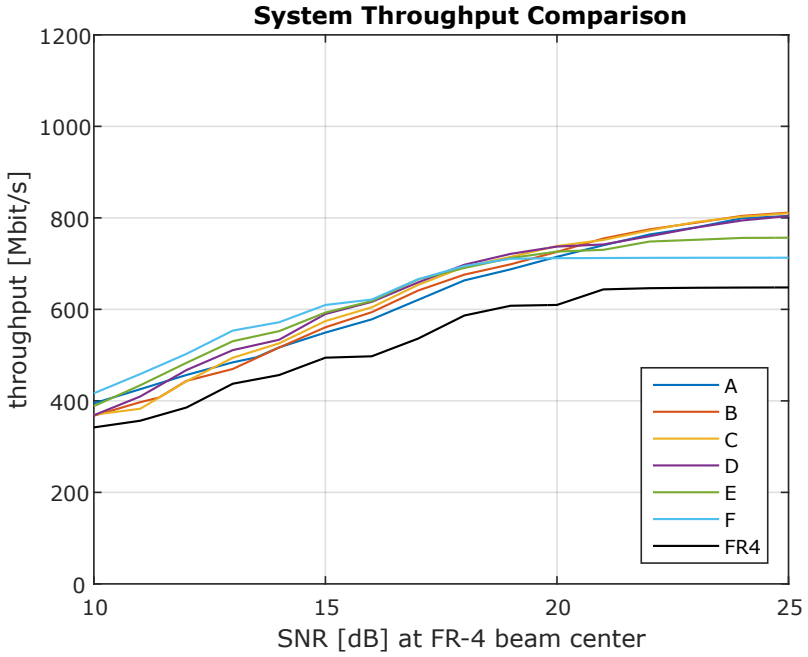

Figure 9.25: Throughput performance [15]

9.6 Scheduler

The scheduler decides between the different ways of information and reception in the system. The analysis points to the need that an optimized scheduling for each operation mode is required. The scheduler aims to balance the throughput in the system and ensures the fairness of assigned resources to the users.

For the IAN scenario, the scheduling is not critical since there is no dependency between the performances of different users in the systems. The scheduling becomes important for the MAC-MUD and is even more crucial in a SC-MUD scenario. For the MAC-MUD system performance the identification of a MODCOD pair that provides the highest performance based on the present interference scenario for the user terminal of interest is of utmost importance. The performance in MAC-MUD is not directly depending on other users, except for the time component since another user cannot be served while one user is served with MAC-MUD, requiring both beams for 100% of the scheduled time.

The scheduling for the SC-MUD has to ensure especially fair traffic share between the users since in this case they are not dependent in terms of time, but in terms of the assigned MODCOD. The scheduler actually needs to assign MODCOD pairs, despite single carriers are received. The difficulty is the fact that both user terminals see the same MODCOD pair but vice versa, while facing different local interference levels. The scheduler thus tries to identify the MODCOD pair that fits best for both users.

For this analysis, different scheduling schemes were examined using the described operation modes. The tested scheduling concepts examined are:

1. Random interference levels

$$\begin{aligned} \mathsf{UT_0} : C/I_1 &= 0 \text{ to } 10\ dB \\ \mathsf{UT_1} : C/I_1 &= 0 \text{ to } 10\ dB \end{aligned}$$

2. Significantly different interference levels

$$\begin{aligned} \mathsf{UT_0} : C/I_1 &= 0 \text{ to } \ \ 4\ dB \\ \mathsf{UT_1} : C/I_1 &= 6 \text{ to } 10\ dB \end{aligned}$$

All performance results of this section are provided for clear sky conditions, not taking into account tropospheric events.

9.6.1 Scheduling Approaches

In the following, the two scheduling approaches, that consider different pairing of interference levels, are introduced in more detail.

Scheduling Approach 1

The first scheduling approach considers interference levels from the full set of interference scenarios for the individual user terminal. The C/I range in curly brackets denotes the FR-2 C/I scenario ID, as specified in Table 3.1, representing the interference scenarios characterized by the strongest interferer C/I_1 from 0 dB to 10 dB.

$$C/I\ (UT_0)\ =\ \{1,2,3,4,5,6\}$$
$$C/I\ (UT_1)\ =\ \{1,2,3,4,5,6\}$$

In addition to the interference level, the same C/N condition was assumed at both user terminals:

$$C/N\ (UT_0)\ =\ C/N\ (UT_1)$$

The performance in terms of spectral efficiency and throughput for this scheduling approach is shown in Figure 9.26 and Figure 9.27, respectively.

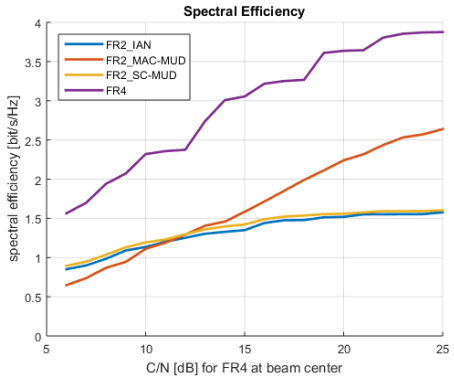

Figure 9.26: Spectral efficiency performance obtained with scheduling type 1

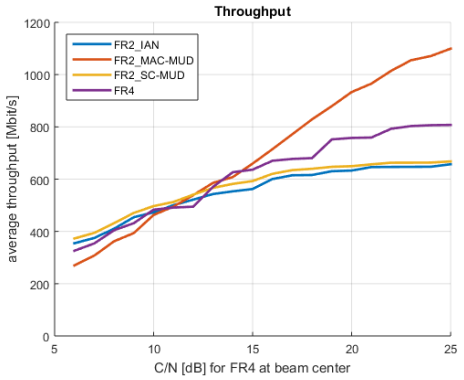

Figure 9.27: Throughput performance obtained with scheduling type 1

Scheduling Approach 2

The second scheduling approach considers contrasting interference level combinations for both users. Following this concept, UT_0 draws random interference scenarios from a set of high interference scenarios, while UT_1 draws random interference scenarios from a set of scenarios with low interference. Again, also for this approach the C/N condition was identical for both terminals.

$$C/I\ (UT_0)\ =\ \{1,2,3\}$$
$$C/I\ (UT_1)\ =\ \{4,5,6\}$$
$$C/N\ (UT_0)\ =\ C/N\ (UT_1)$$

The spectral efficiency and throughput results obtained with this scheduling approach are illustrated in Figure 9.28 and Figure 9.29, respectively.

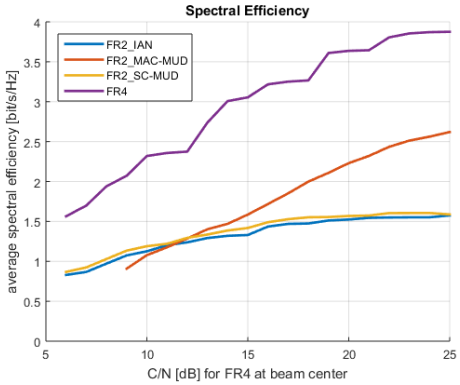

Figure 9.28: Spectral efficiency performance obtained with scheduling type 2

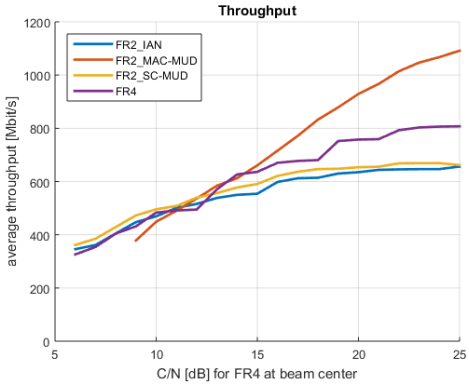

Figure 9.29: Throughput performance obtained with scheduling type 2

Inspecting the performance achieved by both scheduling approaches leads to the conclusion that selecting contradistinct scenarios does not result in a performance improvement. For this reason the approach 1 is selected as optimum scheduling approach since it does not constrain the pairing of two user terminals by the scheduler.

9.6.2 Optimum Scheduling without Impairments

Based on these quasi identical results it was decided to assume exclusively random interference levels for further performance tests. This section now compares the performance of FR-4 with FR-2 in terms of spectral efficiency and throughput without the consideration of system impairments. Since this comparison is done based on the average system performance, the FR-2 envelope performance obtained by the scheduling Approach 1 in Section 9.6.1, here denoted as optimum scheduling, is used demonstrating the fact that the scheduler selects the optimum configuration based on the present interference and C/N scenario.

In the following, the FR-2 scheduling performance is compared to a traditional FR-4 performance, which is considered as reference. The scheduling results, shown in the following, demonstrate the performance obtained while focusing on throughput optimization.

Figure 9.30 shows the individual spectral efficiency performance at FR-2, while Figure 9.31 compares the spectral efficiency envelope of FR-2 with the FR-4 performance. The individual throughput performance is then illustrated by Figure 9.32, together with Figure 9.33, that represents the scheduling throughput envelope.

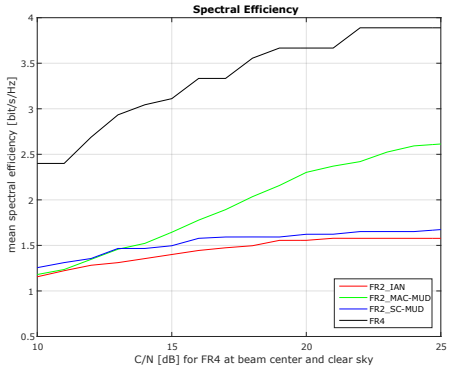

Figure 9.30: Spectral efficiency without impairments

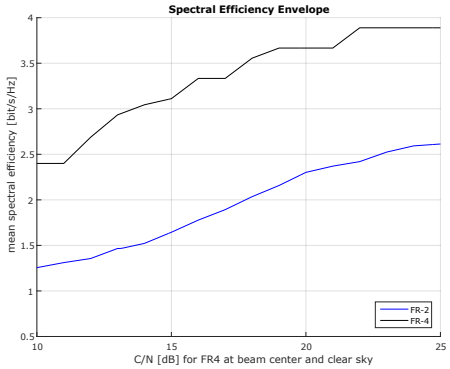

Figure 9.31: Spectral efficiency envelope without impairments

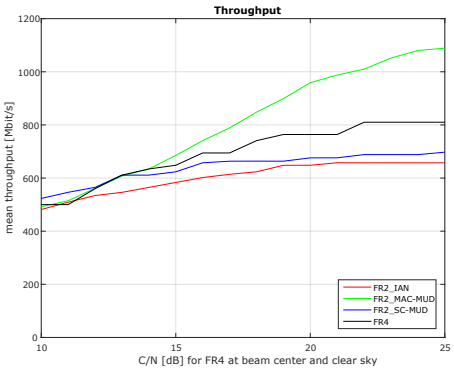

Figure 9.32: Throughput without impairments

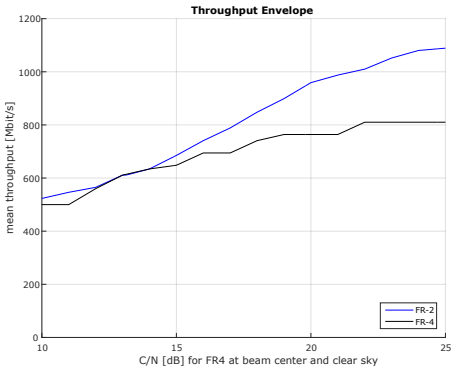

Figure 9.33: Throughput envelope without impairments

9.6.3 Optimum Scheduling with Impairments

After having investigated the ideal system performance, the system impairments are now added in the next step to analyze and compare the effect on the 2-colouring and 4-colouring setup. Since the performance envelope was already explained in the Section 9.6.2 before, the focus is set in the following exclusively on the scheduler envelope performances. The achieved envelope performance including system impairments for spectral efficiency and throughput are shown in Figure 9.34 and Figure 9.35 respectively.

The results show a clear performance degradation that results in a flattening of the throughput envelope. This behaviour was expected due to the presence of impairments, which affects the SNIR level and thus, limits the range of achievable MODCODs. For FR-4 in the performance degradation at 25 dB C/N is in the order of 150 Mbit/s while the performance degradation for FR-2 is in the order of 300 Mbit/s. Nevertheless, the FR-2 scheduling throughput envelope gain w.r.t. FR-4 still persists.

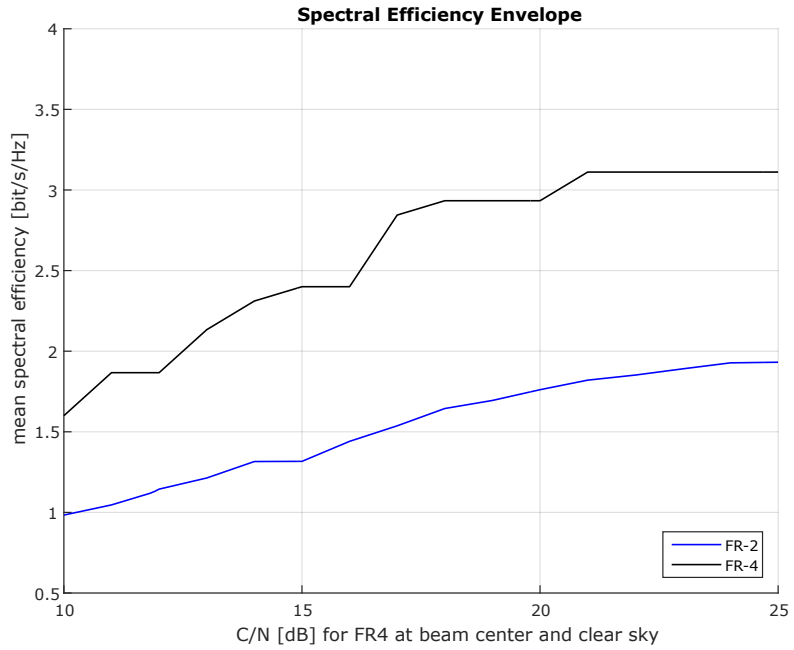

Figure 9.34: Spectral efficiency envelope with impairments [8]

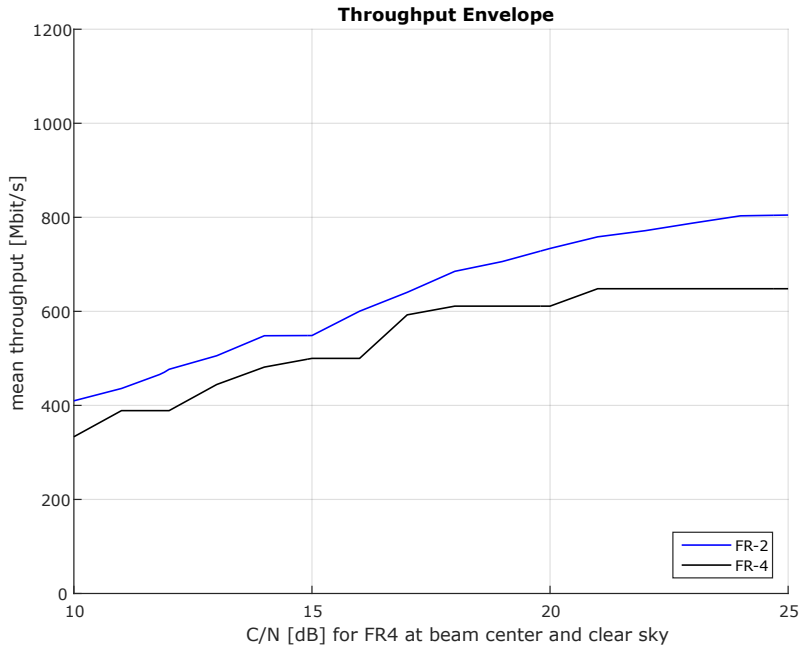

Figure 9.35: Throughput envelope with impairments [8]

9.7 Adaptive Coding and Modulation Performance

The ACM technique is introduced in Annex D of the DVB-S2 standard [5]. The technique relies on a return channel to dynamically adapt the link to propagation conditions of the individual terminal on ground [34].

The target of ACM is thus to achieve highest possible capacities and throughputs for the present tropospheric condition by optimizing the modulation and code rate on a frame basis. This means that for clear sky scenarios where high C/N levels are available, higher modulations such as 16APSK can be utilized. For low C/N levels during critical weather conditions like a thunderstorm, QPSK modulation is preferred since it provides a more robust service while allowing lower throughputs.

To obtain ACM results with the system demonstrator, a sample rain attenuation time series based on the local rain attenuation CCDF at Ka-band for Graz, Austria was generated using the ITU Recommendation ITU-R P.618 [17]. The applied rain attenuation CCDF is shown in Figure 9.36. Two adjacent spot beams in the region of Austria were assumed for this scenario.

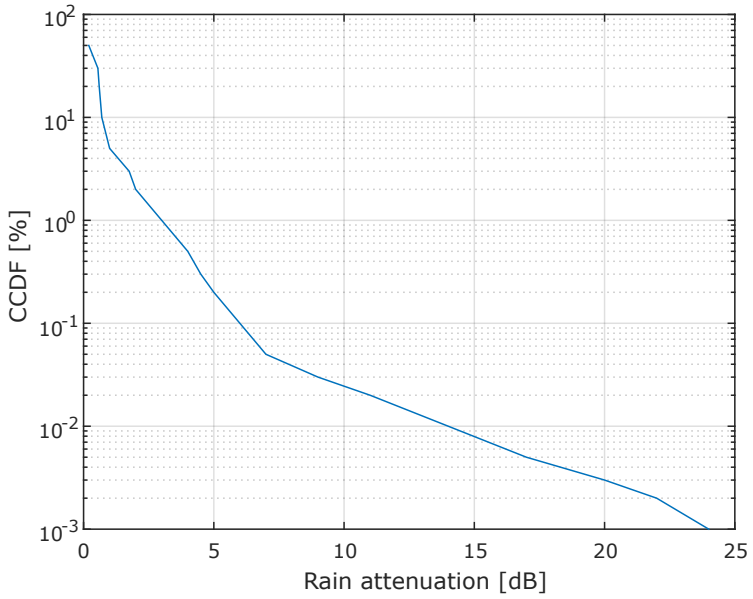

Figure 9.36: Rain attenuation at Ka-band for the region of Austria

9.7.1 Average System Performance without Impairments

The average system performance in terms of spectral efficiency, throughput and availability, obtained with active ACM and excluding the effect of system impairments is provided in Figure 9.37, Figure 9.38 and Figure 9.39, respectively.

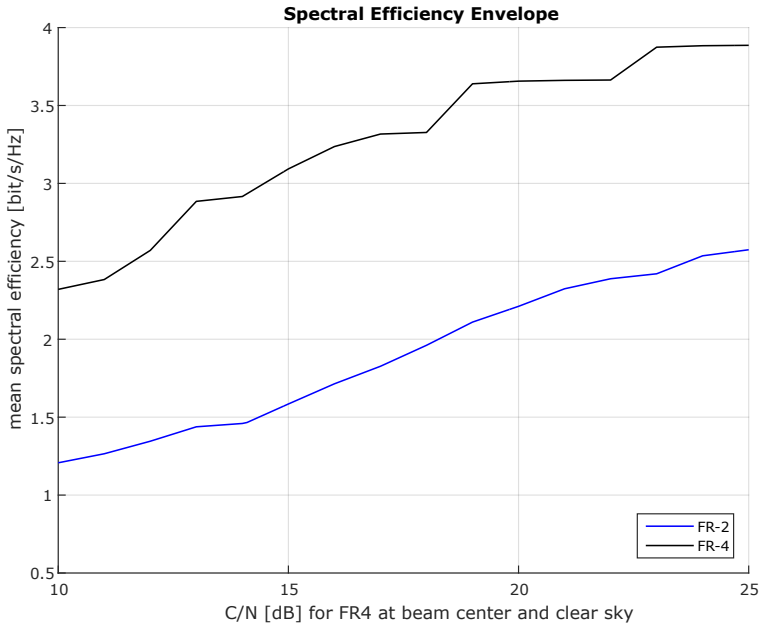

Figure 9.37: ACM spectral efficiency without impairments [8]

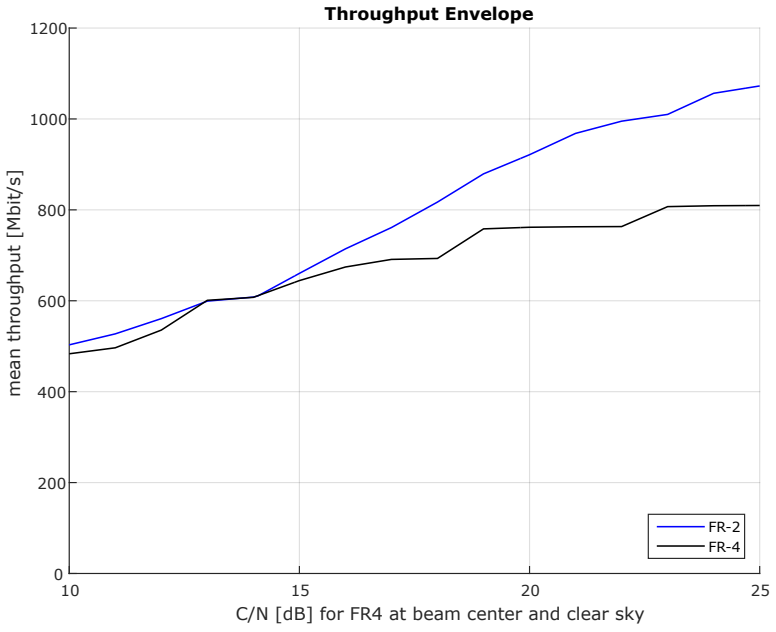

Figure 9.38: ACM throughput without impairments [8]

Since ACM is activated for this analysis, the system availability is provided as well indicating the amount of time that a matching MODCOD was not found due to the presence of low SNIR.

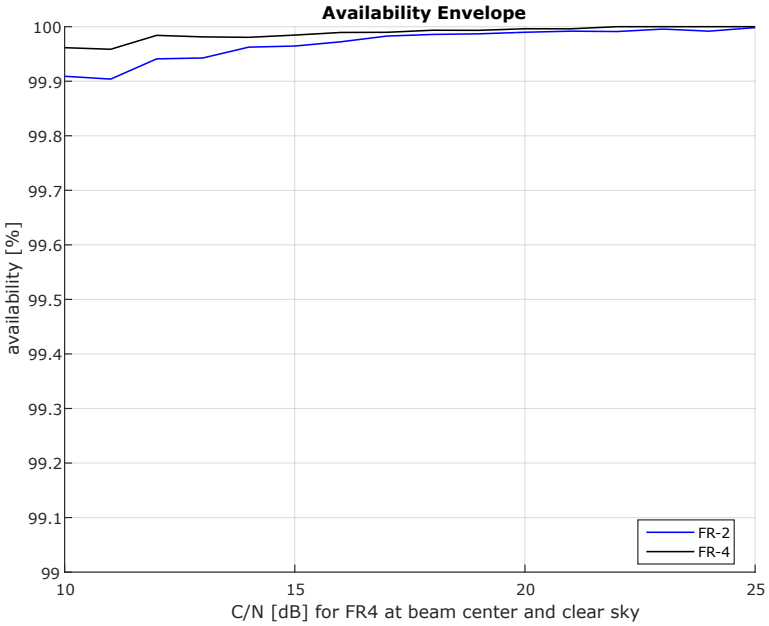

Figure 9.39: ACM availability without impairments [8]

9.7.2 Average System Performance with Impairments

In contrast to the section before, this section compares the FR-4 and FR-2 average system performance envelope including ACM and system impairments in Figure 9.40, Figure 9.41 and Figure 9.42. The impaired ACM results show a clear performance degradation introduced by the present system impairments.

The applied system impairments such as nonlinearities and the phase noise, affect high order modulation schemes, such as 16APSK, significantly more than low order modulation schemes, such as QPSK. Due to this fact, the performance envelope is more degraded in the higher C/N range, while the throughput performance at 10 dB C/N, where QPSK is likely to be applied, drops only slightly.

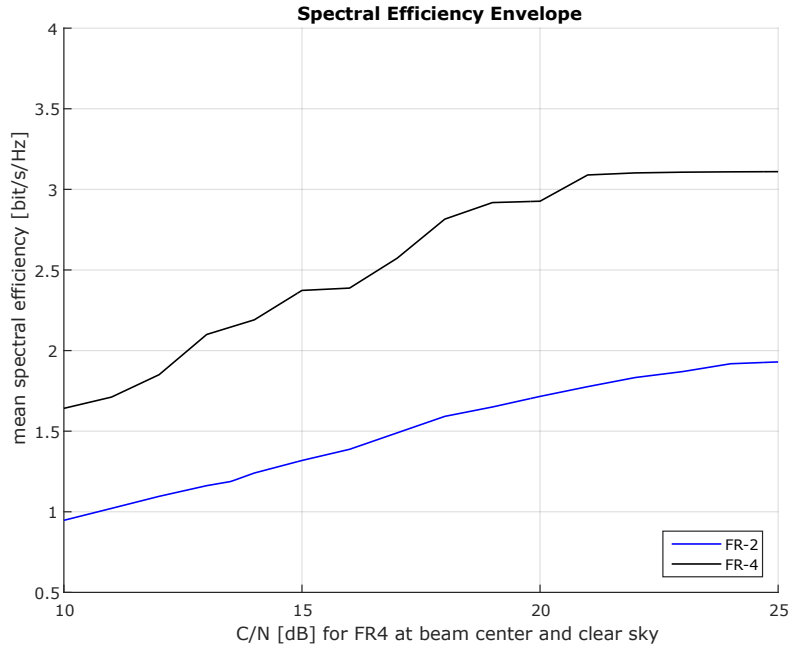

Figure 9.40: Average spectral efficiency with impairments and ACM [8]

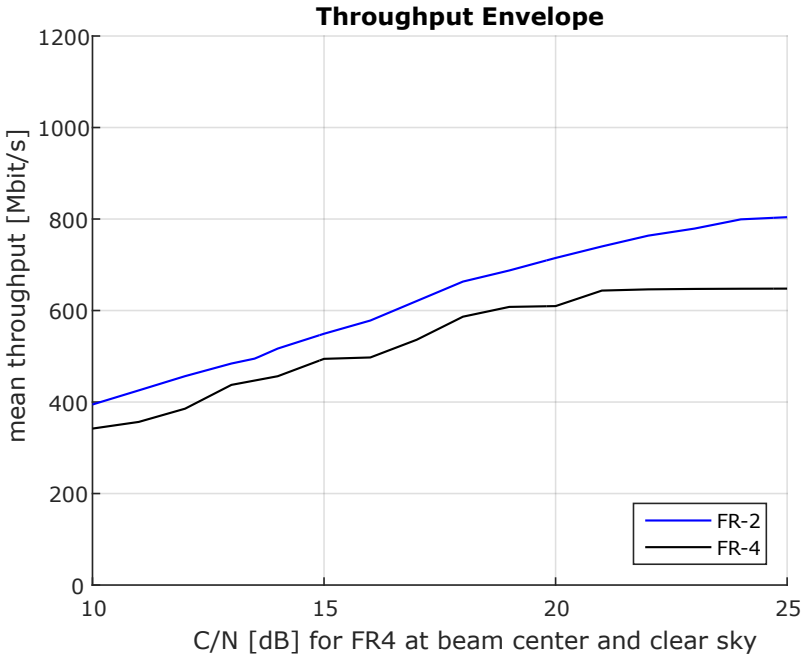

Figure 9.41: Average throughput with impairments and ACM [8]

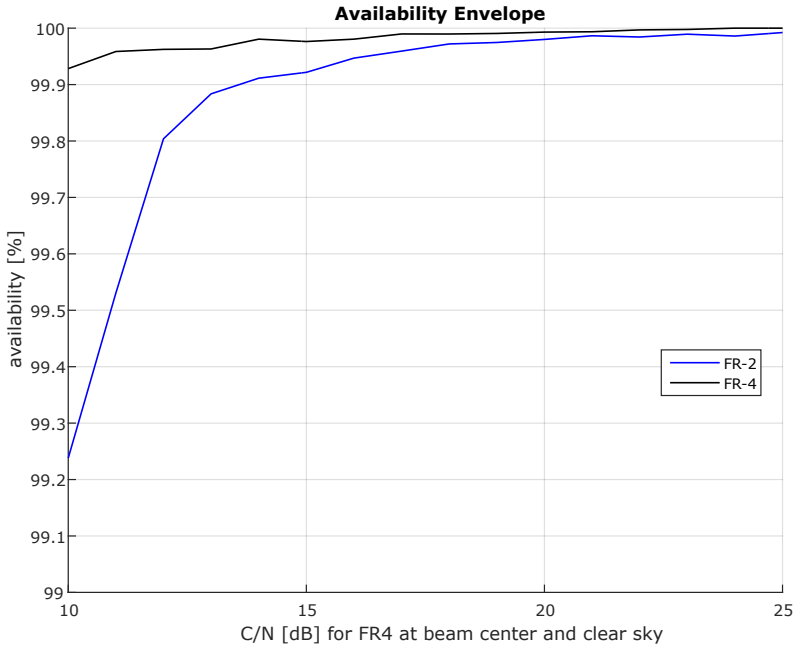

Figure 9.42: Average availability with impairments and ACM [8]

9.8 Achievable Throughput in a Realistic Spot Beam

Inspecting an average spot beam in the considered 200 spot-beam pattern with the C/I_1 levels shown in Figure 3.22, despite the C/I level and SNIR, the achievable throughput at FR-2 is of interest as well, as mentioned [15]. For this purpose the obtained throughput at C/N = 10 dB, 15 dB and 20 dB is shown in Figure 9.44, Figure 9.45 and Figure 9.46, respectively, representing a regular spot beam in the center of the coverage area.

The spot-beam center in terms of received power is marked by a small magenta circle, while the 3 dB cross-over level is indicated by the large red circle. The achievable throughput at 10 dB is approx. 250 MBit/s, which is lower than the results at 15 dB, while the performance at 20 dB C/N achieves approx. 800 Mbit/s, which is roughly 100 MBit/s more than at 15 dB.

This performance again reminds of the fact that MUD does not perform very well at low C/N ranges due to the low SNIR levels. Additionally, it has to be pointed out at this level that the MUD performance needs to be individually analyzed for specific multi-spot beam designs, as reported in [74], in order to determine the expected throughput under the application of MUD considering the actual spot beam shapes, the applied cross-over levels, the C/N ranges and thus, the actually present interference and SNIR levels.

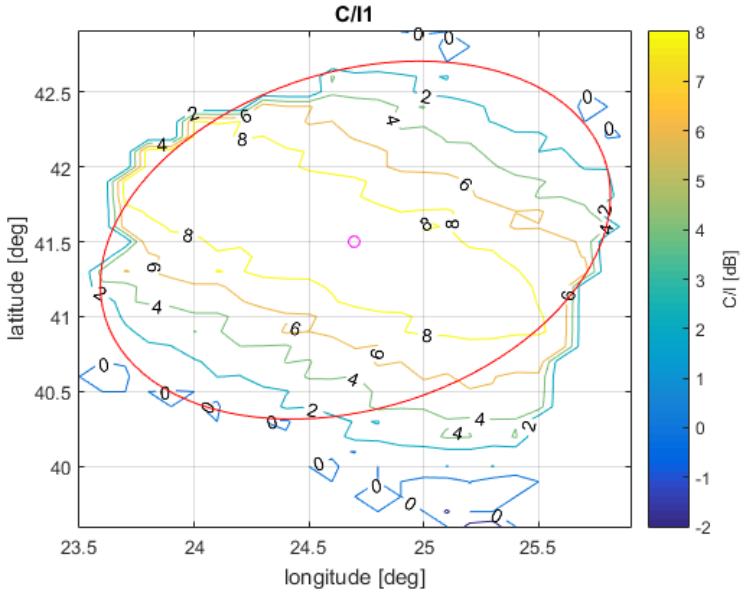

Figure 9.43: FR-2 CNI_1^5R in a sample spot beam at C/N = 20 dB [15]

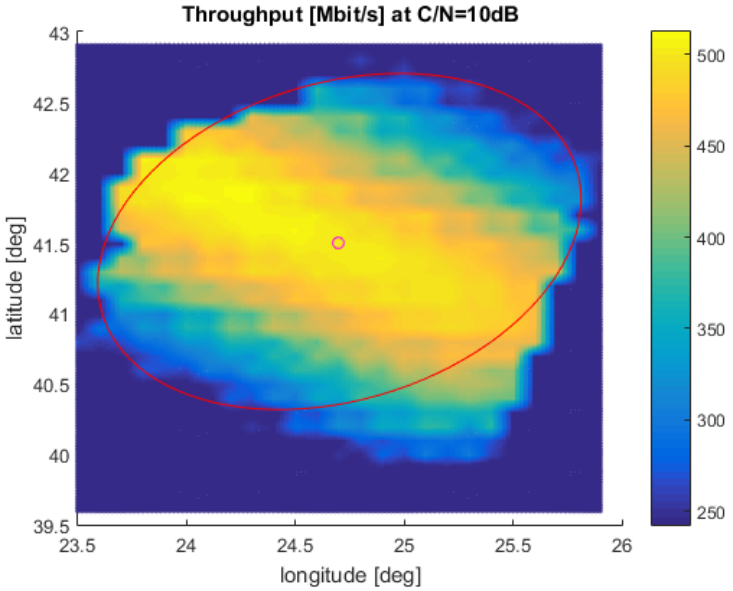

Figure 9.44: Achievable throughput [Mbit/s] in a realistic single spot beam at FR-2 and C/N = 10 dB [15]

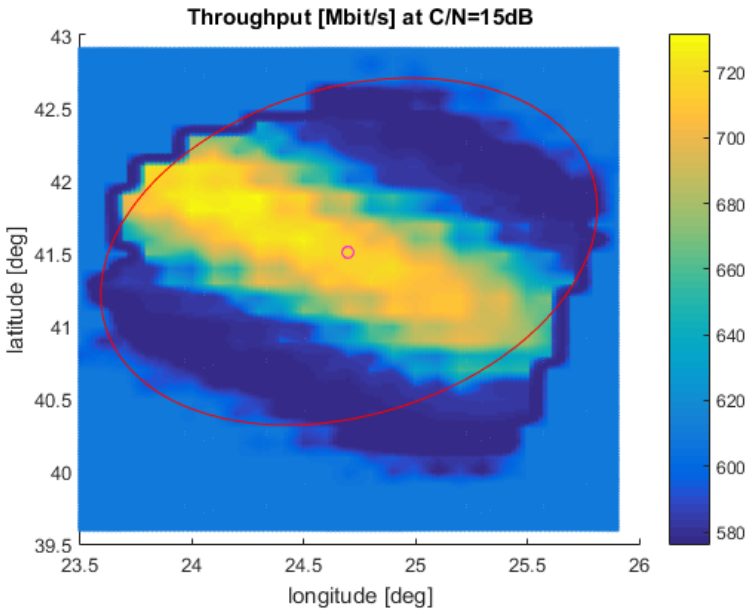

Figure 9.45: Achievable throughput [Mbit/s] in a realistic single spot beam at FR-2 and C/N = 15 dB [15]

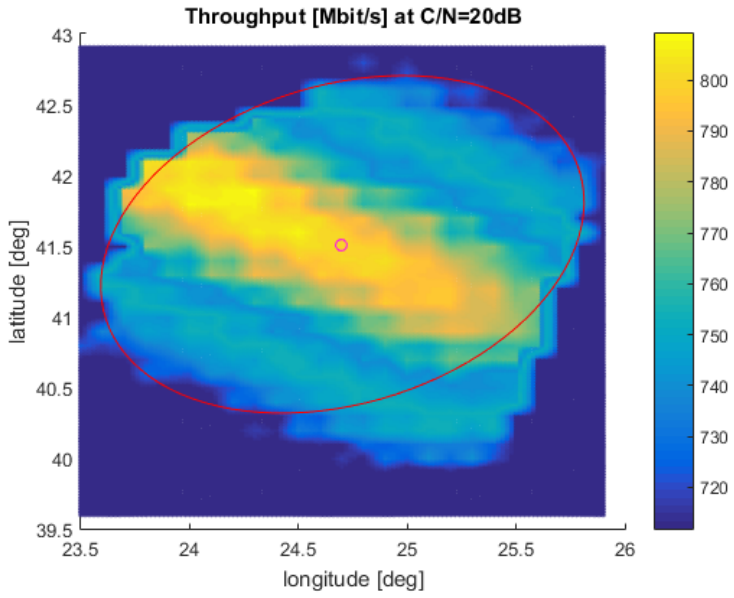

Figure 9.46: Achievable throughput [Mbit/s] in a realistic single spot beam at FR-2 and C/N = 20 dB [15]

9.8.1 Average System Throughput in an Realistic Antenna Pattern

After analyzing the scheduling performance with MUD and the expected throughput within representative spot-beams of a realistic antenna pattern, the average system throughput in the coverage area is provided in this section to complete the picture. In more detail, the average throughput for each of the 200 beams was determined at different C/N levels to demonstrate potential degradations in the system.

The C/I_1 and thus the SNIR at each point within the beam were determined to compute the achievable throughput while applying the same scheduling approach that was identified as the optimum scheduling approach earlier in this chapter. As shown by the scheduling results, the actual C/I_1 pairing of the user terminals can be neglected in this context since a special pairing according to interference levels does not influence the obtained performance.

Since a gain of approx. 15% was determined at FR-2 w.r.t. the traditional FR-4 at a C/N of 20 dB, as shown in this chapter before, it is now interesting to examine if this gain can be confirmed when considering the realistic spot-beam pattern. Note that this comparison considers system impairments but does not include any tropospheric effects and thus ACM.

For this purpose, also the average system throughput achieved by FR-4 is provided in the following.

The average FR-2 throughput per spot-beam including impairments is illustrated in Figure 9.47, Figure 9.48 and Figure 9.49 for the C/N levels of 10 dB, 15 dB and 20 dB respectively.

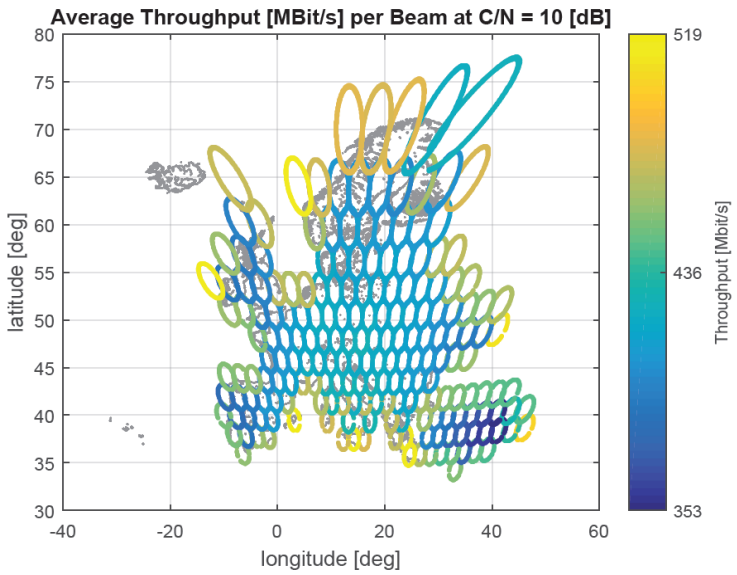

Figure 9.47: Spot beam specific average FR-2 throughput in a 200 beam realistic antenna pattern at C/N = 10 dB

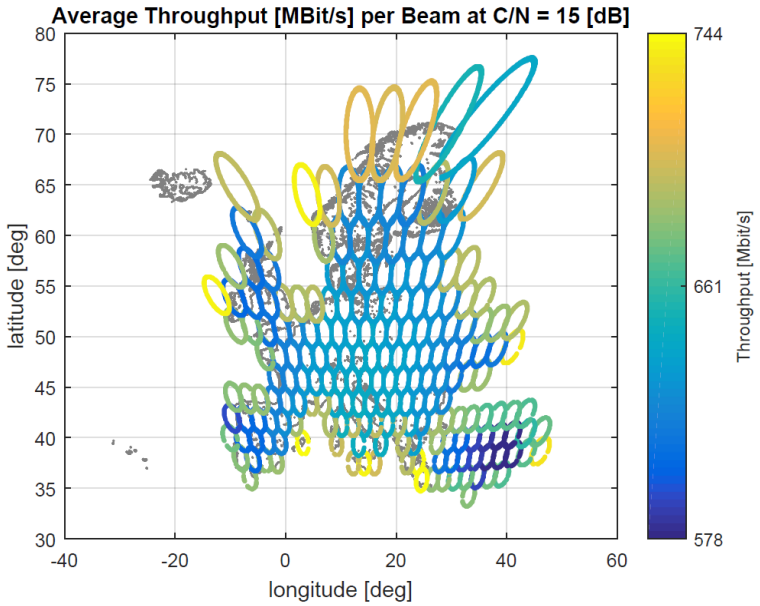

Figure 9.48: Spot beam specific average FR-2 throughput in a 200 beam realistic antenna pattern at C/N = 15 dB

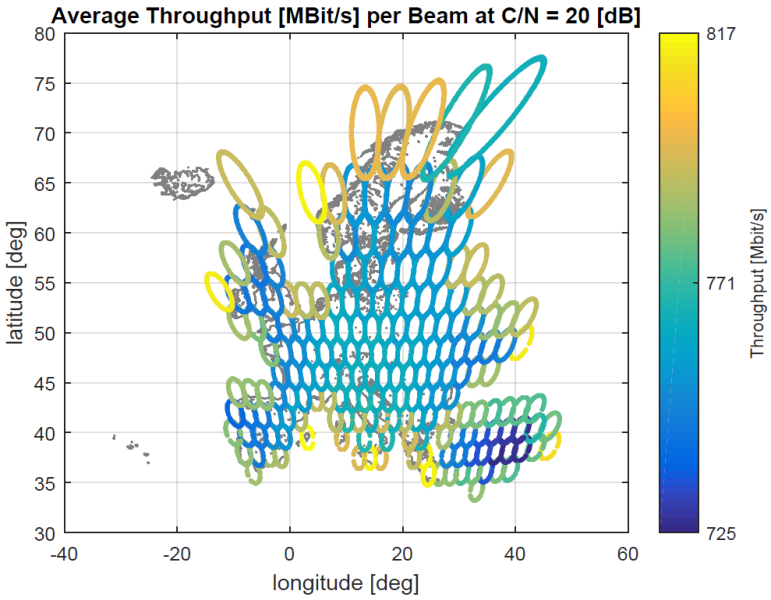

Figure 9.49: Spot beam specific average FR-2 throughput in a 200 beam realistic antenna pattern at C/N = 20 dB

The FR-4 reference setup applied to the same 200 spot-beam antenna pattern would achieve the average throughput per beam as illustrated in Figure 9.50 for C/N=10 dB, Figure 9.51 for C/N=15 dB and Figure 9.52 for C/N=20 dB C/N.

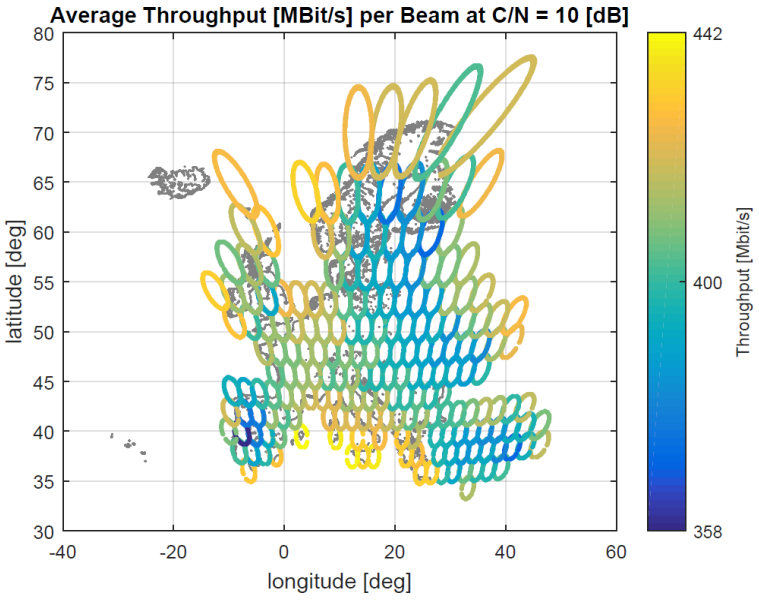

Figure 9.50: Spot beam specific average FR-4 throughput in a 200 beam realistic antenna pattern at C/N = 10 dB projected on Europe using [3]

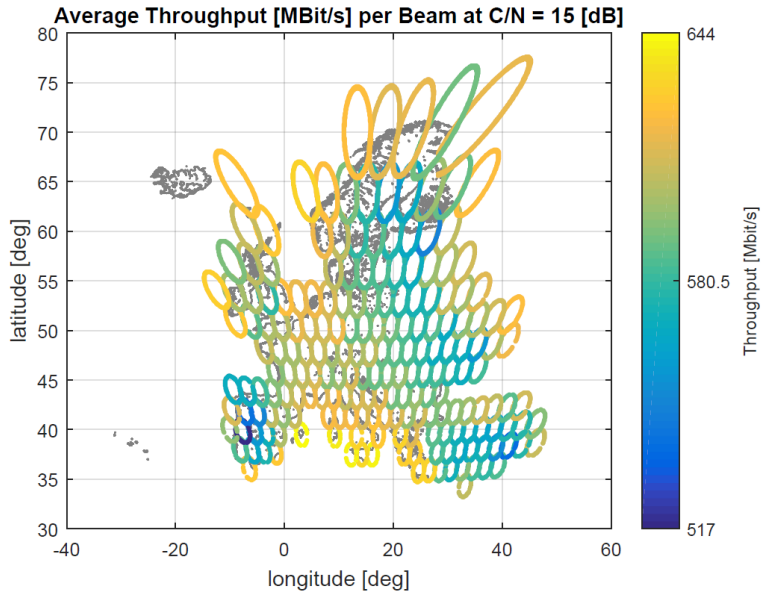

Figure 9.51: Spot beam specific average FR-4 throughput in a 200 beam realistic antenna pattern at C/N = 15 dB projected on Europe using [3]

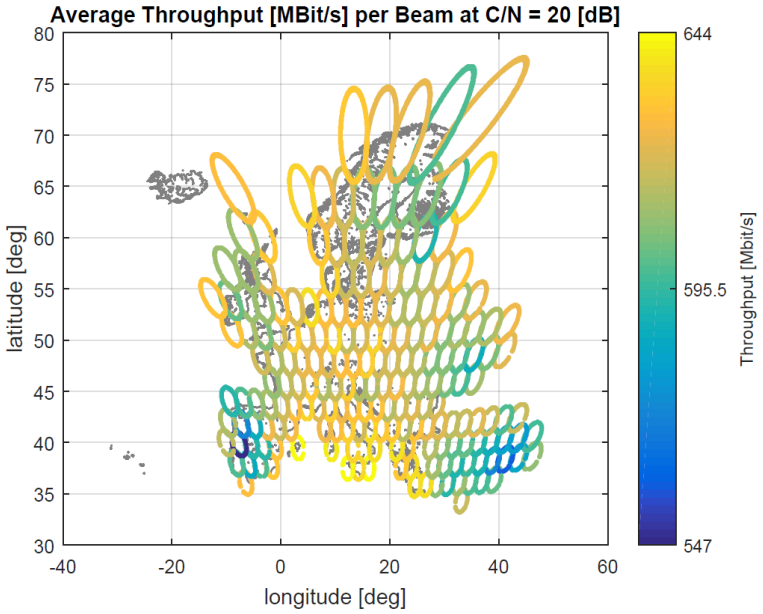

Figure 9.52: Spot beam specific average FR-4 throughput in a 200 beam realistic antenna pattern at C/N = 20 dB projected on Europe using [3]

The individual spot-beam averaged throughput results for FR-2 and FR-4 show a rather stable throughput in the center of the coverage area with anomalies especially at the border of the coverage area. These beams are usually clearly more distorted but on the other hand the area within the 3 dB cross-over level profits in contrast from higher C/I_1 levels, as shown in Figure 3.14 for FR-4 and Figure 3.15 for FR-2.

The resulting average system throughputs for FR-4 and FR-2 at the C/N levels of 10 dB, 15 dB and 20 dB are summarized in Table 9.5. As expected from the results obtained before, the gain of FR-2 w.r.t. FR-4 at C/N levels lower than 20 dB is rather small, below 10%. At a C/N level of 20 dB however, the obtained gain by FR-2 exceeds the expected gain of approx. 15%.

C/N [dB]	**FR-4 Average System Throughput [MBit/s]**	**FR-2 Average System Throughput [MBit/s]**
10	407.5	433.2
15	600	653.8
20	617.5	769.6

Table 9.5: Average system throughput achievable in a 200 spot beam pattern using MUD at various C/N levels

CHAPTER 10

Conclusion and Future Work

10.1 Conclusion

In the course of this work an efficient MUD processing was integrated in the user downlink of a physical layer based system demonstrator for a HTS system. A specific set of interference scenarios was utilized for performance analysis in terms of spectral efficiency and throughput. MUD was applied in a 2-colouring scheme, focusing on the detection of two carriers, represented by the dedicated carrier and strongest interferer, while keeping the classical 4-colouring scheme performance as benchmark. The analysis showed that the detection of several interferers, as required for a full frequency reuse (FR-1) scenario, might not bring a significant benefit due to strong C/I levels and the substantial additional complexity required in the receiver compared to a FR-2 scenario.

The MUD processing was optimized in terms of processing speed, while considering hardware requirements to enable a potential future hardware implementation. A floating-point implementation with high precision served as reference performance for the speed optimized version that combines MUD with a successive interference cancellation approach and introduces a MUD early stop criterion. A decent processing speed was achieved allowing the simulation of MUD performance curves down to FER = 10^{-6}.

The sensitivity of MUD was analyzed at different interference scenarios, which are characterized by the strongest interferer. Results confirm that MUD performs best at high interference scenarios, which are typically present close to the border of a spot beam. Due to this fact the cross-over level selected for the spot beam design is a relevant parameter in this context. In addition to that, tests showed that the MUD detection is also very sensitive to nonlinearities which demands a careful selection of the OBO with respect to the TWTA used in this context.

The performance analysis considers a MUD capable receiver terminal that is able to

operate in three modes, treating interference as noise, decoding information provided via two spot beams by MAC-MUD, and utilizing the MUD detector to decode the main carrier and discard information from the main interferer. In order to obtain the achievable system performance, a scheduling approach was applied aiming to select the best transmission mode to optimize the average system throughput.

For the performance evaluation, the demonstrator was used to generate performance tables with spectral efficiency envelopes indicating the highest performing MODCOD pairs of the individual scenarios to further speed up the scheduling process. Based on the obtained results for the selected scenarios, including ACM and tropospheric effects in the demonstrator, it can be concluded that the MUD scheme relies on strong interference levels. The introduced complexity in the receiver terminal paired with the rather low gain in average system performance are the challenging drawbacks of this interference mitigation method for HTS systems, while on the other hand this interference mitigation method offers great flexibility in terms of the achievable peak performance that could be exploited in scenarios with imbalanced traffic demands.

The analysis of the realistic antenna pattern, however, shows that the achievable gain by MUD has to be re-evaluated based on the present interference levels of each individual multi-beam HTS mission. In addition to that, the channel state information with the current interference level at the user terminals in the coverage area is required by the scheduler in order to reliably classify the situation and select the best performing MODCOD pair for the individual user terminals.

The approx. 15% gain in average system throughput that are achievable with MUD plus the opportunity of more flexibility that would allow the operator more effective provision of internet access in the coverage area comes with the drawback that the MUD system is very sensitive to specific parameters. In other words, the obtained results show that the best performing MODCOD pairs in terms of spectral efficiency are extremely sensitive to the system setup regarding parameters such as OBO, phase noise and frame length. This indicates the necessity to individually evaluate the spectral efficiency envelope for each system under investigation in order to obtain realistic scheduling results.

10.2 Future Work

With the introduction of a successive interference cancellation for the joint detection process in combination with the early stop criterion, the processing speed was improved significantly allowing the analysis of different interference and system scenario settings. For a future prototype implementation of MUD embedded in a user terminal even further investigation in speeding up the detection algorithm could become necessary and, ultimately, the development of a chip that is ready for the

mass market. This further speed improvement could be achieved by slimming down the detector to operate on an 8- to 16-bit arithmetic. Since the detector has to operate with distances, the resolution of the bit field is a critical factor that strongly influences the performance of the detector. As reported in this work, saturation effects occur at 8-bit, whereas increasing the length of the bit field up to 16 bit could provide the intended advantage.

Switching to a 16-bit implementation would allow the detector to utilize the AVX2 command set, which could potentially remove the bottleneck from the detector and improve the system performances in terms of processing speed even further.

Having analyzed the system throughput, the main benefits and drawbacks of MUD as interference mitigation method, and considering the obstacle of the ground segment implementation in the user terminal, which is not trivial due to the vast amount of terminals that would require an upgrade in this respect, another uprising interference mitigation method applied in the gateway should be mentioned. This interference mitigation technique, called precoding, modifies the signal already in the gateway, before the uplink, in order to cancel out the interference in the downlink of the satellite. Similar to MUD also this technique is not yet operational in satellite networks. The obvious advantage of precoding compared to MUD is the fact that the customer hardware is not affected by the introduction of this new technology.

Naturally, also precoding comes with challenges such as the number of interferers that can be precoded, versus its dependency on the CSI accuracy [75]. For this reason, researchers also started to investigate possible approaches to combine both methods and try to compensate the drawbacks of MUD by precoding and vice versa [76].

We know the past but cannot control it.
We control the future but cannot know it.

- Claude Elwood Shannon

Bibliography

[1] Hughes, "The view from JUPITER: high-throughput satellite systems," 2013, (retrieved: 29.12.2018). [Online]. Available: https://www.hughes.com/sites/hughes.com/files/2017-04/JUPITER_H50283_HR_08-01-13.pdf

[2] ETSI EN 302 307, "Digital video broadcasting (DVB). Second generation framing structure, channel coding and modulation systems for broadcasting, interactive services, news gathering and other broadband satellite applications; part II: S2-extensions (S2-X)," European Telecommunications Standards Institute, Standard, 2014.

[3] D. Pape, "CIA World DataBank II," online available: https://www.evl.uic.edu/pape/data/WDB/ (retrieved: 15.01.2019).

[4] J. T. Satre, "www.satellite-calculations.com, satellite motion charts for eutelsat ka-sat 9a," Website, 2018, online available: https://www.satellite-calculations.com/Satellite/satellitemotion.php?26/171/0/37258; (retrieved: 20.01.2019).

[5] ETSI EN 302 307, "Digital video broadcasting (DVB). Second generation framing structure, channel coding and modulation systems for broadcasting, interactive services, news gathering and other broadband satellite applications," European Telecommunications Standards Institute, Standard, 2009.

[6] B. Bandemer, A. El Gamal, and Y.-H. Kim, "Simultaneous nonunique decoding is rate-optimal," in *Proc. IEEE 50th Annual Allerton Conference on Communication, Control, and Computing*, Allerton, USA, 2012, pp. 9–16.

[7] W. Nam, D. Bai, J. Lee, and I. Kang, "Advanced interference management for 5G cellular networks," *IEEE Communications Magazine*, vol. 52, no. 5, pp. 52–60, 2014.

[8] J. Ebert, K. Plimon, H. Schlemmer, E. Tuerkyilmaz, N. Stamenic, M. Caus, and W. Gappmair, "System demonstrator for advanced interference mitigation techniques in satellite networks," ESA Final Report, ARTES 5.1 ESA ESTEC contract 40001110161141NL/AD, Tech. Rep., 2017.

[9] M. Caus, A. Perez-Neira, M. Angelone, and A. Ginesi, "An innovative interference mitigation approach for high throughput satellite systems," in *Proc. IEEE 16th International Workshop on Signal Processing Advances in Wireless Communications (SPAWC)*, Stockholm, Sweden, June 2015, pp. 515–519.

[10] European Space Agency (ESA), "Technology readiness levels," online available, http://sci.esa.int/sci-ft/50124-technology-readiness-level/;, http://sci.esa.int/science-e-media/img/f0/Technology_Readiness_Levels.png; (retrieved: 29.12.2018).

[11] K. Plimon, J. Ebert, N. Stamenic, H. Schlemmer, M. Caus, W. Gappmair, M. Angelone, and A. Ginesi, "Multi-user detection performance demonstrator for realistic high throughput satellite systems," in *Proc. IEEE International Symposium on Communication Systems, Networks and Digital Signal Processing (CSNDSP)*, Budapest, Hungary, July 2018, pp. 1–6.

[12] K. Plimon, J. Ebert, N. Stamenic, and W. Gappmair, "Low complexity multi-user detection in the forward link of high throughput satellite systems," in *Proc. IEEE International Conference on Broadband Communications for Next Generation Networks and Multimedia Applications (CoBCom)*, Graz, Austria, July 2018, pp. 1–6.

[13] E. Casini, R. De Gaudenzi, and A. Ginesi, "DVB-S2 modem algorithms design and performance over typical satellite channels," *International Journal of Satellite Communications and Networking*, vol. 22, no. 3, pp. 281–318, 2004.

[14] A. Ginesi *et al.*, "DVB-S2X channel models," DVB TM-S2 Channel Model Group, Tech. Rep., May 2014.

[15] K. Plimon, J. Ebert, W. Gappmair, M. Angelone, and A. Ginesi, "Interference-dependent performance of multi-user detection in high throughput satellite systems," in *Proc. IEEE International Symposium on Communication Systems, Networks and Digital Signal Processing (CSNDSP)*, Budapest, Hungary, July 2018, pp. 1–6.

[16] ITU Recommendation ITU-R S.484-3, "Station-keeping in longitude of geostationary satellites in the fixed-satellite service," International Telecommunication Union, Standard, March 1992.

[17] ITU Recommendation ITU-R P.618-13, "Propagation data and prediction methods required for the design of earth-space telecommunication systems," International Telecommunication Union, Standard, December 2017.

[18] B. Devillers, A. Perez-Neira, and C. Mosquera, "Joint linear precoding and beamforming for the forward link of multi-beam broadband satellite systems," in *Proc. IEEE Global Telecommunications Conference (GLOBECOM)*, Kathmandu, Nepal, December 2011, pp. 1–6.

[19] G. Gallinaro, "Novel intra-system interference mitigation techniques & technologies for next generations broadband satellite systems," ESA/ESTEC Final Report, February 2008, contract No. 180/04/NL/US.

[20] J. Arnau, B. Devillers, C. Mosquera, and A. Perez-Neira, "Performance study of multiuser interference mitigation schemes for hybrid broadband multibeam satellite architectures," *EURASIP Journal on Wireless Communications and Networking*, vol. 132, pp. 1–19, 2012.

[21] M. L. Moher, "Multiuser decoding for multibeam systems," *IEEE Transactions on Vehicular Technology*, vol. 49, no. 4, pp. 1226–1234, 2000.

[22] G. Colavolpe, D. Fertonani, and A. Piemontese, "SISO detection over linear channels with linear complexity in the number of interferers," *IEEE Journal of Selected Topics in Signal Processing*, vol. 5, no. 8, pp. 1475–1485, 2011.

[23] J. Millerioux, M. Boucheret, C. Bazile, and A. Ducasse, "Iterative multiuser detection and channel estimation in a multibeam satellite communication system," in *Proc. 7th Workshop on IEEE Signal Processing Advances in Wireless Communications (SPAWC)*, Cannes, France, July 2006, pp. 1–5.

[24] D. Christopoulos, S. Chatzinotas, G. Zheng, J. Grotz, and B. Ottersten, "Linear and nonlinear techniques for multibeam joint processing in satellite communications," *EURASIP Journal on Wireless Communications and Networking*, vol. 162, pp. 1–13, 2012.

[25] D. Christopoulos, J. Arnau, S. Chatzinotas, C. Mosquera, and B. Ottersten, "MMSE performance anaylsis of generalized multibeam satellite channels," *IEEE Communications Letters*, vol. 17, pp. 1332–1335, July 2013.

[26] C. Studer, A. Burg, and H. Boelcskei, "Soft-output sphere decoding: Algorithms and VLSI implementation," *IEEE Journal on Selected Areas in Communications*, vol. 26, no. 2, pp. 290–300, 2008.

[27] C. Studer and H. Boelcskei, "Soft–input soft–output single tree-search sphere decoding," *IEEE Transactions on Information Theory*, vol. 56, no. 10, pp. 4827–4842, 2010.

[28] L. Bahl, J. Cocke, F. Jelinek, and J. Raviv, "Optimal decoding of linear codes for minimizing symbol error rate," *IEEE Transactions on Information Theory*, vol. 20, no. 2, pp. 284–287, 1974.

[29] S. Andrenacci, M. Angelone, E. A. Candreva, G. Colavolpe, A. Ginesi, F. Lombardo, A. Modenini, C. Morel, A. Piemontese, and A. Vanelli-Coralli, "Physical layer performance of multi-user detection in broadband multi-beam systems based on DVB-S2," in *Proc. 20th European Wireless Conference*, Barcelona, Spain, May 2014, pp. 1–5.

[30] M. Angelone, A. Ginesi, M. Caus, A. I. Perez-Neira, and J. Ebert, "System performance of an advanced multi-user detection technique for high throughput satellite systems," in *Proc. 21st Ka and Broadband Communications Conference*, Bologna, Italy, October 2015, pp. 1–9.

[31] G. Colavolpe, A. Modenini, A. Piemontese, and A. Ugolini, "Multiuser detection in multibeam satellite systems: Theoretical analysis and practical schemes," *IEEE Transactions on Communications*, vol. 65, no. 2, pp. 945–955, February 2017.

[32] A. Ugolini, G. Colavolpe, and A. Vanelli-Coralli, "A system level approach to the application of multiuser detection in multibeam satellite systems," in *Proc. IEEE International Symposium on Wireless Communication Systems (ISWCS)*, Bologna, Italy, August 2017, pp. 66–71.

[33] S. Tahcfulloh, "Co-channel interference in broadband satellite communication systems," in *Proc. IEEE International Conference on Radar, Antenna, Microwave, Electronics and Telecommunications (ICRAMET)*, Surabaya, Indonesia, March 2013, pp. 14–16.

[34] G. Maral, M. Bousquet, and Z. Sun, *Satellite Communications Systems*, 5th ed. New York: Wiley, 2009.

[35] E. Lutz, "Co-channel interference in high-throughput multibeam satellite systems," in *Proc. IEEE International Conference on Communications (ICC)*, London, UK, June 2015, pp. 885–891.

[36] S. Andrenacci, M. Angelone, E. A. Candreva, G. Colavolpe, A. Ginesi, F. Lombardo, A. Modenini, C. Morel, A. Piemontese, and A. Vanelli-Coralli, "Physical layer performance of multi-user detection in broadband multi-beam systems based on DVB-S2," in *Proc. 20th European Wireless Conference 2014*, May 2014, pp. 1–5.

[37] G. Cocco, M. Angelone, and A. I. Pèrez-Neira, "Co-channel interference cancelation at the user terminal in multibeam satellite systems," *International Journal of Satellite Communications and Networking*, vol. 35, no. 1, pp. 45–65, 2014.

[38] M. Angelone, N. Alagha, and A. Ginesi, "Advanced physical layer techniques: Performance limits within future multi-spot Ka-band networks," in *Proc. 1st IEEE AESS European Conference on Satellite Telecommunications (ESTEL)*, Rome, Italy, October 2012, pp. 1–6.

[39] P. K. Bailleul, "A new era in elemental digital beamforming for spaceborne communications phased arrays," *Proceedings of the IEEE*, vol. 104, no. 3, pp. 623–632, 2016.

[40] P. Romero and J. M. Gambi, "Optimal control in the east/west station-keeping manoeuvres for geostationary satellites," *Aerospace Science and Technology*, vol. 8, no. 8, pp. 729 – 734, 2004. [Online]. Available: http://www.sciencedirect.com/science/article/pii/S1270963804000987

[41] J. Arnau and C. Mosquera, "Multiuser detection performance in multibeam satellite links under imperfect csi," in *Proc. Asilomar Conference on Signals, Systems and Computers*, Pacific Grove, California, November 2012, pp. 458–472.

[42] D. J. MacKay, *Information Theory, Inference and Learning Algorithms.* Cambridge University Press, 2003.

[43] S. Verdu *et al.*, *Multiuser Detection.* Cambridge University Press, 1998.

[44] J. Hagenauer, E. Offer, and L. Papke, "Iterative decoding of binary block and convolutional codes," *IEEE Transactions on Information Theory*, vol. 42, no. 2, pp. 429–445, 1996.

[45] D. Tse and P. Viswanath, *Fundamentals of Wireless Communication.* Cambridge University Press, 2005.

[46] T. M. Cover and J. A. Thomas, *Elements of Information Theory*, 2nd ed. John Wiley & Sons, 2006.

[47] N. Letzepis and A. Grant, "Information capacity of multiple spot beam satellite channels," in *Proc. 6th Australian Communications Theory Workshop*, Brisbane, Australia, February 2005, pp. 168–174.

[48] ——, "Capacity of the multiple spot beam satellite channel with Rician fading," *IEEE Transactions on Information Theory*, vol. 54, pp. 5210–5222, November 2008.

[49] S. Chatzinotas, B. Ottersten, and R. De Gaudenzi, *Cooperative and Cognitive Satellite Systems.* Academic Press: Amsterdam, 2015.

[50] R. Gallager, "Low density parity check codes," 1963.

[51] L. S. and D. J. Costello, *Error Constrol Coding: Fundamentals of Applications.* Prentice Hall, 1983.

[52] C. Berrou, A. Glavieux, and P. Thitimajshima, "Near Shannon limit error-correcting coding and decoding: Turbo codes," in *Proc. IEEE International Conference on Communications*, Geneva, Switzerland, May 1993, pp. 1064–1070.

[53] D. J. C. MacKay and R. M. Neal, "Near shannon limit performance of low density parity check codes," *Electronics Letters*, vol. 33, pp. 457–458, March 1997.

[54] J. Chen and M. P. Fossorier, "Density evolution for two improved BP-based decoding algorithms of LDPC codes," *IEEE Communications Letters*, vol. 6, no. 5, pp. 208–210, 2002.

[55] R. Y. Shao, S. Lin, and M. P. C. Fossorier, "Two simple stopping criteria for turbo decoding," *IEEE Transactions on Communications*, vol. 47, pp. 1117–1120, August 1999.

[56] W. Zhanji, P. Mugen, and W. Wenbo, "A new parity-check stopping criterion for turbo decoding," *IEEE Communications Letters*, vol. 12, pp. 304–306, April 2008.

[57] M. P. Fossorier, M. Mihaljevic, and H. Imai, "Reduced complexity iterative decoding of low-density parity check codes based on belief propagation," *IEEE Transactions on Communications*, vol. 47, no. 5, pp. 673–680, 1999.

[58] J. Zhang, M. Fossorier, and D. Gu, "Two-dimensional correction for min-sum decoding of irregular LDPC codes," *IEEE Communications Letters*, vol. 10, no. 3, pp. 180–182, 2006.

[59] J. Arnau, D. Christopoulos, S. Chatzinotas, C. Mosquera, and B. Ottersten, "Performance of the multibeam satellite return link with correlated rain attenuation," *IEEE Transactions of Wireless Communications*, vol. 13, pp. 6286–6298, 2014.

[60] M. S. Kay, *Fundamentals of Statistical Signal Processing: Estimation Theory*. Prentice Hall: Englewood Cliffs, NJ, 1993.

[61] U. Mengali and A. N. D'Andrea, *Synchronization Techniques in Digital Receivers*. Plenum Press: New York, 1997.

[62] W. Gappmair, K. Plimon, and A. Ginesi, "Coarse recovery of carrier frequency and symbol timing in multibeam satellite channels," *International Journal of Satellite Communications and Networking*, vol. 37, pp. 31–42, 2019.

[63] A. N. D'Andrea and U. Mengali, "Performance of a quadri-correlator driven by modulated signals," *IEEE Transactions on Communications*, vol. 38, pp. 1952–1957, 1990.

[64] W. Gappmair, K. Plimon, J. Ebert, and M. Bergmann, "Joint recovery of carrier frequency and symbol timing for extremely bandwidth-efficient satellite links," *IET Communications*, vol. 12, pp. 44–51, 2018.

[65] F. M. Gardner, "A BPSK/QPSK timing-error detector for sampled receivers," *IEEE Transactions on Communications*, vol. 34, pp. 423–429, 1986.

[66] M. Morelli and M. Mengali, "Feedforward frequency estimation for PSK: a tutorial review," *European Transactions on Telecommunications*, vol. 9, pp. 103–116, 1998.

[67] A. J. Viterbi and A. M. Viterbi, "Nonlinear estimation on PSK-modulated carrier phase with application to burst digital transmission," *IEEE Transactions on Information Theory*, vol. 29, pp. 543–551, July 1983.

[68] J. Ebert, H. Schlemmer, and W. Gappmair, "The code-aided FEPE algorithm for joint frequency and phase estimation at low snr," in *Proc. IEEE 6th Advanced Satellite Multimedia Systems Conference*, Baiona, Spain, September 2012, pp. 350–354.

[69] J. Ebert, H. Schlemmer, E. Tuerkyilmaz, J. Rivera-Castro, S. Cioni, and W. Gappmair, "An efficient receiver architecture for burst reception at very low SNR," in *Proc. IEEE 14th International Conference on Telecommunications*, Zagreb, Croatia, June 2017, pp. 47–54.

[70] D. R. Pauluzzi and N. C. Beaulieu, "A comparison of SNR estimation techniques for the AWGN channel," *IEEE Transactions on Communications*, vol. 48, pp. 1681–1691, October 2000.

[71] ITU Recommendation ITU-R P.1511-1, "Topography for earth-to-space propagation modelling," International Telecommunication Union, Standard, July 2015.

[72] ITU Recommendation ITU-R P.837-7, "Characteristics of precipitation for propagation modelling," International Telecommunication Union, Standard, June 2017.

[73] ITU Recommendation ITU-R P.839-4, "Rain height model for prediction methods," International Telecommunication Union, Standard, September 2013.

[74] A. Kyrgiazos, B. Evans, P. Thompson, P. T. Mathiopoulos, and S. Papaharalabos, "A terabit/second satellite system for European broadband access: A feasibility study," *International Journal of Satellite Communications and Networking*, vol. 32, pp. 63–92, 2014.

[75] A. I. Pérez-Neira, M. Á. Vázquez, S. Maleki, M. R. B. Shankar, and S. Chatzinotas, "Signal processing for high throughput satellite systems: Challenges in new interference-limited scenarios," *CoRR*, vol. abs/1802.03958, 2018. [Online]. Available: http://arxiv.org/abs/1802.03958

[76] M. A. Vazquez, M. Caus, and A. Pérez-Neira, "Performance analysis of joint precoding and mud techniques in multibeam satellite systems," in *Proc. IEEE Global Communications Conference (GLOBECOM)*, Washington D.C., USA, December 2016, pp. 1–5.

Publication List Related to Thesis

- K. Plimon, J. Ebert, N. Stamenic, H. Schlemmer, M. Caus, W. Gappmair, M. Angelone, and A. Ginesi, "Multi-user detection performance demonstrator for realistic high throughput satellite systems", in *Proc. IEEE International Symposium on Communication Systems, Networks and Digital Signal Processing (CSNDSP)*, Budapest, Hungary, July 2018, pp. 1–6.

- K. Plimon, J. Ebert, W. Gappmair, M. Angelone, and A. Ginesi, "Interference-dependent performance of multi-user detection in high throughput satellite systems", in *Proc. IEEE International Symposium on Communication Systems, Networks and Digital Signal Processing (CSNDSP)*, Budapest, Hungary, July 2018, pp. 1–6.

- K. Plimon, J. Ebert, N. Stamenic, and W. Gappmair, "Low complexity multi-user detection in the forward link of high throughput satellite systems", in *Proc. IEEE International Conference on Broadband Communications for Next Generation Networks and Multimedia Applications (CoBCom)*, Graz, Austria, July 2018, pp. 1–6.

- W. Gappmair, K. Plimon, J. Ebert, and M. Bergmann, "Joint Recovery of Carrier Frequency and Symbol Timing for Extremely Bandwidth-Efficient Satellite Links", *IET Communications*, vol. 12, pp. 44-51, 2018.

- W. Gappmair, K. Plimon, A. Ginesi, "Coarse Recovery of Carrier Frequency and Symbol Timing in Multibeam Satellite Channels", *International Journal of Satellite Communications and Networking*, vol. 37, pp. 31-42, 2019.

- J. Ebert, K. Plimon, H. Schlemmer, E. Tuerkyilmaz, N. Stamenic, M. Caus, and W. Gappmair, "System demonstrator for advanced interference mitigation techniques in satellite networks", ESA, Final Report, ARTES 5.1 ESA ESTEC contract 40001110161141NL/AD, 2017.

APPENDIX A

Additional Material

A.1 Sample SimFile

In the following the content of a sample MUD Simfile is shown. The modular concept as well as the categorization in transmit, channel and receive part are demonstrated. The module name is indicated by the keyword MODULE followed by the module specific list of parameters and their initialization values. Other keywords, written in uppercase, such as PIPE and LABEL serve to manage data flow between the modules and handle the program flow.

```
//////////////////////////////////////////
//
// CONFIGURATION
//
//////////////////////////////////////////

MODULE SimulationControl
        maxContainerLength          2000000
        maxLargeContainerLength     10000000
        containerNumber             2000
        largeContainerNumber        75
        loopsPerPoint               2147483647
        loopsPerIntermediateResult  2147483647
        infoRate                    -1
        maxPendingBurstsPerServer   5
        randomGeneratorSeed         0
        streamingMode               1

MODULE SkipFinalBurst

MODULE CountContainers
        viewModulo                  1000

MODULE Scheduler
```

```
        number_of_carriers              2
        info_flow_mode                  0
        acm                             0
        time_share                      10
        mud_iterations                  4
        c_i_scenario                    2
        detector_mode                   1
        mud_num_interferer_detect       1
        useAimtConfiguration            1
        fecFrameLength                  1
        modcodUser0                     4
        modcodUser1                     14
        configModulo                    1

REMOTE_START                            5

MODULE MultipleContainerCopies
        multiplicationFactor            36

STATIC_PIPE                             -1

//////////////////////////////////////////
//
//  TRANSMITTER
//
//////////////////////////////////////////

MODULE DVBS2XStreamConfiguration
        transponderID                   0
        carrier_center_frequency_Hz     0
        baud_rate                       100000
        modcod                          7
        roll_off_factor                 0.25
        superframe                      1
        frame_length                    1
        pilots                          1
        power                           10
        WH-pilots                       0
        WH-SOSF                         0
        payloadScramblerID              0

STATIC_PIPE                             -1

MODULE DVBS2XStreamConfiguration
        transponderID                   1
        carrier_center_frequency_Hz     0
        baud_rate                       100000
        modcod                          9
        roll_off_factor                 0.25
        superframe                      1
        frame_length                    1
        pilots                          1
        power                           10
        WH-pilots                       1
        WH-SOSF                         1
        payloadScramblerID              1
```

```
STATIC_PIPE                                 -1

MODULE PacketGenerator
        mode                                1
        pkt_bodyContent                     0
        pkt_content                         5
        pkt_type                            4
        multiUser                           1
        randomSeqNr                         1

MODULE ByteToBit

MODULE BCHencoder

MODULE LDPCencoder
        mode                                0

MODULE DVBS2BitInterleaver IF UID 0
        mode                                0
        userID                              0

MODULE DVBS2BitInterleaver IF UID 1
        mode                                0
        userID                              1

MODULE MapperBitToSymbol
        outputMode                          11

MODULE DVBS2XSuperFrameComposer IF UID 0

STATIC_PIPE                                 -1

MODULE DVBS2XSuperFrameComposer IF UID 1

STATIC_PIPE                                 -1

MODULE ZeroPadding IF UID 0
        oversampling                        4

MODULE RRCosFilter IF UID 0
        symbols_length                      20
        roll_off_factor                     0.25
        oversampling                        4
        sampling_error                      0.0
        mode                                3

MODULE ZeroPadding IF UID 1
        oversampling                        4

MODULE RRCosFilter IF UID 1
        symbols_length                      20
        roll_off_factor                     0.25
        oversampling                        4
        sampling_error                      0.0
        mode                                3
```

```
//////////////////////////////////////////
//
//  CHANNEL USER 0
//
//////////////////////////////////////////

MODULE ZeroPadding IF UID 0
        oversampling                    4

MODULE SliceToNormalOrCombineToLargeContainer IF UID 0
        mode                            0

STATIC_PIPE                             -1

MODULE ImuxOmuxFilter IF UID 0
        filterType                      3
        scaleToOS                       4

MODULE TWT_Impairments IF UID 0
        rrcosTxSymbols                  0
        oversampling                    10
        typeOfNonlinearity              2
        IBO_dB                          -6

MODULE Power_NormerExpAvg IF UID 0
        alpha                           0.001
        normPowerTo                     0.125

//////////////////////////////////////////
//
//  CHANNEL USER 1
//
//////////////////////////////////////////

MODULE ZeroPadding IF UID 1
        oversampling                    4

MODULE SliceToNormalOrCombineToLargeContainer IF UID 1
        mode                            0

STATIC_PIPE                             25

MODULE ImuxOmuxFilter IF UID 1
        filterType                      3
        scaleToOS                       4

MODULE TWT_Impairments IF UID 1
        rrcosTxSymbols                  0
        oversampling                    10
        typeOfNonlinearity              2
        IBO_dB                          -6

MODULE Power_NormerExpAvg IF UID 1
        alpha                           0.001
        normPowerTo                     0.125
```

```
//////////////////////////////////////////
//
//  COMMON CHANNEL IMPAIRMENTS
//
//////////////////////////////////////////

MODULE AddAllCarrierStreamFloat
        add_carrier_phase           1

MODULE ImuxOmuxFilter
        filterType                  4
        scaleToOS                   4

MODULE Downsampling
        downsamplingFactor          4

MODULE ConverterFloatToDouble

STATIC_PIPE                         30

MODULE PhaseNoiseGeneration
        fs                          1280000000
        maskId                      4
        testId                      0

MODULE ConverterDoubleToFloat

MODULE AWGN
        snr                         12.6

MODULE AddAdditionalInterferers

MODULE FrequencyErrorNew
        delta_fT                    0.001
        phaseStaticOffsetDeg        0
        mode                        1
        oversampling                4

//////////////////////////////////////////
//
//  RECEIVER
//
//////////////////////////////////////////

MODULE SignalBasedMeasures
        Mode                        4
        Center_freq                 0
        Freq_span                   300000
        Freq_resolution             1
        Limit_points                4096
        Num_points                  8192

MODULE RRCosFilter
        symbols_length              20
        roll_off_factor             0.25
        oversampling                4
        mode                        3
```

```
LABEL 3

MODULE AIMTInitSync

LABEL 4

STATIC_PIPE                                 -1

MODULE S2XAddLastTrailerAndNextHeaderToCurrentFrame
        oversampling                        4
LABEL 5

STATIC_PIPE                                 -1

MODULE S2XFineFreqCorr
        oversampling                        4
        useTimingEst                        1

MODULE AimtCoarseSync
        driftcorr                           0
        filterSymbols                       4
        os                                  4
        symbolsout                          1
        analyzeRefIfDiff                    0
        analyzeIF                           0
        mode                                0
        peaksExternal                       1
        driftExternal                       0
        labelDriftCorr                      3
        labelInitSync                       4
        labelAddLastTrailerAndNextHeader    5

MODULE AimtPhaseSync
        mode                                3
        os                                  1

STATIC_PIPE                                 -1

MODULE DVBS2XSuperFrameDecomposer

STATIC_PIPE                                 -1

MODULE SymbolBasedMeasures
        ScatterPlot_NumPoints               100

MODULE MUD_SymbolToChar

MODULE LDPCPacketcollector
        mode                                1

STATIC_PIPE                                 40

LABEL 1

// ------------ USER0 --------------------
MODULE MultiUserDetector
        userID                              0
```

```
        mode                            2
        multiFrame                      1
        useExternalChannelEstimates     1

MODULE DVBS2BitDeinterleaver
        mode                            2
        userID                          0

MODULE LDPCdecoder
        maxIterations                   200
        mode                            10
        multiFrame                      32
        User_ID                         0
        mud_bundled_frame               1

MODULE MUD_ExtrinsicInformation
        usr_id                          0
        multiFrame                      1
        mode                            1

MODULE DVBS2BitInterleaver
        mode                            2
        userID                          0

// ---------- USER1 ----------
MODULE MultiUserDetector
        userID                          1
        mode                            2
        multiFrame                      1

MODULE DVBS2BitDeinterleaver
        mode                            2
        userID                          1

MODULE LDPCdecoder
        maxIterations                   200
        mode                            10
        multiFrame                      32
        User_ID                         1
        mud_bundled_frame               1

MODULE MUD_ExtrinsicInformation
        usr_id                          1
        multiFrame                      1
        mode                            1

MODULE DVBS2BitInterleaver
        mode                            2
        userID                          1

MODULE MUD_CheckIteration
        label                           1
        early_stop                      1

LABEL 2

MODULE SplitFrames
```

```
        user_id                 0
        info_mode               2
        mode                    4
        mud_active              2
        multiFrame              1

STATIC_PIPE                     -1

MODULE RemoveParityCheckBits

MODULE MapperSoftBitToHardBit

MODULE BCHdecoder

MODULE BitToByte

MODULE PacketAnalyser
        pkt_content             5
        ignoreSynchLoss         1
        pkt_bodyContent         0
        outputStatistics        1
        multiUser               1

REMOTE_END                      180

MODULE CountContainers

MODULE StatisticsReceiver
        viewModulo              10
        autoReset               1

MODULE  LuaOutput

END
```

A.2 Spectral Efficiency Results for Short Frame

A.2.1 MUD Float Reference Performance

The MUD floating-point reference spectral efficiency performance excluding channel impairments following Caus et al. [9] was confirmed with the MUD system demonstrator using the LDPC decoder with belief propagation.

C/I_1 **[dB]**	**MODCOD** (B_0)	**MODCOD** (B_1)	**SNR [dB]**	**specEffPair [bit/s/Hz]**
0	QPSK 1/2	32APSK 9/10	17.4	2.71
0	QPSK 1/2	32APSK 8/9	17.0	2.68
0	QPSK 2/5	32APSK 5/6	15.3	2.44
0	QPSK 2/5	32APSK 4/5	14.5	2.36
0	QPSK 1/2	16APSK 9/10	13.9	2.27
0	QPSK 1/2	16APSK 8/9	13.6	2.25
0	QPSK 2/5	32APSK 3/4	13.5	2.24
0	QPSK 1/2	16APSK 5/6	13.3	2.14
0	QPSK 2/5	16APSK 5/6	12.1	2.04
0	PSK8 8/9	QPSK 3/5	12.0	1.91
0	QPSK 2/5	16APSK 4/5	11.5	1.97
0	QPSK 2/5	16APSK 3/4	10.6	1.87
0	QPSK 1/2	8PSK 5/6	9.8	1.72

Table A.1: Spectral efficiency result of MUD float for the $C/I_1 = 0\ dB$ scenario compared to the reference performance with floating-point [9], [8], short frame

C/I_1 [dB]	MODCOD (B_0)	MODCOD (B_1)	SNR [dB]	specEffPair [bit/s/Hz]
2	QPSK 2/3	32APSK 8/9	19.7	2.85
2	QPSK 3/5	32APSK 4/5	16.9	2.56
2	QPSK 3/5	32APSK 3/4	15.9	2.44
2	QPSK 2/3	16APSK 8/9	16.0	2.42
2	QPSK 2/3	16APSK 5/6	14.5	2.31
2	QPSK 2/3	16APSK 4/5	14.25	2.24
2	QPSK 3/5	16APSK 4/5	14.0	2.17
2	QPSK 3/5	16APSK 3/4	13.0	2.07
2	QPSK 3/5	8PSK 5/6	12.0	1.82
2	QPSK 1/2	8PSK 3/4	13.3	1.60

Table A.2: Spectral efficiency result of MUD float for the $C/I_1 = 2\ dB$ scenario compared to the reference performance with floating-point [9], [8], short frame

C/I_1 [dB]	MODCOD (B_0)	MODCOD (B_1)	SNR [dB]	specEffPair [bit/s/Hz]
4	QPSK 5/6	32APSK 4/5	20.2	2.8
4	QPSK 5/6	32APSK 3/4	19.1	2.7
4	QPSK 4/5	16APSK 8/9	18.6	2.55
4	QPSK 5/6	16APSK 5/6	18.1	2.48
4	QPSK 4/5	16APSK 5/6	16.8	2.44
4	QPSK 4/5	16APSK 4/5	16.1	2.37
4	QPSK 4/5	16APSK 3/4	15.2	2.27
4	QPSK 3/4	16APSK 3/4	15.0	2.22
4	QPSK 3/4	16APSK 2/3	14.7	2.05
4	QPSK 4/5	8PSK 5/6	14.3	2.02
4	QPSK 3/4	8PSK 3/4	12.5	1.85
4	QPSK 3/4	8PSK 2/3	11.3	1.73
4	QPSK 2/3	8PSK 3/5	10.0	1.55

Table A.3: Spectral efficiency result of MUD float for the $C/I_1 = 4\ dB$ scenario compared to the reference performance with floating-point [9], [8], short frame

C/I_1 [dB]	MODCOD (B_0)	MODCOD (B_1)	SNR [dB]	specEffPair [bit/s/Hz]
6	8PSK 2/3	16APSK 5/6	19.8	2.64
6	8PSK 2/3	16APSK 4/5	18.9	2.57
6	8PSK 2/3	16APSK 3/4	17.7	2.47
6	8PSK 2/3	8PSK 5/6	16.8	2.23
6	8PSK 2/3	8PSK 3/4	14.8	2.10
6	QPSK 8/9	8PSK 3/5	12.2	1.77
6	8PSK 3/5	QPSK 5/6	11.6	1.71
6	QPSK 5/6	QPSK 4/5	11.1	1.62
6	QPSK 5/6	QPSK 3/4	10.4	1.57

Table A.4: Spectral efficiency result of MUD float for the $C/I_1 = 6\ dB$ scenario compared to the reference performance with floating-point [9], [8], short frame

C/I_1 [dB]	MODCOD (B_0)	MODCOD (B_1)	SNR [dB]	specEffPair [bit/s/Hz]
8	16APSK 2/3	8PSK 5/6	20.0	2.55
8	16APSK 2/3	8PSK 3/4	18.7	2.43
8	8PSK 3/4	8PSK 3/4	17.6	2.22
8	16APSK 2/3	QPSK 8/9	16.6	2.20
8	8PSK 3/4	8PSK 2/3	16.1	2.10
8	8PSK 3/4	QPSK 8/9	15.2	2.00
8	8PSK 2/3	8PSK 3/5	14.6	1.88
8	8PSK 2/3	8PSK 5/6	13.9	1.82
8	8PSK 2/3	QPSK 4/5	13.4	1.78
8	8PSK 2/3	QPSK 3/4	12.7	1.73
8	8PSK 2/3	QPSK 2/3	11.6	1.65
8	8PSK 3/5	QPSK 3/5	10.6	1.48
8	QPSK 8/9	QPSK 1/2	9.6	1.37

Table A.5: Spectral efficiency result of MUD float for the $C/I_1 = 8\ dB$ scenario compared to the reference performance with floating-point [9], [8], short frame

C/I_1 **[dB]**	**MODCOD** (B_0)	**MODCOD** (B_1)	**SNR [dB]**	**specEffPair [bit/s/Hz]**
10	16APSK 3/4	QPSK 8/9	19.7	2.36
10	16APSK 5/6	8PSK 3/5	18.2	2.20
10	16APSK 3/4	QPSK 5/6	17.2	2.14
10	16APSK 3/4	QPSK 4/5	16.5	2.11
10	16APSK 2/3	QPSK 3/5	14.7	1.91
10	8PSK 3/4	QPSK 3/5	13.1	1.70
10	8PSK 3/4	QPSK 1/2	12.0	1.60
10	8PSK 2/3	QPSK 1/2	11.7	1.40
10	8PSK 2/3	QPSK 2/5	10.2	1.38

Table A.6: Spectral efficiency result of MUD float for the $C/I_1 = 10\,dB$ scenario compared to the reference performance with floating-point [9], [8], short frame

A.2.2 MUD Performance 8-bit

C/I_1 [dB]	MODCOD (B_0)	MODCOD (B_1)	SNR [dB]	specEffPair [bit/s/Hz]
0	QPSK 1/3	32APSK 8/9	18.4	2.56
0	QPSK 14/45	32APSK 8/9	18.0	2.53
0	QPSK 7/15	32APSK 5/6	17.2	2.52
0	QPSK 1/2	32APSK 5/6	16.7	2.50
0	QPSK 7/15	32APSK 4/5	16.0	2.41
0	QPSK 1/2	32APSK 4/5	15.7	2.39
0	QPSK 8/15	16APSK 8/9	15.5	2.31
0	QPSK 7/15	32APSK 3/4	15.2	2.30
0	QPSK 7/15	16APSK 8/9	14.4	2.24
0	QPSK 1/2	16APSK 8/9	14.2	2.20
0	QPSK 2/5	32APSK 32/45	14.1	2.18
0	QPSK 7/15	16APSK 5/6	13.0	2.10
0	QPSK 1/2	16APSK 5/6	12.9	2.09
0	QPSK 2/5	16APSK 5/6	12.8	2.04
0	QPSK 7/15	16APSK 4/5	12.2	2.02
0	QPSK 1/3	16APSK 4/5	12.1	1.89
0	QPSK 2/5	16APSK 3/4	11.3	1.87
0	QPSK 8/15	8PSK 5/6	10.8	1.77
0	QPSK 7/15	8PSK 5/6	10.6	1.70
0	QPSK 1/2	8PSK 5/6	10.5	1.68
0	QPSK 3/4	QPSK 8/9	10.4	1.62
0	QPSK 2/5	16APSK 3/5	9.5	1.60
0	QPSK 7/15	8PSK 3/4	9.1	1.57
0	QPSK 7/15	8PSK 32/45	8.9	1.53
0	QPSK 1/3	16APSK 26/45	8.5	1.49
0	QPSK 8/15	QPSK 8/9	7.8	1.42
0	QPSK 7/15	QPSK 8/9	7.2	1.36
0	QPSK 8/9	QPSK 1/2	7.1	1.33
0	QPSK 2/5	8PSK 3/5	7.0	1.30
0	QPSK 7/15	QPSK 5/6	6.6	1.29
0	QPSK 5/6	QPSK 2/5	5.9	1.20
0	QPSK 2/5	QPSK 4/5	5.6	1.18
0	QPSK 2/5	QPSK 3/4	5.3	1.13
0	QPSK 4/5	QPSK 1/3	5.1	1.10
0	QPSK 3/4	QPSK 1/3	4.5	1.07
0	QPSK 32/45	QPSK 1/3	4.4	1.04
0	QPSK 32/45	QPSK 14/45	4.2	1.02
0	QPSK 2/3	QPSK 14/45	4.0	0.98

0	QPSK 2/3	QPSK 4/15	3.7	0.93
0	QPSK 3/5	QPSK 4/15	3.5	0.87
0	QPSK 14/45	QPSK 8/15	3.4	0.84
0	QPSK 4/15	QPSK 8/15	2.8	0.80
0	QPSK 8/15	QPSK 11/45	2.3	0.78
0	QPSK 11/45	QPSK 7/15	1.9	0.71
0	QPSK 11/45	QPSK 1/2	1.6	0.69
0	QPSK 1/4	QPSK 2/5	1.2	0.60
0	QPSK 1/4	QPSK 1/3	1.0	0.53
0	QPSK 1/4	QPSK 14/45	0.9	0.51
0	QPSK 11/45	QPSK 11/45	0.6	0.49
0	QPSK 1/4	QPSK 11/45	0.4	0.44

Table A.7: Spectral efficiency result of MUD for the $C/I_1 = 0\,dB$ scenario compared to the reference performance with floating-point [8], short frame

C/I_1 **[dB]**	**MODCOD** (B_0)	**MODCOD** (B_1)	**SNR [dB]**	**specEffPair [bit/s/Hz]**
2	QPSK 2/3	32APSK 5/6	19.2	2.72
2	QPSK 3/5	32APSK 5/6	18.7	2.66
2	QPSK 3/5	32APSK 4/5	17.7	2.54
2	QPSK 3/4	16APSK 8/9	17.3	2.51
2	QPSK 32/45	16APSK 8/9	17.0	2.49
2	QPSK 2/3	16APSK 8/9	16.5	2.40
2	QPSK 3/5	16APSK 8/9	16.4	2.38
2	QPSK 2/3	16APSK 5/6	15.2	2.31
2	QPSK 8/15	16APSK 5/6	15.1	2.18
2	QPSK 3/5	16APSK 4/5	14.8	2.16
2	QPSK 8/15	16APSK 4/5	14.4	2.09
2	QPSK 7/15	16APSK 4/5	14.3	2.02
2	QPSK 8/15	16APSK 3/4	13.6	2.00
2	QPSK 7/15	16APSK 3/4	13.5	1.93
2	PSK8 2/3	QPSK 8/9	13.3	1.89
2	QPSK 8/15	16APSK 2/3	12.2	1.87
2	PSK8 26/45	QPSK 8/9	12.1	1.76
2	QPSK 8/15	16APSK 3/5	11.2	1.73
2	QPSK 8/15	16APSK 26/45	10.8	1.69
2	QPSK 7/15	16APSK 26/45	10.7	1.62
2	QPSK 2/3	QPSK 8/9	9.9	1.56
2	QPSK 3/5	QPSK 8/9	9.7	1.49
2	QPSK 8/15	PSK8 3/5	9.2	1.40

2	QPSK 8/15	QPSK 5/6	8.3	1.36
2	QPSK 8/15	QPSK 4/5	7.7	1.31
2	QPSK 8/15	QPSK 3/4	7.4	1.27
2	QPSK 8/15	QPSK 32/45	7.2	1.24
2	QPSK 8/9	QPSK 1/3	6.8	1.20
2	QPSK 5/6	QPSK 1/3	6.6	1.16
2	QPSK 5/6	QPSK 14/45	6.2	1.13
2	QPSK 5/6	QPSK 4/15	5.7	1.09
2	QPSK 4/5	QPSK 4/15	5.5	1.04
2	QPSK 4/5	QPSK 11/45	5.1	1.02
2	QPSK 3/4	QPSK 11/45	4.9	0.98
2	QPSK 3/4	QPSK 1/4	4.5	0.93
2	QPSK 2/5	QPSK 7/15	4.2	0.87
2	QPSK 2/5	QPSK 1/2	4.1	0.84
2	QPSK 2/5	QPSK 2/5	4.0	0.80
2	QPSK 1/3	QPSK 1/2	3.8	0.78
2	QPSK 1/3	QPSK 2/5	3.1	0.73
2	QPSK 1/3	QPSK 1/3	2.6	0.67
2	QPSK 14/45	QPSK 1/3	2.2	0.64
2	QPSK 14/45	QPSK 14/45	2.1	0.62
2	QPSK 4/15	QPSK 1/3	2.0	0.60
2	QPSK 14/45	QPSK 11/45	1.8	0.56
2	QPSK 4/15	QPSK 11/45	1.6	0.51
2	QPSK 11/45	QPSK 11/45	1.4	0.49

Table A.8: Spectral efficiency result of MUD for the $C/I_1 = 2\,dB$ scenario compared to the reference performance with floating-point [8], short frame

C/I_1 **[dB]**	**MODCOD** (B_0)	**MODCOD** (B_1)	**SNR [dB]**	**specEffPair [bit/s/Hz]**
4	QPSK 5/6	32APSK 5/6	21.1	2.88
4	QPSK 3/4	32APSK 5/6	21.0	2.79
4	QPSK 5/6	32APSK 4/5	20.1	2.77
4	QPSK 4/5	32APSK 4/5	20.0	2.72
4	QPSK 5/6	32APSK 3/4	19.9	2.66
4	QPSK 4/5	32APSK 3/4	19.1	2.61
4	QPSK 3/4	32APSK 3/4	19.0	2.57
4	QPSK 4/5	32APSK 32/45	18.4	2.56
4	QPSK 32/45	32APSK 32/45	18.3	2.49
4	QPSK 4/5	32APSK 2/3	17.9	2.44
4	QPSK 4/5	16APSK 5/6	17.4	2.42

4	QPSK 3/4	16APSK 5/6	17.5	2.38
4	QPSK 4/5	16APSK 4/5	16.7	2.33
4	QPSK 3/4	16APSK 4/5	16.6	2.29
4	QPSK 4/5	16APSK 3/4	15.9	2.24
4	QPSK 3/4	16APSK 3/4	15.8	2.20
4	QPSK 4/5	16APSK 2/3	15.3	2.11
4	QPSK 3/4	16APSK 2/3	14.4	2.07
4	QPSK 8/9	8PSK 32/45	14.3	1.96
4	QPSK 3/4	16APSK 3/5	13.3	1.93
4	QPSK 3/4	16APSK 26/45	13.0	1.89
4	QPSK 2/3	16APSK 26/45	12.9	1.82
4	QPSK 4/5	8PSK 2/3	12.7	1.78
4	PSK8 26/45	QPSK 8/9	12.2	1.76
4	PSK8 8/15	QPSK 8/9	11.9	1.69
4	QPSK 4/5	QPSK 8/9	11.4	1.67
4	QPSK 4/5	QPSK 5/6	11.3	1.60
4	QPSK 2/3	PSK8/3/5	11.1	1.57
4	QPSK 3/4	QPSK 5/6	10.4	1.56
4	QPSK 3/4	QPSK 4/5	10.1	1.51
4	QPSK 32/45	QPSK 4/5	9.9	1.49
4	QPSK 32/45	QPSK 3/4	9.8	1.44
4	QPSK 2/3	QPSK 3/4	9.2	1.40
4	QPSK 32/45	QPSK 2/3	9.1	1.38
4	QPSK 2/3	QPSK 2/3	8.5	1.33
4	QPSK 8/9	QPSK 1/3	7.6	1.22
4	QPSK 8/9	QPSK 14/45	7.4	1.20
4	QPSK 8/9	QPSK 4/15	6.7	1.16
4	QPSK 5/6	QPSK 11/45	6.3	1.07
4	QPSK 5/6	QPSK 1/4	6.1	1.02
4	QPSK 8/15	QPSK 1/2	6.0	0.98
4	QPSK 8/15	QPSK 2/5	5.3	0.93
4	QPSK 8/15	QPSK 4/15	5.2	0.80
4	QPSK 7/15	QPSK 1/3	4.2	0.80
4	QPSK 7/15	QPSK 14/45	4.0	0.78
4	QPSK 7/15	QPSK 11/45	3.8	0.71
4	QPSK 1/2	QPSK 11/45	3.6	0.69
4	QPSK 2/5	QPSK 4/15	3.7	0.67
4	QPSK 2/5	QPSK 11/45	3.5	0.64
4	QPSK 1/3	QPSK 11/45	3.4	0.58
4	QPSK 11/45	QPSK 11/45	3.3	0.49

Table A.9: Spectral efficiency result of MUD for the $C/I_1 = 4\,dB$ scenario compared to the reference performance with floating-point [8], short frame

C/I_1 **[dB]**	**MODCOD** (B_0)	**MODCOD** (B_1)	**SNR [dB]**	**specEffPair [bit/s/Hz]**
6	QPSK 8/9	32APSK 3/4	21.8	2.72
6	QPSK 8/9	32APSK 32/45	21.1	2.67
6	QPSK 5/6	32APSK 32/45	21.0	2.60
6	QPSK 8/9	32APSK 2/3	20.3	2.56
6	QPSK 8/9	16APSK 5/6	19.9	2.53
6	QPSK 5/6	16APSK 5/6	19.8	2.47
6	QPSK 8/9	16APSK 4/5	19.0	2.44
6	QPSK 8/9	16APSK 3/4	18.2	2.36
6	8PSK 3/5	16APSK 2/3	18.0	2.23
6	QPSK 8/9	16APSK 2/3	16.8	2.22
6	8PSK 3/5	16APSK 3/5	17.1	2.10
6	QPSK 8/9	16APSK 3/5	15.7	2.09
6	QPSK 3/4	16APSK 2/3	16.8	2.07
6	8PSK 3/5	16APSK 26/45	16.6	2.06
6	QPSK 8/9	16APSK 26/45	15.2	2.04
6	8PSK 3/5	8PSK 2/3	14.9	1.90
6	QPSK 8/9	8PSK 2/3	14.6	1.89
6	8PSK 2/3	QPSK 5/6	13.5	1.82
6	8PSK 3/5	QPSK 5/6	13.1	1.72
6	QPSK 8/9	QPSK 5/6	12.6	1.71
6	8PSK 3/5	QPSK 4/5	12.2	1.68
6	QPSK 8/9	QPSK 4/5	12.1	1.67
6	QPSK 8/9	QPSK 3/4	11.5	1.62
6	QPSK 8/9	QPSK 2/3	11.1	1.56
6	QPSK 5/6	QPSK 2/3	10.7	1.49
6	QPSK 8/9	QPSK 8/15	10.3	1.42
6	QPSK 8/9	QPSK 7/15	9.7	1.36
6	QPSK 8/9	QPSK 1/2	9.4	1.33
6	QPSK 4/5	QPSK 8/15	9.2	1.31
6	QPSK 8/9	QPSK 2/5	9.0	1.29
6	QPSK 5/6	QPSK 1/2	8.8	1.27
6	QPSK 4/5	QPSK 7/15	8.7	1.24
6	QPSK 8/9	QPSK 1/3	8.2	1.22
6	QPSK 8/9	QPSK 14/45	8.1	1.20
6	QPSK 8/9	QPSK 4/15	7.6	1.16
6	QPSK 8/9	QPSK 11/45	7.3	1.13
6	QPSK 8/9	QPSK 1/4	7.1	1.09
6	QPSK 4/5	QPSK 4/15	7.0	1.04
6	QPSK 4/5	QPSK 11/45	6.8	1.02

6	QPSK 2/3	QPSK 1/3	6.4	1.00
6	QPSK 2/3	QPSK 4/15	6.3	0.93
6	QPSK 2/3	QPSK 11/45	6.0	0.91
6	QPSK 8/15	QPSK 4/15	5.9	0.80
6	QPSK 8/15	QPSK 11/45	5.5	0.78

Table A.10: Spectral efficiency result of MUD for the $C/I_1 = 6\,dB$ scenario compared to the reference performance with floating-point [8], short frame

C/I_1 **[dB]**	**MODCOD** (B_0)	**MODCOD** (B_1)	**SNR [dB]**	**specEffPair [bit/s/Hz]**
8	QPSK 8/9	32APSK 5/6	28.9	2.94
8	QPSK 8/9	32APSK 4/5	27.3	2.83
8	16APSK 2/3	16APSK 2/3	23.4	2.67
8	16APSK 26/45	16APSK 3/4	23.2	2.62
8	16APSK 3/5	16APSK 2/3	21.7	22.53
8	16APSK 26/45	16APSK 2/3	21.5	2.49
8	16APSK 4/5	QPSK 8/9	20.2	2.44
8	16APSK 2/3	8PSK 3/4	19.8	2.43
8	16APSK 2/3	8PSK 32/45	19.2	2.40
8	16APSK 3/4	QPSK 8/9	18.7	2.36
8	16APSK 3/4	QPSK 5/6	18.6	2.29
8	16APSK 2/3	QPSK 8/9	16.6	2.22
8	16APSK 2/3	QPSK 5/6	16.5	2.16
8	16APSK 3/5	QPSK 5/6	15.1	2.02
8	16APSK 3/5	QPSK 4/5	14.9	1.98
8	16APSK 26/45	QPSK 4/5	14.5	1.93
8	16APSK 26/45	QPSK 3/4	14.2	1.89
8	16APSK 26/45	QPSK 32/45	14.1	1.87
8	16APSK 26/45	QPSK 2/3	14.0	1.82
8	8PSK 32/45	QPSK 32/45	13.8	1.78
8	8PSK 32/45	QPSK 2/3	13.5	1.73
8	8PSK 2/3	QPSK 2/3	13.2	1.67
8	8PSK 2/3	QPSK 3/5	13.1	1.60
8	8PSK 2/3	QPSK 8/15	12.0	1.53
8	8PSK 3/5	QPSK 8/15	11.7	1.43
8	8PSK 26/45	QPSK 8/15	11.6	1.40
8	8PSK 3/5	QPSK 7/15	11.0	1.37
8	QPSK 8/9	QPSK 7/15	10.9	1.36
8	8PSK 3/5	QPSK 1/2	10.6	1.34
8	8PSK 3/5	QPSK 2/5	10.7	1.30

8	QPSK 8/9	QPSK 2/5	9.8	1.289
8	QPSK 8/9	QPSK 1/3	8.7	1.20
8	QPSK 8/9	QPSK 4/15	8.4	1.16
8	QPSK 8/9	QPSK 11/45	8.2	1.13
8	QPSK 8/9	QPSK 1/4	8.1	1.09
8	QPSK 5/6	QPSK 11/45	7.9	1.07
8	QPSK 7/15	QPSK 11/45	7.8	0.71
8	QPSK 1/4	QPSK 11/45	7.7	0.44

Table A.11: Spectral efficiency result of MUD for the $C/I_1 = 8\,dB$ scenario compared to the reference performance with floating-point [8], short frame

C/I_1 **[dB]**	**MODCOD** (B_0)	**MODCOD** (B_1)	**SNR [dB]**	**specEffPair [bit/s/Hz]**
10	16APSK 5/6	QPSK 8/9	22.0	2.53
10	16APSK 5/6	QPSK 5/6	21.8	2.47
10	16APSK 4/5	QPSK 8/9	20.1	2.44
10	16APSK 4/5	QPSK 5/6	19.9	2.38
10	16APSK 4/5	QPSK 4/5	19.8	2.33
10	16APSK 3/4	QPSK 5/6	18.6	2.29
10	16APSK 3/4	QPSK 4/5	18.0	2.24
10	16APSK 3/4	QPSK 3/4	17.8	2.20
10	16APSK 3/4	QPSK 2/3	17.9	2.13
10	16APSK 2/3	QPSK 3/4	17.2	2.07
10	16APSK 2/3	QPSK 32/45	17.0	2.04
10	16APSK 2/3	QPSK 2/3	16.5	2.00
10	16APSK 2/3	QPSK 3/5	16.2	1.93
10	16APSK 2/3	QPSK 8/15	14.9	1.87
10	16APSK 2/3	QPSK 1/2	14.8	1.78
10	16APSK 3/5	QPSK 7/15	13.9	1.67
10	16APSK 3/5	QPSK 1/2	13.6	1.64
10	16APSK 3/5	QPSK 2/5	13.3	1.60
10	16APSK 26/45	QPSK 2/5	12.8	1.56
10	16APSK 26/45	QPSK 1/3	12.1	1.49
10	16APSK 26/45	QPSK 4/15	11.9	1.42
10	8PSK 32/45	QPSK 1/3	11.6	1.40
10	8PSK 32/45	QPSK 14/45	11.5	1.38
10	8PSK 32/45	QPSK 4/15	11.4	1.33
10	8PSK 32/45	QPSK 11/45	11.3	1.31
10	8PSK 2/3	QPSK 4/15	11.0	1.27
10	8PSK 2/3	QPSK 11/45	10.4	1.24

10	QPSK 8/9	QPSK 11/45	10.3	1.13

Table A.12: Spectral efficiency result of MUD for the $C/I_1 = 10\,dB$ scenario compared to the reference performance with floating-point [8], short frame

A.2.3 Performance Including Impairments

C/I_1 [dB]	MODCOD (B_0)	MODCOD (B_1)	SNR [dB]	specEffPair [bit/s/Hz]
0	QPSK 5/6	QPSK 8/9	13.3	1.71
0	QPSK 1/2	8PSK 5/6	11.9	1.68
0	QPSK 2/3	QPSK 8/9	11.2	1.56
0	QPSK 4/5	QPSK 374	10.9	1.51
0	QPSK 1/3	16APSK 26/45	10.1	1.49
0	QPSK 2/5	8PSK 32/45	9.4	1.47
0	QPSK 8/9	QPSK 8/15	8.9	1.42
0	QPSK 7/15	QPSK 8/9	7.7	1.36
0	QPSK 7/15	QPSK 5/6	7.6	1.29
0	QPSK 5/6	QPSK 1/2	7.4	1.27
0	QPSK 5/6	QPSK 2/5	6.6	1.22
0	QPSK 2/5	QPSK 4/5	6.1	1.18
0	QPSK 2/5	QPSK 3/4	6.0	1.133
0	QPSK 1/3	QPSK 3/4	5.2	1.07
0	QPSK 1/3	QPSK 32/45	5.0	1.04
0	QPSK 1/3	QPSK 2/3	4.5	1.00
0	QPSK 14/45	QPSK 2/3	4.4	0.98
0	QPSK 3/5	QPSK 14/45	4.2	0.91
0	QPSK 8/15	QPSK 14/45	4.0	0.84
0	QPSK 4/15	QPSK 8/15	3.1	0.80
0	QPSK 8/15	QPSK 11/45	3.0	0.78
0	QPSK 1/4	QPSK 8/15	2.9	0.73
0	QPSK 7/15	QPSK 11/45	2.4	0.71
0	QPSK 7/15	QPSK 1/4	2.1	0.67
0	QPSK 1/4	QPSK 1/2	1.8	0.64
0	QPSK 1/3	QPSK 1/4	1.4	0.53
0	QPSK 14/45	QPSK 1/4	1.3	0.51
0	QPSK 11/45	QPSK 11/45	1.0	0.49
0	QPSK 11/45	QPSK 1/4	0.6	0.44

Table A.13: Spectral efficiency result with impairments for the $C/I_1 = 0\,dB$ scenario compared to the reference performance with floating-point [8], short frame

C/I_1 [dB]	MODCOD (B_0)	MODCOD (B_1)	SNR [dB]	specEffPair [bit/s/Hz]
2	8PSK 3/4	QPSK 5/6	18.0	1.92
2	QPSK 7/15	16APSK 32/45	16.3	1.89

2	QPSK 7/15	16APSK 2/3	14.9	1.80
2	QPSK 1/2	16APSK 2/3	14.6	1.78
2	QPSK 8/15	8PSK 5/6	14.0	1.77
2	8PSK 8/15	QPSK 8/9	13.0	1.69
2	QPSK 8/15	8PSK 3/4	12.0	1.63
2	QPSK 8/15	7PSK 32/45	11.4	1.60
2	QPSK 1/2	16APSK 8/15	11.2	1.51
2	QPSK 2/3	QPSK 5/6	10.6	1.49
2	QPSK 8/15	PSK8 3/5	10.0	1.43
2	QPSK 7/15	PSK8 3/5	9.4	1.37
2	QPSK 8/9	QPSK 1/2	9.3	1.33
2	QPSK 8/9	QPSK 2/5	8.2	1.29
2	QPSK 7/15	QPSK 4/5	8.0	1.24
2	QPSK 8/9	QPSK 1/3	7.5	1.22
2	QPSK 7/15	QPSK 3/4	7.3	1.20
2	QPSK 1/2	QPSK 3/4	7.2	1.18
2	QPSK 1/2	QPSK 32/45	7.0	1.10
2	QPSK 1/2	QPSK 2/3	6.5	1.11
2	QPSK 4/5	QPSK 14/45	6.4	1.09
2	QPSK 4/5	QPSK 11/45	5.8	1.02
2	QPSK 3/4	QPSK 11/45	5.1	0.98
2	QPSK 2/5	QPSK 8/15	4.9	0.93
2	QPSK 32/45	QPSK 1/4	4.8	0.91
2	QPSK 1/3	QPSK 7/15	4.2	0.80
2	QPSK 14/45	QPSK 7/15	4.1	0.78
2	QPSK 14/45	QPSK 1/2	3.8	0.76
2	QPSK 1/3	QPSK 2/5	3.3	0.73
2	QPSK 14/45	QPSK 2/5	3.0	0.71
2	QPSK 4/15	QPSK 1/3	2.2	0.60
2	QPSK 11/45	QPSK 1/3	2.1	0.58
2	QPSK 4/15	QPSK 4/15	1.9	0.53
2	QPSK 11/45	QPSK 11/45	1.8	0.49

Table A.14: Spectral efficiency result with impairments for the $C/I_1 = 2\,dB$ scenario compared to the reference performance with floating-point [8], short frame

C/I_1 **[dB]**	**MODCOD** (B_0)	**MODCOD** (B_1)	**SNR [dB]**	**specEffPair [bit/s/Hz]**
4	QPSK 32/45	16APSK 3/4	19.7	2.18
4	QPSK 3/4	16APSK 32/45	18.7	2.16
4	QPSK 32/45	16APSK 32/45	18.8	2.13

4	QPSK 2/3	16APSK 2/3	17.4	2.00
4	QPSK 3/5	16APSK 2/3	17.1	1.93
4	QPSK 5/6	8PSK 32/45	16.6	1.89
4	QPSK 4/5	8PSK 32/45	15.6	1.84
4	QPSK 2/3	16APSK 26/45	14.6	1.82
4	QPSK 32/45	8PSK 3/4	14.4	1.81
4	QPSK 3/4	8PSK 32/45	13.9	1.80
4	QPSK 3/4	8PSK 2/3	13.1	1.73
4	8PSK 8/15	QPSK 8/9	12.5	1.69
4	QPSK 3/4	QPSK 8/9	12.1	1.62
4	QPSK 3/4	QPSK 5/6	11.3	1.56
4	PSK8 7/15	QPSK 5/6	11.2	1.52
4	QPSK 2/3	QPSK 5/6	10.6	1.49
4	QPSK 2/3	QPSK 4/5	10.0	1.44
4	QPSK 2/3	QPSK 32/45	9.4	1.38
4	QPSK 3/5	QPSK 3/4	9.3	1.33
4	QPSK 8/9	QPSK 1/3	8.1	1.22
4	QPSK 5/6	QPSK 1/3	8.0	1.16
4	QPSK 5/6	QPSK 14/45	7.9	1.13
4	QPSK 5/6	QPSK 4/15	7.1	1.09
4	QPSK 4/5	QPSK 11/45	6.5	1.02
4	QPSK 3/4	QPSK 11/45	6.3	0.98
4	QPSK 3/4	QPSK 1/4	6.2	0.93
4	QPSK 7/15	QPSK 1/2	5.7	0.91
4	QPSK 2/5	QPSK 2/5	5.1	0.80
4	QPSK 7/15	QPSK 4/15	4.5	0.73
4	QPSK 2/5	QPSK 14/45	4.2	0.71
4	QPSK 1/3	QPSK 1/3	4.1	0.67
4	QPSK 2/5	QPSK 11/45	3.6	0.64
4	QPSK 1/3	QPSK 11/45	3.5	0.58
4	QPSK 4/15	QPSK 11/45	3.4	0.51

Table A.15: Spectral efficiency result with impairments for the $C/I_1 = 4\,dB$ scenario compared to the reference performance with floating-point [8], short frame

C/I_1 **[dB]**	**MODCOD** (B_0)	**MODCOD** (B_1)	**SNR [dB]**	**specEffPair [bit/s/Hz]**
6	QPSK 3/4	16APSK 32/45	23.7	2.16
6	QPSK 3/4	16APSK 2/3	21.3	2.07
6	QPSK 8/9	8PSK 3/4	17.3	1.99
6	QPSK 8/9	8PSK 32/45	16.5	1.96

6	QPSK 8/9	8PSK 2/3	15.5	1.89
6	QPSK 8/9	16APSK 7/15	15.4	1.82
6	QPSK 8/9	8PSK 3/5	14.4	1.789
6	8PSK 26/45	8PSK 26/45	14.2	1.73
6	QPSK 8/9	QPSK 4/5	13.1	1.67
6	QPSK 8/9	QPSK 3/4	12.7	1.62
6	QPSK 5/6	QPSK 4/5	12.3	1.60
6	QPSK 5/6	QPSK 3/4	11.7	1.56
6	QPSK 5/6	8PSK 7/15	11.5	1.52
6	QPSK 4/5	QPSK 32/45	11.3	1.49
6	QPSK 4/5	QPSK 3/5	10.5	1.38
6	QPSK 3/4	QPSK 3/5	10.4	1.33
6	QPSK 5/6	QPSK 7/15	10.1	1.29
6	QPSK 3/4	QPSK 8/15	9.1	1.27
6	QPSK 3/4	QPSK 7/15	8.6	1.20
6	QPSK 3/4	QPSK 1/2	8.4	1.18
6	QPSK 2/3	QPSK 7/15	8.2	1.13
6	QPSK 2/3	QPSK 1/2	7.9	1.11
6	QPSK 2/3	QPSK 2/5	7.2	1.07
6	QPSK 3/5	QPSK 2/5	7.1	1.00
6	QPSK 3/5	QPSK 1/3	7.0	0.93
6	QPSK 3/5	QPSK 14/45	6.9	0.91
6	QPSK 7/15	QPSK 1/3	6.1	0.80
6	QPSK 7/15	QPSK 14/45	6.0	0.78
6	QPSK 2/5	QPSK 11/45	5.5	0.64

Table A.16: Spectral efficiency result with impairments for the $C/I_1 = 6\,dB$ scenario compared to the reference performance with floating-point [8], short frame

C/I_1 [dB]	MODCOD (B_0)	MODCOD (B_1)	SNR [dB]	specEffPair [bit/s/Hz]
8	QPSK 8/9	8PSK 3/4	21.7	1.99
8	8PSK 3/5	16APSK 8/15	20.8	1.97
8	8PSK 32/45	QPSK 8/9	19.0	1.96
8	8PSK 32/45	QPSK 5/6	16.0	1.89
8	8PSK 32/45	QPSK 4/5	15.3	1.84
8	8PSK 32/45	QPSK 2/3	15.1	1.73
8	QPSK 8/9	QPSK 4/5	14.9	1.67
8	QPSK 5/6	QPSK 3/4	14.2	1.56
8	8PSK 26/45	QPSK 2/3	13.0	1.53
8	QPSK 8/9	QPSK 8/15	11.4	1.42
8	QPSK 8/9	QPSK 1/2	10.5	1.33
8	QPSK 5/6	QPSK 2/5	9.3	1.22
8	QPSK 5/6	QPSK 1/3	8.6	1.16
8	QPSK 5/6	QPSK 4/15	8.4	1.09
8	QPSK 3/4	QPSK 1/3	8.3	1.07
8	QPSK 4/5	QPSK 11/45	7.8	1.02
8	QPSK 1/3	QPSK 11/45	7.7	0.58

Table A.17: Spectral efficiency result with impairments for the $C/I_1 = 8\,dB$ scenario compared to the reference performance with floating-point [8], short frame

C/I_1 [dB]	MODCOD (B_0)	MODCOD (B_1)	SNR [dB]	specEffPair [bit/s/Hz]
10	8PSK 3/4	QPSK 3/4	17.8	1.83
10	8PSK 3/4	QPSK 3/5	16.1	1.70
10	8PSK 32/45	QPSK 8/15	14.2	1.60
10	8PSK 32/45	QPSK 7/15	13.2	1.53
10	8PSK 32/45	QPSK 2/5	12.5	1.47
10	8PSK 26/45	QPSK 2/5	11.8	1.27
10	QPSK 5/6	QPSK 2/5	11.7	1.22
10	8PSK 26/45	QPSK 1/3	10.7	1.20
10	QPSK 5/6	QPSK 1/3	10.5	1.16
10	8PSK 8/15	QPSK 4/15	10.4	1.07
10	QPSK 4/5	QPSK 11/45	10.2	1.02
10	8PSK 7/15	QPSK 11/45	9.9	0.94

Table A.18: Spectral efficiency result with impairments for the $C/I_1 = 10\,dB$ scenario compared to the reference performance with floating-point [8], short frame

A.3 Spectral Efficiency Results for Normal Frame

The MUD spectral efficiency envelopes for normal frames including system impairments are provided in the following.

A.3.1 MUD Performance 8-bit Including Impairments

C/I_1 **[dB]**	**MODCOD** (B_0)	**MODCOD** (B_1)	**SNR [dB]**	**specEffPair [bit/s/Hz]**
0	PSK8 23/36	16APSK 5/6	22.0	2.62
0	QPSK 2/5	32APSK 8/9	17.4	2.62
0	QPSK 1/2	32APSK 5/6	16.5	2.58
0	QPSK 9/20	32APSK 5/6	16.1	2.53
0	QPSK 9/20	32APSK 4/5	15.4	2.45
0	QPSK 2/5	32APSK 4/5	15.3	2.40
0	QPSK 9/20	32APSK 3/4	14.2	2.33
0	QPSK 1/2	16APSK 8/9	14.0	2.28
0	QPSK 1/2	16APSK 5/6	13.2	2.17
0	QPSK 9/20	16APSK 5/6	12.7	2.12
0	QPSK 9/20	16APSK 4/5	12.0	2.05
0	QPSK 9/20	16APSK 3/4	11.3	1.95
0	QPSK 9/20	16APSK 13/18	10.9	1.89
0	QPSK 2/5	16APSK 25/36	10.1	1.79
0	QPSK 2/5	16APSK 23/36	9.4	1.68
0	QPSK 2/5	16APSK 28/45	9.1	1.65
0	QPSK 1/3	16APSK 3/5	8.7	1.53
0	QPSK 1/3	16APSK 26/45	8.3	1.49
0	QPSK 1/2	QPSK 9/10	7.3	1.40
0	QPSK 2/5	8PSK 23/36	7.0	1.36
0	QPSK 2/5	8PSK 3/5	6.6	1.30
0	QPSK 9/20	QPSK 5/6	6.5	1.28
0	QPSK 9/20	QPSK 4/5	6.2	1.25
0	QPSK 5/6	QPSK 2/5	5.8	1.23
0	QPSK 2/5	QPSK 3/4	5.1	1.15
0	QPSK 3/4	QPSK 1/3	4.5	1.08
0	QPSK 2/3	QPSK 1/3	4.4	1.00
0	QPSK 1/3	QPSK 3/5	3.5	0.93
0	QPSK 3/5	QPSK 13/45	3.2	0.89
0	QPSK 13/45	QPSK 11/20	3.0	0.84
0	QPSK 11/20	QPSK 1/4	2.6	0.80

0	QPSK 1/2	QPSK 1/4	1.8	0.75
0	QPSK 1/4	QPSK 2/5	1.0	0.65
0	QPSK 1/4	QPSK 1/3	0.9	0.58
0	QPSK 1/4	QPSK 13/45	0.6	0.54

Table A.19: Spectral efficiency result of MUD for the $C/I_1 = 0\ dB$ scenario compared to the reference performance with floating-point [8], normal frame

C/I_1 **[dB]**	**MODCOD** (B_0)	**MODCOD** (B_1)	**SNR [dB]**	**specEffPair [bit/s/Hz]**
2	QPSK 11/20	32APSK 8/9	19.9	2.77
2	QPSK 2/3	32APSK 5/6	19.5	2.75
2	QPSK 3/5	32APSK 5/6	18.4	2.68
2	QPSK 3/5	32APSK 4/5	17.6	2.60
2	QPSK 3/5	32APSK 3/4	16.7	2.475
2	QPSK 2/3	16APSK 9/10	16.6	2.47
2	QPSK 2/3	16APSK 8/9	16.4	2.44
2	QPSK 3/5	16APSK 8/9	16.2	2.38
2	QPSK 2/3	16APSK 5/6	16.0	2.33
2	QPSK 3/5	16APSK 5/6	14.9	2.27
2	QPSK 3/5	16APSK 4/5	14.4	2.20
2	QPSK 3/5	16APSK 3/4	13.6	2.10
2	QPSK 3/5	16APSK 13/18	13.5	2.04
2	QPSK 11/20	16APSK 13/18	12.9	1.99
2	QPSK 11/20	16APSK 25/36	12.4	1.94
2	QPSK 11/20	16APSK 28/45	11.9	1.79
2	QPSK 1/2	16APSK 23/36	11.6	1.78
2	QPSK 1/2	16APSK 28/45	11.2	1.74
2	QPSK 1/2	16APSK 3/5	10.9	1.70
2	QPSK 1/2	16APSK 26/45	10.5	1.66
2	QPSK 2/3	QPSK 9/10	10.3	1.57
2	QPSK 11/20	8PSK 2/3	10.4	1.55
2	QPSK 3/5	QPSK 9/10	9.5	1.50
2	QPSK 1/2	8PSK 23/36	9.1	1.46
2	QPSK 3/5	QPSK 5/6	8.7	1.43
2	QPSK 11/20	QPSK 5/6	8.3	1.38
2	QPSK 1/2	QPSK 4/5	7.8	1.30
2	QPSK 1/2	QPSK 3/4	7.1	1.25

Table A.20: Spectral efficiency result of MUD for the $C/I_1 = 2\ dB$ scenario compared to the reference performance with floating-point [8], normal frame

C/I_1 **[dB]**	**MODCOD** (B_0)	**MODCOD** (B_1)	**SNR [dB]**	**specEffPair [bit/s/Hz]**
4	QPSK 5/6	32APSK 5/6	20.9	2.92
4	QPSK 5/6	32APSK 4/5	20.3	2.83
4	QPSK 4/5	32APSK 4/5	20.0	2.80
4	QPSK 5/6	32APSK 3/4	19.5	2.71
4	QPSK 4/5	32APSK 3/4	18.9	2.68
4	QPSK 4/5	16APSK 8/9	18.5	2.58
4	QPSK 4/5	16APSK 5/6	17.2	2.47
4	QPSK 4/5	16APSK 4/5	16.5	2.40
4	QPSK 3/4	16APSK 3/4	15.7	2.25
4	QPSK 3/4	16APSK 13/18	15.2	2.19
4	QPSK 3/4	16APSK 25/36	14.6	2.14
4	QPSK 3/4	16APSK 23/36	13.8	2.03
4	QPSK 3/4	16APSK 3/5	13.7	1.95
4	QPSK 2/3	16APSK 28/45	13.4	1.91
4	QPSK 2/3	16APSK 3/5	13.1	1.87
4	PSK8 23/36	QPSK 9/10	12.6	1.86
4	PSK8 3/5	QPSK 9/10	12.3	1.80
4	QPSK 3/4	8PSK 23/36	12.2	1.71
4	QPSK 4/5	QPSK 9/10	11.8	1.70
4	QPSK 3/4	QPSK 9/10	11.6	1.65
4	QPSK 2/3	8PSK 23/36	11.3	1.63
4	QPSK 3/4	QPSK 5/6	10.6	1.58
4	QPSK 3/4	QPSK 3/4	10.5	1.50
4	QPSK 2/3	QPSK 4/5	10.0	1.47
4	QPSK 2/3	QPSK 3/4	9.3	1.42
4	QPSK 9/10	QPSK 2/5	8.4	1.30
4	QPSK 9/10	QPSK 1/3	7.4	1.23
4	QPSK 9/10	QPSK 13/45	6.9	1.189
4	QPSK 8/9	QPSK 1/4	6.6	1.14
4	QPSK 5/6	QPSK 1/4	6.1	1.08
4	QPSK 1/2	QPSK 9/20	5.9	0.95
4	QPSK 2/3	QPSK 1/4	5.7	0.92
4	QPSK 1/2	QPSK 2/5	5.1	0.90
4	QPSK 1/2	QPSK 1/3	4.4	0.83
4	QPSK 1/2	QPSK 1/4	4.2	0.75
4	QPSK 9/20	QPSK 13/45	4.1	0.74
4	QPSK 9/20	QPSK 1/4	4.0	0.70
4	QPSK 2/5	QPSK 13/45	3.9	0.69
4	QPSK 1/3	QPSK 1/4	3.7	0.58

Table A.21: Spectral efficiency result of MUD for the $C/I_1 = 4\ dB$ scenario compared to the reference performance with floating-point [8], normal frame

C/I_1 **[dB]**	**MODCOD** (B_0)	**MODCOD** (B_1)	**SNR [dB]**	**specEffPair [bit/s/Hz]**
6	QPSK 8/9	32APSK 5/6	23.9	2.97
6	QPSK 9/10	32APSK 4/5	23.0	2.90
6	PSK8 25/36	16APSK 4/5	21.2	2.64
6	PSK8 23/36	16APSK 5/6	20.8	2.63
6	PSK8 2/3	16APSK 4/5	20.4	2.60
6	QPSK 9/10	16APSK 5/6	19.7	2.57
6	QPSK 9/10	16APSK 4/5	19.1	2.50
6	QPSK 5/6	16APSK 4/5	19.0	2.43
6	PSK8 23/36	16APSK 13/18	18.7	2.40
6	QPSK 9/10	16APSK 3/4	18.2	2.40
6	QPSK 9/10	16APSK 13/18	17.6	2.34
6	QPSK 8/9	16APSK 25/36	17.0	2.28
6	QPSK 9/10	16APSK 23/36	16.2	2.18
6	QPSK 9/10	16APSK 28/45	15.7	2.14
6	QPSK 9/10	16APSK 3/5	15.5	2.10
6	QPSK 9/10	16APSK 26/45	14.9	2.06
6	QPSK 9/10	8PSK 2/3	14.5	1.90
6	QPSK 9/10	8PSK 23/36	13.5	1.86
6	QPSK 9/10	QPSK 5/6	12.6	1.73
6	PSK8 3/5	QPSK 4/5	12.3	1.70
6	PSK8 3/5	QPSK 3/4	11.6	1.65
6	QPSK 9/10	QPSK 3/5	10.9	1.50
6	QPSK 8/9	QPSK 3/5	10.7	1.49
6	QPSK 5/6	QPSK 3/5	10.1	1.43
6	QPSK 9/10	QPSK 1/2	9.8	1.40
6	QPSK 4/5	QPSK 11/20	9.5	1.35
6	QPSK 9/10	QPSK 2/5	8.8	1.30
6	QPSK 9/10	QPSK 1/3	8.1	1.23
6	QPSK 9/10	QPSK 13/45	7.8	1.189
6	QPSK 9/10	QPSK 1/4	7.2	1.15
6	QPSK 4/5	QPSK 1/4	6.9	1.05
6	QPSK 3/4	QPSK 1/4	6.6	1.00
6	QPSK 3/5	QPSK 1/3	6.5	0.93
6	QPSK 3/5	QPSK 13/45	6.1	0.89
6	QPSK 3/5	QPSK 1/4	5.8	0.85

Table A.22: Spectral efficiency result of MUD for the $C/I_1 = 6\ dB$ scenario compared to the reference performance with floating-point [8], normal frame

C/I_1 **[dB]**	**MODCOD** (B_0)	**MODCOD** (B_1)	**SNR [dB]**	**specEffPair [bit/s/Hz]**
8	QPSK 8/9	32APSK 5/6	28.9	2.94
8	QPSK 8/9	32APSK 4/5	27.3	2.83
8	APSK16 2/3	16APSK 2/3	23.4	2.67
8	APSK16 26/45	16APSK 3/4	23.2	2.62
8	APSK16 3/5	16APSK 2/3	21.7	2.53
8	APSK16 26/45	16APSK 2/3	21.5	2.49
8	APSK16 4/5	QPSK 8/9	20.2	2.44
8	APSK16 2/3	8PSK 3/4	19.8	2.43
8	APSK16 2/3	8PSK 32/45	19.2	2.40
8	APSK16 3/4	QPSK 8/9	18.7	2.36
8	APSK16 3/4	QPSK 5/6	18.6	2.29
8	APSK16 2/3	QPSK 8/9	16.6	2.22
8	APSK16 2/3	QPSK 5/6	16.5	2.16
8	APSK16 3/5	QPSK 5/6	15.1	2.02
8	APSK16 3/5	QPSK 4/5	14.9	1.98
8	APSK16 26/45	QPSK 4/5	14.5	1.93
8	APSK16 26/45	QPSK 3/4	14.2	1.8
8	APSK16 26/45	QPSK 32/45	14.1	1.87
8	APSK16 26/45	QPSK 2/3	14.0	1.82
8	8PSK 32/45	QPSK 32/45	13.8	1.78
8	8PSK 32/45	QPSK 2/3	13.5	1.73
8	8PSK 2/3	QPSK 2/3	13.2	1.67
8	8PSK 2/3	QPSK 3/5	13.1	1.60
8	8PSK 2/3	QPSK 8/15	12.0	1.53
8	8PSK 3/5	QPSK 8/15	11.7	1.43
8	8PSK 26/45	QPSK 8/15	11.6	1.40
8	8PSK 3/5	QPSK 7/15	11.0	1.37
8	QPSK 8/9	QPSK 7/15	10.9	1.35
8	8PSK 3/5	QPSK 1/2	10.6	1.34
8	8PSK 3/5	QPSK 2/5	10.7	1.30
8	QPSK 8/9	QPSK 2/5	9.8	1.29
8	QPSK 8/9	QPSK 1/3	8.7	1.22
8	QPSK 8/9	QPSK 4/15	8.4	1.16
8	QPSK 8/9	QPSK 11/45	8.2	1.13
8	QPSK 8/9	QPSK 1/4	8.1	1.09

8	QPSK 5/6	QPSK 11/45	7.9	1.07
8	QPSK 7/15	QPSK 11/45	7.8	0.71
8	QPSK 1/4	QPSK 11/45	7.7	0.44

Table A.23: Spectral efficiency result of MUD for the $C/I_1 = 8\ dB$ scenario compared to the reference performance with floating-point [8], normal frame

C/I_1 **[dB]**	**MODCOD** (B_0)	**MODCOD** (B_1)	**SNR [dB]**	**specEffPair [bit/s/Hz]**
10	16APSK 4/5	QPSK 8/9	20.1	2.49
10	16APSK 4/5	QPSK 5/6	20.0	2.43
10	16APSK 3/4	QPSK 8/9	19.8	2.39
10	16APSK 3/4	QPSK 5/6	18.7	2.33
10	16APSK 3/4	QPSK 4/5	18.1	2.30
10	16APSK 3/4	QPSK 3/4	17.9	2.25
10	16APSK 13/18	QPSK 3/4	17.4	2.19
10	16APSK 13/18	QPSK 3/5	16.7	2.04
10	16APSK 25/36	QPSK 3/5	15.7	1.99
10	16APSK 25/36	QPSK 11/20	15.5	1.94
10	16APSK 23/36	QPSK 11/20	15.2	1.83
10	16APSK 23/36	QPSK 1/2	14.1	1.78
10	16APSK 23/36	QPSK 9/20	13.8	1.73
10	16APSK 28/45	QPSK 9/20	13.6	1.69
10	16APSK 28/45	QPSK 2/5	13.1	1.64
10	16APSK 26/45	QPSK 2/5	12.7	1.56
10	16APSK 26/45	QPSK 1/3	11.8	1.49
10	8PSK 25/36	QPSK 13/45	11.6	1.33
10	8PSK 2/3	QPSK 13/45	11.2	1.29
10	8PSK 2/3	QPSK 1/4	10.9	1.25
10	8PSK 23/36	QPSK 1/4	10.8	1.21
10	8PSK 3/5	QPSK 1/4	10.7	1.15
10	QPSK 4/5	QPSK 1/4	10.6	1.05

Table A.24: Spectral efficiency result of MUD for the $C/I_1 = 10\ dB$ scenario compared to the reference performance with floating-point [8], normal frame